Structural Nexus and Divide: the Western Tauern Window, Eastern Alps

Susanne Schneider[1], Claudio Luca Rosenberg[2], Andreas Scharf[3], Konrad Hammerschmidt[4], and Lothar Ratschbacher[5]

[1]Technische Universität Bergakademie Freiberg
[2]Sorbonne Universités
[3]Sultan Qaboos University
[4]Freie Universitaet Berlin
[5]Geologie, Technische Universität Bergakademie Freiberg, 09599 Freiberg, Germany

November 22, 2022

Abstract

The western Tauern Window of the Eastern Alps constitutes a mature transpressive wrench zone generated by Oligocene-Miocene convergence between the Dolomites Indenter and the European foreland. As a major structural divide, it translates convergence-parallel north-south shortening into convergence-perpendicular eastward lateral extrusion. About 7000 foliation, lineation, fold-axis, axial-plane, shear-zone, and shear-band measurements at ˜1800 sites detail the structural geometry and evolution during indentation and transpression, modeled by numerical and analogue-material experiments. The results outline the western Tauern Window as an orogen-scale zone of localized deformation, consisting of tight, upright folds, reactivated by a sinistral shear-zone network. It connects the Giudicarie Belt southwest of the indenter salient with the Salzach-Ennstal-Mariazell-Puchberg Fault (SEMP) in the northeast. This transpressive zone has a sigmoidal vortex geometry, decoupling the Ötztal Basement in the west from the extruding wedges of the Eastern Alps in the east. Shortening was successively absorbed by nappe stacking, upright folding, and dome formation and then maintained by transpressional shearing that led to lateral extrusion, probably promoted by a change in the lithospheric configuration. The western part of the SEMP likely rotated [?]20deg clockwise around a pole approximately halfway along its entire length during the indentation.

Hosted file

schneider-et-al-supporting-information-agu210609.docx available at https://authorea.com/users/538229/articles/599564-structural-nexus-and-divide-the-western-tauern-window-eastern-alps

Hosted file

essoar.10507291.1.docx available at https://authorea.com/users/538229/articles/599564-structural-nexus-and-divide-the-western-tauern-window-eastern-alps

Hosted file

schneider-et-al-tectonics-agu210609.docx available at https://authorea.com/users/538229/articles/599564-structural-nexus-and-divide-the-western-tauern-window-eastern-alps

Structural Nexus and Divide: the Western Tauern Window, Eastern Alps

Susanne Schneider[1], Claudio L. Rosenberg[2], Andreas Scharf[3], Konrad Hammerschmidt[4, †], Lothar Ratschbacher[1]

[1]Geologie, Technische Universität Bergakademie Freiberg, Freiberg, Germany.

[2]Institut des Sciences de la Terre Paris, ISTeP UMR 7193, Sorbonne Université, CNRS-INSU, Paris, France.

[3]Department of Earth Sciences, Sultan Qaboos University, Muscat, Sultanate of Oman.

[4]Institute of Geological Sciences, Freie Universität Berlin, Berlin, Germany.

[†] Retired.

Corresponding author: Susanne Schneider ()

(ORCID IDs: Susanne Schneider: 0000-0002-8392-7711, Lothar Ratschbacher: 0000-0001-9960-2084).

Key Points:

- The western Tauern Window forms a mature transpressive wrench zone with a sigmoidal vortex geometry
- The western Tauern Window links the Giudicarie Belt to the SEMP Fault, translating orogen-perpendicular shortening into -parallel extension
- The western Tauern Window decouples the Ötztal Basement in the west from the extruding wedges of the Eastern Alps in the east

Abstract

The western Tauern Window of the Eastern Alps constitutes a mature transpressive wrench zone generated by Oligocene-Miocene convergence between the Dolomites Indenter and the European foreland. As a major structural divide, it translates convergence-parallel north-south shortening into convergence-perpendicular eastward lateral extrusion. About 7000 foliation, lineation, fold-axis, axial-plane, shear-zone, and shear-band measurements at ~1800 sites detail the structural geometry and evolution during indentation and transpression, modeled by numerical and analogue-material experiments. The results outline the western Tauern Window as an orogen-scale zone of localized deformation, consisting of tight, upright folds, reactivated by a sinistral shear-zone network. It connects the Giudicarie Belt southwest of the indenter salient with the Salzach-Ennstal-Mariazell-Puchberg Fault (SEMP) in the northeast. This transpressive zone has a sigmoidal vortex geometry, decoupling the Ötztal Basement in the west from the extruding wedges of the Eastern Alps in the east.

Shortening was successively absorbed by nappe stacking, upright folding, and dome formation and then maintained by transpressional shearing that led to lateral extrusion, probably promoted by a change in the lithospheric configuration. The western part of the SEMP likely rotated 20° clockwise around a pole approximately halfway along its entire length during the indentation.

Plain Language Summary

The Alps constitute one of Earth's best-studied continent-continent collision orogens. There, the Apulian plate, a continental sliver of the African plate, started to collide with the European plate ~66 million years ago. In the north, the Apulian plate has a triangular shape, the Dolomites Indenter. The Tauern Window at the tip of the Dolomites Indenter deformed stronger than its neighboring areas, exposing deeply-buried European-plate rocks that are surrounded by Apulian-plate upper crustal rocks. We studied the deformation within the western Tauern Window and found that it connects two major fault zones, i.e., the Giudicarie Belt in the southwest that accommodates orogen-perpendicular shortening, and the SEMP Fault in the northeast that accompanies orogen-parallel extension. Based on kinematic models and field data, the western SEMP Fault likely rotated clockwise 20°.

1 Introduction

Salients or oroclines (e.g., Bandar Abbas, Pamir-Hindu Kush, Hazare-Kashmir, Namche Barwa, Nanga Parbat), where promontories advance into weak crust, are studied to deduce the kinematics of indenter tectonics and the associated displacements in the lithosphere (e.g., Critelli & Garzanti, 1994; Kufner et al., 2016; Molinario et al., 2004). Commonly observed processes are strain partitioning and localization, decoupling between tectonic blocks, deep-crustal exhumation, transpression, transtension, and slab breakoff (e.g., Chopin et al., 2012; Dewey et al., 1998; Fossen et al., 2013; Frehner, 2016; Kufner et al., 2016; Reiter et al., 2011; Reiter et al., 2018; Robin & Cruden, 1994). The structural evolution at indenter fronts has been modeled by numerical and analogue-material experiments, but controversies on the boundary conditions, reference systems and directions, and displacement amounts and rates in orogens hinder the transfer of their results to the natural systems (Burg & Podladchikov, 1999; Ratschbacher et al., 1991a, 1991b; Reiter et al., 2011; Rosenberg et al., 2004, 2007; Schueller & Davy, 2008). In addition, pre-existing anisotropies, common in orogens, may induce a structural evolution that deviates from the predicted one. Another difficulty is the quantification of shortening at the indenter fronts. Shortening in transpressional zones is often overestimated, as the wrench component of deformation remains underconsidered due to the lateral material movements out of the cross sections used to quantify the shortening (Tikoff & Peterson, 1998). To overcome this problem, we herein derive the kinematic vorticity number W_{k} to estimate the amounts of convergence-parallel shortening (contraction) and fold-hinge-parallel extension (stretching) based on the convergence angle , measured between the convergence direction and the active shear plane (Supporting Information Figure S1); this reflects the ratio between the simple and pure shear components of the bulk deformation (Fossen & Tikoff, 1993; Tikoff & Fossen, 1993).

We studied the western Tauern Window (TW) in front of the Dolomites Indenter in the European Alps (Figure 1a). The structural maps outline areas of dominate transpression and subordinate transtension, for example outlined by non-cylindrical folds and transecting foliations. In the field, we took foliation, lineation, fold axis, fold axial plane, shear zone, and shear band measurements. Based on their orientation, we defined five structural domains (A to E). We focus on the spatial distribution and relative temporal evolution of these structures and calculate the dihedral angles (section 4 Methods and section 5 Results) between the mean values of two distinct structures that formed in kinematic succession. We use the rotational direction of the dihedral angles (being clockwise or counterclockwise) and the kinematic vorticity number W_k to (1) deduce the kinematic connections between major fault systems, (2) discriminate between wrench-dominated and pure-shear-dominated transpressional domains, and (3) quantify the amounts of shortening and extension within the transpressional folds of the western TW. We review the existing hypotheses on the structural development of the TW and, based on our findings, modify them regarding the role of indentation, lateral extrusion, and fault linkage and rotation. Finally, we discuss the coupling between major fault zones, the decoupling of tectonic blocks, and complement the ongoing discussion about fault linkage and absolute displacements in the western TW by developing the Proto-SEMP hypothesis.

2 Geological Setting

The TW (Figure 1a) is the largest tectonic window of the Eastern Alps (Frisch, 1976), where lower plate rocks have been exhumed from >35-km-depth in the Cenozoic (e.g., Kurz et al., 2008; Selverstone & Spear, 1985; Spear & Franz, 1986). In this east-west elongate structural and metamorphic dome, the arcuate dome axis coincides with rocks recording the peak temperatures of high-grade Barrovian metamorphism (Grundmann & Morteani, 1985; Rosenberg et al., 2018; Selverstone, 1985; Schneider et al., 2015) and the youngest cooling ages (Bertrand et al., 2017; Luth & Willingshofer, 2008; Most, 2003; Rosenberg & Berger, 2009). We subdivided the TW into the eastern, central, and western sub-domes; the eastern and western sub-domes are characterized by elongate and concentric metamorphic isograd trajectories (Grundmann & Morteani, 1985; Scharf et al., 2013b) and intersecting and bordering shear zones (Figure 1a; e.g., Linzer et al., 2002; Neubauer et al., 1999; Rosenberg et al., 2004; Scharf et al., 2013a; Schneider et al., 2013). Framing shear zones are absent in the central dome; there, only structurally high nappes are exposed (e.g., Bousquet et al., 2012a; Schmid et al., 2013), partly folded into a map-scale sheet fold (Groß et al., 2020).

Two end-member models are debated for the formation of the TW. One emphasizes orogen-parallel, large-scale extension, exhuming the rocks of the TW along low-angle normal faults (e.g., Frisch et al., 2000; Neubauer et al., 1999), the other upright folding associated with erosional denudation (e.g., Cornelius, 1940; Laubscher, 1990). Yet, most authors agree on the activity of two kinematically-coupled processes, namely shortening due to the northward displacement of the Dolomites Indenter and eastward lateral material transport, associated with orogen-parallel extension; Ratschbacher et al. (1991a, 1991b) defined these as lateral extrusion, encompassing extension collapse, i.e., gravitational spreading of thickened and uplifted crust in an orogen, and tectonic escape. However, the amounts of shortening, displacement, and extension remain controversial (Frisch et al., 2000; Fügenschuh et al., 2012; Linzer et al., 2002; Luth et al., 2013; Neubauer et al., 1999; Pomella et al., 2011, 2012; Rosenberg & Berger, 2009; Rosenberg & Garcia, 2011, 2012; Scharf et al., 2013a; Schmid et al., 2013; Wolff et al., 2020). We contribute to this discussion with a compilation of structural measurements in the western TW to distinguish structural domains, and to assess the traces and interconnections of major shear zones.

2.1 Tectonostratigraphic Framework

Mesozoic ocean-derived and ophiolite-bearing units of the Glockner Nappe and Matreier Zone and siliciclastic rocks of the European distal margin were imbricated during European continental margin subduction (Figure 1a). The deepest structural units of the TW consist of Europe-derived, late-Variscan intrusions and their para-autochthonous, pre-Variscan host rocks covered by post-Variscan metasediments (Figure 1a), forming the Venediger Duplex, an antiformal stack generated by north-vergent nappe emplacement during the Adria-Europe collision. Above the intervening ocean-derived units of the Glockner Nappe and Matreier Zone, the hanging, Adria-derived Austroalpine nappes include the Meran-Mauls Basement, Ötztal Basement, Northern Calcareous Alps, Niedere Tauern, Gurktal Alps, and the DAV Basement (Figure 1a). All these units were thrusted over the European continental-margin units with the units in the TW shortened due to nappe stacking (D_1) and upright folding (D_2) during the Alpine collision in the Eocene to Oligocene. This resulted in a thickened European crust (e.g., Frisch, 1976; Lammerer et al., 2008; Lammerer & Weger, 1998; Rosenberg et al., 2014, 2018; Schmid et al., 2013) with a declining thickeness east of the TW (Spada et al., 2013). In the late stage of the orogenic evolution, in the Oligocene-Miocene, east-west extension and strike-slip motion (D_3) have accompanied shortening.

2.2 Structural Framework

The western TW consists of the (D_2) upright Ahorn-, Tuxer-, and Zillertaler antiforms that fold the Early Alpine (D_1) foliation of the Venediger Duplex (Figure 1a; Schmid et al., 2013; Lammerer & Weger, 1998). Estimates of the amount of shortening accommodated by these folds vary between ~60 km (Rosenberg et al., 2015), ~49 km (Rosenberg & Berger, 2009), and ~32 km (Schmid et al., 2013), based on line-length balancing and assuming constant nappe thicknesses. The tight folds strike ENE, show sub-horizontal, doubly-plunging fold axes and sub-vertical axial planes; they are often associated with axial-plane foliations, and have up to ~17 km amplitudes (Figure 1b). In contrast, the upright folds in the central and eastern TW strike east to ESE, are open and flat-topped (box-type) with amplitudes of up to ~10 km, and lack axial-plane foliations (Figures 1c to 1d). These structural differences point to an abrupt along-strike change in the way shortening has been accommodated (Figure 2a).

The Brenner Fault at the western margin of the TW (Figure 1a) is subdivided in this study into the Brenner Mylonites (BM) and the Silltal Fault (SF, Figure 2b; Behrmann, 1988; Schmidegg, 1953; Selverstone, 1988). The top-west, normal-slip Brenner Fault detaches the Ötztal Basement from the underlying Glockner nappe. The steep limbs of the antiforms and the cores of the tight synforms in the westernmost TW are overprinted by sinistral shear zones, striking sub-parallel to their axial planes. From north to south, the map-scale sinistral shear zones are the Ahorn (ASZ), Greiner (GSZ), and Ahrntal (AhSZ) Shear Zones, each ~1 to 3-km-wide and tens of kilometers long (Figures 1a and 2b). In addition, several 10s to 100s of meters wide sinistral shear zones, e.g., the Tuxer (TSZ) and the Olperer (OSZ) Shear Zones, occur.

2.3 Surrounding Fault Zones

2.3.1 Giudicarie Belt The sinistral transpressive Giudicarie Belt (GB, Figure 1a) forms the western margin of the Dolomites Intender, a ~77-km-long, N30°E-striking fault system, that offsets the ESE-striking Periadriatic Fault System. Displacement estimates along the GB vary between 15 to 30 km (e.g., Müller et al., 2001; Picotti et al., 1995; Viola et al., 2001) and ~70 km (e.g., Laubscher, 1988; Ratschbacher et al., 1991b; Werling, 1992) due to differing assumptions on its pre-indentation orientation and the amount of shortening accommodated at its southwestern tail. The former group of authors assumes an originally bent Periadriatic Fault System and therefore argues for moderate displacement along the GB, whereas the latter group assumes a straight, pre-indentation Periadriatic Fault System, requiring a larger displacement. Based on balanced cross-sections across the Southern Alps (Nussbaum, 2000; Schönborn, 1992), we favor an originally straight Periadriatic Fault System, hence a sinistral displacement of ~70 km along the GB. The GB includes the Pejo (PeF) and the Northern (NGF) and Southern Giudicarie Faults (SGF), and terminates in the north in the Jaufen (JF), Meran-Mauls (MMF), and Passeier Faults (PaF); the latter delimit, together with the southwestern corner of the TW, the N55°E-striking Meran-Mauls Basement (Figure 1a) (Pomella et al., 2011, 2012). The PaF cuts the JF and the MMF (Müller et al., 2001; Pomella et al., 2011). The thrust geometries inside the Dolomites Indenter exhibit an arcuate shape, indicating north-south (±10°) shortening when applying the bow-and-arrow rule (e.g., Elliot, 1976) to its major thrusts. GNSS measurements of the present-day Alpine kinematics indicate a counterclockwise rotation of Adria against Europe (Caporali & Martin, 2000; Le Breton et al., 2017).

Seismic tomography outlined two lithospheric slabs whose lateral terminations spatially coincide with the GB. The eastern slab was interpreted as the Adriatic plate subducted northward down to 250 km depth; the western slab, likely part of the European plate, features incipient slab break-off (Kästle et al., 2020; Lippitsch et al., 2003; Mitterbauer et al., 2011; Zhao et al., 2016). This discontinuity in the lithospheric structure coincides with a change in seismic anisotropy (Bokelmann et al., 2013; Hetényi et al., 2018; Qorbani et al., 2015). Earthquakes with a magnitude M_L 5 (Richter scale) and hypocentral depths of 20 km have strike-slip focal mechanisms along the GB (Reiter et al., 2018).

2.3.2 Salzach-Ennstal-Mariazell-Puchberg Fault The sinistral transpressive (west) to transtensive (east) Salzach-Ennstal-Mariazell-Puchberg Fault (SEMP, Figure 1a) strikes N70°E from Mittersill along the northern margin of the TW to the Vienna Basin (e.g., Cole et al., 2007; Frost et al., 2009; Linzer et al., 1995). Currently, the SEMP is a structural divide between the seismically active Northern Calcareous Alps in the north and the low-seismicity TW in the south (Reiter et al., 2018). Piercing points imply ~60 km displacement along the SEMP (Linzer et al., 2002), equivalent to ~56 km of east-west extension. Analogue-material models (Ratschbacher et al., 1991a; Rosenberg et al., 2004), simulating the indentation of the Dolomites Intender into the Eastern Alps, suggest that the sinistral faults along the northern boundary of the extruding wedges, e.g., the Proto-SEMP (chapter 6.5), initiated in the earliest stages of indentation and then rotated clockwise during progressive indentation. For the west-central SEMP, Wang and Neubauer (1998) inferred six evolution stages from paleostress analysis. Two involve predominantly strike-slip faulting and four are dominated by fault-normal compression; the maximum compressive stress axes rotated counterclockwise from NE to NW over time. Throughout the evolution of the SEMP, its northeastern tail has been confined to the southeastern salient of the European Platform, the southeastern tip of the Bohemian Massif (Ratschbacher et al., 1991b). At present, the southeastern tip of the Bohemian spur is located below the subparallel Mur-Mürz Fault (Figure 1a) at the Semmering Pass, close to Glognitz (16°00'East, 47'40'North; van Gelder et al., 2020). Geophysical data outline its subsurface extent (Grad et al., 2009; Baroň et al., 2019; Reinecker & Lenhardt, 1999) and suggest that the Bohemian spur is still acting as a buttress.

2.3.3 Pustertal-Gailtal Fault The dextral, N100°E-striking Pustertal-Gailtal Fault (PGF), a segment of the Periadriatic Fault System, divides the Eastern from the Southern Alps (Figure 1a, Polinski & Eisbacher, 1992) and defines the southern margin of the extruding wedges of the Eastern Alps (Ratschbacher et al., 1991b). Estimates of the Oligo-Miocene displacement along the PGF are indefinite. Frisch et al. (1998) and Laubscher (1988) argued for 100 150 km, pre-Miocene dextral displacement along the entire Periadriatic Fault System based on apparent map-view offsets and palinspastic reconstructions. The dextral, NE-dipping Sprechenstein-Mauls Fault (SMF, Figure 2b), the youngest and westernmost, purely brittle segment of the PGF, offsets the western ductile tail of the PGF by ~2 km (Bistacchi et al., 2010). Earthquakes with focal mechanisms M_L 4 and hypocentral depths 10 km indicate dextral strike-slip along the PGF (Reiter et al., 2018).

2.3.4 Brenner Mylonites and Silltal Fault First estimates of east-west extension across the west-dipping BM varied between ~9 and 14 km (Behrmann, 1988) and "several to tens" of kilometers (Selverstone, 1988). Recent estimates are ~70 km (Fügenschuh et al., 1997), 4 to 12 km (Rosenberg & Garcia, 2011, 2012), 35 ± 10 km (Wolff et al., 2020), and ~44 km (Fügenschuh et al., 2012). The throw across the BM varies continuously along strike (Rosenberg & Garcia, 2011, 2012), with a maximum of ~17 km in the area of the Brenner Pass along the hinge of the Tuxer Antiform (Figure 1a); there, the BM are thickest (Axen et al., 1995; Behrmann, 1988; Selverstone, 1988). Towards the northern and southern tails of the BM and SF, the throw decreases to ~5 km, which cannot be explained by folding of the footwall (Rosenberg & Garcia, 2011). Reassessment (Fügenschuh et al., 2012; Rosenberg & Garcia, 2011, 2012) showed that extension was overestimated because exhumation was entirely attributed to normal faulting, ignoring the contributions of folding and erosion (Axen et al., 1995; Fügenschuh et al., 1997; Selverstone et al., 1995; Wolff et al., 2020). Following structural arguments (Rosenberg & Garcia, 2011, 2012) and using the average 29° dip of the BM obtained in this study (chapter 5.7.5 Extensional Shear Zones), we calculated 10 km extension across the BM, in agreement with the first estimates (Behrmann, 1988; Selverstone, 1988).

The moderately west-dipping SF strikes ~30 km from Innsbruck to Sterzing (Figure 2b and 2c). North of Steinach (Figure 2c), syn- and antithetic normal faults occur in the hanging wall of the SF (Figures 1a and 2b; Reiser, 2010; Reiter et al., 2018). The seismically active Brenner-Inntal Transfer zone connects the SF with the Inntal Fault System (Figure 1a) with transtensive and transpressive faults in the hanging and footwall of the SF, respectively (Ortner et al., 2006). The hypocentral depths of the M_L 4 earthquakes are between 5 and 15 km (Reiter et al., 2018).

2.3.5 Tauern-Northern-Boundary Fault

The Tauern-Northern-Boundary Fault (TNBF) between the Glockner Nappe and the Lower Austroalpine nappes in the northwestern TW was interpreted to link the BM to the SEMP (Töchterle et al., 2011), to transform extensional into strike-slip displacements (Fügenschuh et al., 2012), and to have a throw of ~3 km, deduced from the TRANSALP seismic section (Lammerer et al., 2008). The TNBF is an outcrop-scale, 50-m-thick, poorly exposed fault zone with varying shear sense indicators, perhaps with dominant top-north reverse and minor sinistral displacements (Bergmeister, 2010; Töchterle et al., 2011).

3 Deformation Fabrics

In the following, we present new and published structural data from the western TW (Figure 2) (Angel & Staber, 1950; Becker, 1993; Exner, 1956, 1962a, 1962b, 1979, 1980, 1983, 1989; Frank & Pestal, 2008; Frank et al., 1987; Giese, 2004; Höck et al., 1994; Karl et al., 1979; Lichtenheld, 2004; Moser, 2006; Rockenschaub & Nowotny, 2009, 2011). These data highlight a structural difference between the central and eastern and the western TW. Based on the mean orientation of the structures, we subdivided the western TW into five structural domains (Figure 2c, Domains A to E) and discriminated three deformation phases (D_1 to D_3), associated with foliations S_1 to S_3.

S_1 foliations formed prior to the upright folds (D_2; Figure 2d). Although of possibly varying ages, S_1 are associated with D_1 nappe stacking and Eocene/Oligocene metamorphism (Bousquet et al., 2012b; Glodny et al., 2005; Nagel et al., 2013; Schmid et al., 2013). The widespread sub-vertical axial-plane foliations (S_{2a}) of the D_2 tight and upright folds strike ENE and cut the folded nappe contacts in the tight D_2 synforms of the western TW (Figure 2d and 2c). The micro- and meso-scale D_2 folds are disharmonic passive shear folds, with thickened hinges, thinned limbs (measured perpendicular to bedding), and Z- and S-shaped second-order folds. Along the margins of the western TW and in the Austroalpine nappes, flexural-slip folds dominate. Along the western margin of the TW, the anticline hinges plunge west, indicated by the circular strike of the nappe contacts with outward pointing bedding. There, the folded S_1 are cut by or form composite foliations with moderately west-dipping S_{2b} foliations, part of the normal-slip shear zones along the BF. S_{2a} and S_{2b} are spatially separated, occurring NE and NW of the indenter salient, respectively (S_{2a} and S_{2b} appear as solid and dashed trajectories in Figure 2d).

D_2 folds and S_2 foliations are overprinted by D_3 km- to meter-scale, subvertical strike-slip and extensional shear zones (Figure 2b). Major NNE- to ENE-striking, sinistral (C_{sin}) shear zones and minor ESE- to ENE-striking, dextral (C_{dex}) ones occur (Pennacchioni and Mancktelow, 2007; Bistacchi et al., 2010). The west-dipping extensional shear zones (C_{nor}) along the western margin of the TW (Figure 2b) formed contemporaneously with the strike-slip shear zones because of mutual overprinting relationships (Axen et al., 1995; Behrmann, 1988; Fügenschuh et al., 1997; Selverstone, 1988). All D_3 shear zones are mylonitic, often brittle-ductile, have higher mica content and smaller grain size than the host rocks, and show clear shear-sense indicators (e.g., Mancktelow & Pennacchioni, 2005; Pennacchioni & Mancktelow, 2007; Schneider et al., 2013; Selverstone, 1993).

4 Methods

We first summarize the geometry, kinematics, and metamorphism associated with the major shear zones of the western TW (Figure 2b). Most of these structures have been described (e.g., Behrmann, 1988; Behrmann & Frisch, 1990;

Lammerer and Weger 1998; Neubauer et al., 1999; Müller et al., 2001; Pomella et al., 2011; Reicherter et al., 1993; Schneider et al., 2013; Spiess, 1995; Steffen & Selverstone, 2006; Viola et al., 2001), but their extent and location differ in the literature. Therefore, we reassess the structures and the shear-zone pattern based on our new structural data and a literature compilation. Then, we present and discuss the field measurements and mean orientation values of specific structures shown in equal area, lower hemisphere stereoplots (created by Stereo32 version 0.9; Röller & Trepmann, 2008). When the data show a preferred orientation and number >15, we contoured them using a cosine exponential equation. If lineations and foliations are shown together, we contoured only the foliations. Mean values were deduced graphically from the data maxima. The individual field measurements of the Domains A to E are listed in the Supporting Information Dataset S1. Rotation of these structures during transpression led to deactivation and replacement by new structures representing the prevailing deformation field during the progressive deformation. The rotational sense of the successively formed structures is opposed to the material paths. We calculated dihedral angles between the mean values of structures, which formed in the prevailing deformational field, and that we infer to have formed in kinematic succession. This illustrates and quantifies their transpressional character and yielded different rotational senses for Domains A to E during transpression (Borradaile, 1987; Treagus and Treagus, 1981). 's algebraic sign is positive (blue arrows) or negative (purple arrows) when the rotation from one mean value to the succeeding one is clockwise or counterclockwise, respectively (Figure S1).

5 Results and Interpretation

5.1 Ahorn Shear Zone

The ~2.5-km-wide and ~50-km-long, ~ENE-striking Ahorn Shear Zone (ASZ) is a transpressive mylonitic belt located along the northern limb of the western TW (Rosenberg & Schneider, 2008), extending the SEMP westward into deeper crustal levels (Figure 2b; Cole et al., 2007). The ASZ shows sinistral-oblique, south-side-up kinematics with a sub-vertical to steeply SSE-dipping mylonitic foliation and a shallowly west-plunging stretching lineation (Rosenberg & Schneider, 2008). The ASZ transitions into the SEMP in the area of Mittersill and Krimml where sinistral, brittle-ductile and ductile shear zones strike ~NNE and turn abruptly into the east-striking SEMP (Figure 2b and 2c; Cole et al., 2007; Reicherter et al., 1993). The metamorphic grade of the mylonites increases westward along-strike and southward perpendicular to the ASZ strike from 300°C to 400 500°C based on the quartz and feldspar recrystallization mechanisms and the stability of biotite (Schneider et al., 2013).

5.2 Tuxer Shear Zones

Lammerer & Weger (1998) described two sinistral shear zones of >40 km length within the Tuxer Antiform (Salzach-Riffler Fault), striking ESE from the Olperer and Riffel summits in the west to Krimml in the east (Figure 2b and 2c). At Lammerer & Weger's (1998) locations, we mapped an interconnected network of outcrop-scale, 1- to 10-m-thick, lower amphibolite-facies, sinistral shear zones, the Tuxer Shear Zones (TSZ, Figure 2b). The TSZ strike NE to east, dip sub-vertically to steeply south, and connect to the ASZ and the Greiner Shear Zone (see chapter 5.4) at their northeastern and southwestern tails, respectively (Figure 2b).

5.3 Olperer Shear Zones

We divided Lammerer & Weger's (1998) shear zones in the Tuxer Antiform into the TSZ (section 5.2) and the Olperer Shear Zones (OSZ) because of their different orientations and kinematics. In agreement with Ebner et al. (2004), the OSZ constitute two shear zones of 10 to 15 km length, NE to north strike, and moderate to sub-vertical NW to west dip. Sinistral and top-NW normal shear occurred within these ~300-m-thick zones at their western tails. Feldspar ductility and biotite stability indicate syn-kinematic flow at amphibolite-facies conditions.

5.4 Greiner Shear Zone

The ~1-km-thick and ~50-km-long Greiner Shear Zone (GSZ) cuts all D_1 nappe contacts of the western TW and attains a maximum thickness in the Glockner Nappe (Figure 2b and 2e; Selverstone, 1993; Steffen et al., 2001). It strikes east to ENE, is sub-vertical, and has a sub-horizontal stretching lineation. Kinematic indicators imply sinistral (Behrmann & Frisch, 1990; De Vecchi & Baggio, 1982) and dextral (Barnes et al., 2004) shear. Metamorphism in the GSZ mylonites increases eastward along strike from greenschist to amphibolite facies, controlled by the west-plunging Greiner Synform (Figure 1a; e.g., Selverstone, 1985; Selverstone & Spear, 1985).

5.5 Ahrntal Shear Zone

The ~2-km-wide and ~70-km-long transpressive Ahrntal Shear Zone (AhSZ) at the southern limb of the western TW strikes NE to ENE, dips sub-vertically to steeply NNW, and shows sinistral and minor dextral and north-side-up shear (Figure 2b; Behrmann & Frisch, 1990; Reicherter et al., 1993; Schneider et al., 2009). The AhSZ cuts all D_1 nappe contacts and shows predominantly shallowly east-plunging stretching lineations. Metamorphism increases eastwards along strike from greenschist to lower amphibolite facies and northward, perpendicular to the strike, from 300°C to 400 500°C based on quartz and feldspar recrystallization mechanisms, biotite stability, and epidote composition (Kitzig, 2010; Reicherter et al., 1993; Wollnik, 2012). Hence, the metamorphic trends are complementary to the ASZ. Key outcrops in the Vals Valley, south of the Grabspitz summit (Figure 2c), show upright, open to tight folds in the north progressing into isoclinal and rootless folds with axial-plane foliations in the south, overprinted by sinistral shear zones (Figure 3a to 3d).

5.6 Jaufen Fault and Meran-Mauls Basement

The ~200- to 300-m-wide, >15-km-long JF strikes ~ENE; its ductile-brittle mylonites formed at lower greenschist-facies conditions (Müller et al., 2001; Spiess, 1995, 2001; Viola et al., 2001). The JF splits into two branches, one with top-west normal shear in the area of Gasteig (Viola et al., 2001), and one with sinistral-transpressive shear at the Penserjoch road NW of Elzenbaum (Figures 2b and 4; Müller et al., 2001). Our structural data, collected in the Meran-Mauls Basement and summarized in chapter 5.7 as Domain C, indicate that the upright folds of the western TW can be traced into the Austroalpine nappes (Figures 2c to 2d and 4).

5.7 Structural Elements of the Western Tauern Window

5.7.1 S_1 Foliation In Domains A to C (Figure 2c), the folded S_1 strike ENE and dip moderately to steeply NNW but locally SSE (Figure 3a and 3b), indicating an upright to slightly south-vergent sub-dome structure. The sub-vertical -circle of S_1 in Domain A traces a sub-horizontal, WSW-trending fold axis, whereas the -circles of S_1 in Domains B and C indicate gently ENE- and WSW-plunging fold axes, respectively (Figure 5a to 5c; -circle: great circle that fits best the distribution of poles to a folded surface). S_1 and S_2 form a composite foliation along the steep limbs of the D_2 antiforms. A crenulation cleavage, comprising the folded S_1 cut by the axial-plane S_{2a} foliation (Figure 3a and 3b), dominates the fold hinges.

5.7.2 D_2 Fold Axes and Axial Planes The D_2 axial planes (AP_2) of Domains A and B strike ENE, whereas those of Domain C strike NE, sub-parallel to the northwestern margin of the Dolomites Indenter (Figure 5k to 5m). In a cylindrical fold, the -circle and the mean axial plane should be orthogonal to each other and the -axis should be the fold axis (Ramsay & Huber, 1987, p. 334). However, the values for $_1$ (mean AP_2 − -axis; i.e., angle between the strike of the mean D_2 axial planes and the pole to the -circle) in Domains A and B show a -5° (counterclockwise) deviation from being orthogonal, whereas the $_1$ value in Domain C indicates a +11° (clockwise) deviation (Figures 5a to 5c, 5k to 5m, and S1a to S1c, S1g in the supporting information). The D_2 fold axes (FA_2) of Domain A are sub-horizontal and trend ENE, whereas the fold axes in Domains B and C plunge moderately ENE and SW, respectively (Figure 5a to 5c and 5f to 5h). Further, the $_2$ values (mean FA_2 − -axis) indicate a deviation of -8° and -6° in Domains B and A, in contrast to a deviation of +8° in Domain C (Figures 5f to 5h, 5k to 5m, and S1). The orientation of successively formed structures (deformation fields) during the D_2 folding of S_1, indicated by $_1$ and $_2$, thus rotated counterclockwise in Domains A and B and clockwise in Domain C; the corresponding material paths rotated opposite to the deformation field, i.e., counterclockwise in Domain C and clockwise in Domains A and B (chapter 6.4).

The FA_2− -axis deviations ($_1$ and $_2$) in Domains A, B, and C indicate non-cylindrical folding in the western TW, which is diagnostic for transpressional or transtensional folding (Dewey et al., 1998; Ramsay & Huber, 1987; Tikoff & Peterson, 1998; Treagus & Treagus, 1981). The opposite rotations in Domains A and B respectively Domain C (Figures 5a to 5c, 5k to 5m, and S1) reflect the different strikes of the indenter margins causing dextral transpressive folds in domain C and sinistral ones in domains A and B (Figure S1). The different strikes are governed by the orientation of indenter margins and their angle to the convergence direction.

5.7.3 S_2 Foliation and L_2 Stretching Lineation In Domain A, the sub-vertical S_{2a} axial-plane foliations strike ENE, whereas in Domains B and C, they strike ENE–NE, i.e., slightly more to the north, and dip oppositely, SE and NW, respectively (Figure 6a to 6c). The angle $_3$ (mean AP_2–mean S_{2a}) describes the transection of the axial planes (AP_2) by the axial plane foliation (S_{2a}); S_{2a} deviates counterclockwise from AP_2 in Domains A and B and clockwise in Domain C (Figures 5k to 5m, 6a to 6c, and S1). Equally, the $_4$ values (mean FA_2–mean S_{2a}) in Domains A to C deviate clockwise in Domain C and counterclockwise in Domains A and B. According to Borradaile (1978), the $_3$ and $_4$ values obtained from cleavage-transected folds indicate dextral transpressive shear for Domains A and B, and sinistral one for Domain C. However, Treagus and Treagus (1981) showed that the relationship between cleavage-transected folds and transpressive shear sense rather depends on the initial orientation of the convergence direction to the shear zone boundary. Accordingly, the dihedral angles $_1$ to $_4$ indicate clockwise rotation of the deformation field in Domain C west of the indenter salient and counterclockwise rotation in Domains A and B east of the indenter salient during the same transpressive event. The dihedral angles $_5$ (-axis–S_{2a}) of Domains A to C are -6°, -4°, and -5°. The L_2 stretching lineations are sub-horizontal in Domain B (Figure 6b), sub-horizontal to gently WSW-, rarely ENE-plunging in Domain A, and mostly shallowly WSW-plunging in Domain C, with an increasing WSW-plunge along-strike from Domain B to C (Figure 6a to 6c).

5.7.4 Transcurrent Shear Zones In Domains A, B, and C, the values for $_6$ (mean S_{2a}–mean C_{sin}) are -7°, -15°, and -18°, respectively; these are typical but especially for Domain A relatively small angles for sinistral S-C fabrics (Figures 6a to 6c, 6f to 6h, and S1; Passchier & Trouw, 2005). The values for $_7$ (mean C_{sin}–mean C'_{sin}) are -20°, -16°, and -18°, indicating typical C-C' angular relationships in all Domains (Figures 6f to 6h, 6k to 6m, and S1). The relatively small $_6$ angle in Domain A and the typical $_7$ angles suggest a mature shear zone system formed by prolonged activity. In Domain A, the sinistral shear zones (C_{sin}) are sub-vertical and strike ~ENE; in Domain B and C, they strike NE with opposing dips, steeply SE and NW, respectively (Figure 6g to 6h). Stretching lineations (L_{sin}) are sub-horizontal in Domain B, plunge shallowly SW in Domain A, and moderately SW to WNW in Domain C (Figure 6f to 6h). In Domains A, C, and D, conjugate dextral shear zones (C_{dex}) are associated with variably-oriented stretching lineations (L_{dex}, Figure 7a, 7e, and 7i). The mean strike of C_{dex} changes from ENE to E to SE across the Domains C, A, and D, forming an arc around the indenter salient.

5.7.5 Extensional Shear Zones Extensional shear zones (C_{nor}) in Domains A and E show a large orientation scatter, but are, in general, sub-parallel to the S_{2b} foliation in Domain E (Figure 7c, 7m, and 7o). Based on the spatial distribution of S_{2b} (Figure 2d), the west-plunging FA_2 (Figures 2c and 5j), and the westward increasing plunge of L_2 (Figure 6e), we infer that the C_{nor} nucleated along the hinges and limbs of the west-plunging D_2 folds, ultimately forming the BM. In the areas of the OSZ and the JF (Figure 2b), outcrop-scale shear zones show sinistral-oblique, top-west normal kinematics, i.e., transtension, connecting the BM to the sinistral shear zones of the western TW. The extensional shear zones dip moderately NW in Domain A and gently NE in Domain C, where they are associated with shallowly NW-plunging stretching lineations (Figure 7c and 7g), parallel the Sprechenstein-Mauls Fault (Bistacchi et al., 2010).

5.7.6 Shear Bands Sinistral shear bands (C'_{sin}) in all five Domains (A to E) have a similar appearance, strike in average N34°E, and dip steeply to sub-vertically, indicating a homogeneous deformation field in and around the western TW (Figure 6k to 6o). Assuming that shear bands form at angles of 15 35° to the shear-zone boundary (Passchier and Trouw, 2005), the MMF (N55°E) with an angle of 21° to the average C'_{sin} strike may constitute the structure that is closest to the shear zone boundary during the C'_{sin} formation. The dextral shear bands (C'_{dex}) in Domains A, C, and D strike east; in Domain E, they strike ESE (Figure 7b, 7f, 7j, and 7l). Moderately west-dipping extensional shear bands (C'_{nor}) are common in Domains E and C, where they parallel the BM (Axen et al., 1995); they are rare in Domain A (Figure 7d, 7h, and 7n).

5.7.7 Structural elements in Domain D: Incipient Extruding Wedge Structural elements like the S_2 foliation (S_{2a} and S_{2b}) and the D_3 shear zones are less developed in Domain D than in Domains A to C. The folded S_1 predominantly dip gently to steeply south, i.e., opposite to those in Domains A to C (Figure 5a to 5d). The sub-horizontal FA_2 trend east (Figure 5d and 5i) and the sub-vertical AP_2 strike east (Figure 5n). Towards the west, the D_2 folds tighten and axial-plane foliations become frequent. The rarely observed, sub-vertical S_{2a} strikes east and the related L_2 lineation plunges gently east (Figure 6d), i.e., opposite to Domain C (Figure 6c). The sub-vertical sinistral shear zones (C_{sin}) strike ENE, show gently west-plunging L_{sin} (Figure 6i); the sub-vertical dextral shear zones (C_{dex}) strike east (Figure 7j). Both the C_{sin} and C_{dex} are more eastward oriented than those in Domains A to C.

5.7.8 Structural elements in Domain E: Western Margin of the Tauern Window The major difference between Domain E and the other Domains is that none of its structural elements is sub-vertical. The folded S_1 dip mainly NNE, indicating south-verging folds (Brandner et al., 2008; Rosenberg & Garcia, 2011); the FA_2 plunge gently west, and the AP_2 dip moderately north (Figure 5e, 5j, and 5o), similar to the D_2 folds in Domain D (Figure 5i and 5n). The S_{2a} axial-plane foliations strike ENE and mainly dip moderately NNW; the associated stretching lineations plunge gently west (Figure 6e). In Domain E and along its transition to Domain A, the shallowly WNW-dipping S_{2b} dominate the structural grain (Figures 5e and 7m o), following the west-plunging hinge of the Tuxer Antiform. We observed only few NE-striking sinistral and ESE-striking dextral shear zones, but numerous, top-west normal shear zones, paralleling the BM, with down-dip stretching lineations (Figures 6j, 7k, and 7m) (e.g., Axen et al., 1995). In our field study, we could not find convincing evidence for the existence of the TNBF (Bergmeister, 2010; Fügenschuh et al., 2012; Töchterle et al., 2011).

A key outcrop in St. Jodok (Figure 2c) exhibits NNW-dipping normal shear zones (C_{nor}) associated with D_3 folds with gently NNW-dipping axial planes (AP_3) (Figure 8a to 8c). The D_3 folds refold the tight, south-verging D_2 folds and are accompanied by subvertical, NE-striking tension gashes (Figure 8d). These relationships indicate that the normal shear zones along the western margin of the TW post-date the D_2 folds. Additionally, the C_{nor} and AP_3 follow the arcuate strike of the folded S_1 along the northern limb of the Tuxer Antiform, delimiting the BM to the north, and connecting them to the ENE-striking sinistral-transtensive OSZ. To the south, the BM are delimited by the sinistral-transtensive JF.

5.8 Estimates of the Amounts of Shortening, Stretching, and Sinistral Strike-Slip

A critical parameter for estimating the amounts of shortening, stretching, and sinistral strike-slip is the movement direction of the Dolomites Indenter; the latter has been assumed to be NNW to N (e.g., Laubscher, 1988; Scharf et al., 2013; Schmid et al., 2013). Based on the analogue-material modeling results of Rosenberg et al., (2007) and the interpretation of the PaF, NGF, and SGF as strike-slip faults formed in a wrench-dominated transpressional regime, we argue for a convergence direction of N20°E; we include a ±10° uncertainty in our calculations (Figure S3). In section 6.3 (Transpressional Hypothesis), we detail the geometry of the western TW as transpressive zone and anticipate the structural orientation of its center, Domain A, as being representative for this zone. The angle between the mean strike (N60°E) of the sinistral shear zones (C_{sin}) in domain A and the inferred N20°E convergence direction is 40°. This indicates pure-shear-dominated transpression with a kinematic vorticity number W_k of 0.22, estimated using the graph proposed by Tikoff & Peterson (1998, Figure S3). Hence, 22% of the N30°E-displacement of ~70 km along the GF, which caused the shortening in the TW in front of the Dolomites Indenter (amount of contraction) (Laubscher, 1988), can be attributed to the hinge parallel stretch and 78% to folding (true amount of contraction). According to Tikoff & Peterson (1998) and using the ±10° uncertainty in the convergence direction, we calculated 55 +6/-9 km of shortening accommodated by folds and 15 +9/-6 km hinge parallel stretch (Figure S3). Our result for shortening is larger than the estimate of ~32 km (Schmid et al., 2013) but similar to the estimates of ~49 km (Rosenberg and Berger, 2009) and ~60 km (Rosenberg et al., 2015) based on balanced cross sections. According to Tikoff & Peterson (1998), the amount of hinge parallel stretch equals the wrench component in transpressive systems. Therefore, sinistral strike-slip together with the hinge parallel stretch in the western TW is 15 +9/-6 km, together contributing 13 +8/-5 km to E-W extension.

6 Discussion

In the following, we discuss three hypotheses for the localized exhumation in the western TW. We also discuss the rotation of the Proto-SEMP during transpression, and wrench zone formation across the Eastern Alps.

6.1 Transtension Hypothesis

The TW was interpreted as a pull-apart structure in a transtensional setting (e.g., Genser & Neubauer, 1989; Neubauer et al., 1999). Strain modeling shows that upright open folds can form during transtension (Fossen et al., 2013). Such experiments indicate that the axial planes of transtensional folds strike perpendicular or at a high angle to the extension direction (Rey et al., 2011), and rotate toward the divergence vector ( ), that is the vector sum of the simple and pure shear components in transtensive (and transpressive) strain fields (Fossen et al., 2013). In sinistral transtension, the orientation of the divergence vector, approximated by the transtensional fold axes, has a clockwise deviation from the shear zone boundary (Fossen et al., 2013, their Figure 2a).

We used the mean strike (N60°E) of C_{sin} in Domain A as approximating the shear zone boundary during the D_2 and D_3 deformation. The mean trend (N57°E) of the FA_2 fold axes is sub-parallel to the shear zone boundary in Domain C (Figure 5h), and deviates 14° and 8° clockwise in Domains A and B, respectively (Figures 5f and 5g). These fold axes–shear zone boundary relationships exclude the formation of D_2 folds as transtensional folds (Fossen et al., 2013). In addition, the geometry of transtensional folds is different from those observed in the western TW, where D_2 fold hinges are sub-parallel, not sub-perpendicular to the extension direction. The axial planes of D_2 folds in the western TW strike at high angles to the BM and are therefore kinematically unsuitable to accommodate large amounts of east-west extension. Only small-scale D_3 folds in Domain E have an appropriate orientation to accommodate east-west extension and could be interpreted as collapse folds (Froitzheim, 1992; Fossen et al., 2013).

6.2 Extensional Unroofing Hypothesis

Exhumation of the western TW by extensional unroofing requires that extension along the BM and SF are transferred to transcurrent sinistral and dextral strike-slip faults at the northern and southern tails of the Brenner Fault, respectively (Fügenschuh et al., 1997; Scharf et al., 2013a; Schmid et al., 2013). Our fieldwork shows that neither a sinistral strike-slip fault at the northern boundary of the western TW nor a km-scale, dextral strike-slip fault at the southern tail of the BM exists. The dextral PGF nucleates at the salient of the Dolomites Indenter that is located ~10 km ESE of the Brenner Fault. We traced the westernmost occurrence of the dextral PGF to the Valler Jöchl that is ~13 km away from the Brenner Fault. In spite of the widespread occurrence of sinistral shear zones throughout the western TW and the Meran-Mauls Basement (Figures 2b and 6f to 6i), Domain E lacks such structures (Figures 2b and 6j). The TNBF is a small-scale structure (section 2.3.5). The northwestern margin of the TW is characterized by south-verging, asymmetric F_2 folds (Figures 2c, 5e, 5j, and 5o) and the folded S_1 of the northern limbs are reactivated/overprinted by S_{2a} and S_{2b} (Figures 6e and 7o). The brittle SMF that possibly connects to the BM at the southwestern margin of the TW (Bistacchi et al., 2010), has no ductile precursor. Hence, it never was part of the pre-indentation Periadriatic Fault System. We predominantly found sinistral and normal-sense shear indicators in the field. Dextral shear indicators along the Meran-Mauls Fault document the pre-existence of dextral strike-slip along the Periadriatic Fault System.

6.3 Transpression Hypothesis

We interpret the large sinistral shear zone network within the western TW as a first-order structure linking the GB to the SEMP, transferring indentation into lateral extrusion. The mean orientation of the structural elements within Domains A to C show four along-strike trends from SW to NE in the western TW (Figures 2b to 2d). First, the S_{2a} foliations and C_{sin} strike NE at the lateral terminations of the western TW (Domains B and C) and ENE in its center (Domain A, Figures 6a to 6c, 6f to 6h, and 9a). Second, these foliations and shear zones show a steepening of the average dip from the lateral terminations (Domains B and C) to the center (Domain A), and third, an along-strike flip in dip direction (Figures 6a to 6c, 6f to 6h, and 9a). Fourth, the fold axes are doubly plunging towards the lateral terminations of the western TW (Domains B and C) and sub-horizontal in its center (Domain A, Figures 5a to 5c, and 5f to 5h). This sigmoidal foliation pattern resembles that of a transpression zone in a sinistral strike-slip system, e.g., a restraining bend or a strike-slip duplex, in which Domain A is the transpression zone and Domains B and C approximate the bordering wrench zones (Dewey et al., 1998; Sanderson & Marchini, 1984; Woodcock & Fischer, 1986). The vortex of the foliation is located in the central Domain A (Figure 9b), as described for transpressive systems (Robin & Cruden, 1994).

Generally, the stretching lineations are shallowly plunging but scatter between sub-horizontal and steeply westward plunging along the axis of the western TW. The variable bearing and plunge agree with numerical model results of stretching lineations formed in transpression (Robin & Cruden, 1994). Further, the fold amplitudes decrease and the fold wavelengths narrows from the central Domain A towards the outer Domains B and C, indicating non-cylindrical (conical) folds; such style is predicted by numerical models of transpressional folds (Frehner, 2016).

The dihedral angles $_1$ to $_4$ in Domains A to C, which mainly describe the geometric evolution of the D_2 folds, indicate a deviation of the mean strike/trend of the different structures formed in kinematic succession that is consistently clockwise in Domain C and counterclockwise in Domains A and B (Figures S1a to c, S1g). This indicates counterclockwise material-plane rotations in Domain C and clockwise rotations in Domains A and B and can be explained by the orientations of the two margins of the Dolomites Indenter, parallel to the MMF and PGF, causing different deformation fields east and west of the indenter salient, e.g., bending the preexisting S_1 foliations. The dihedral angles $_5$ to $_7$, which mainly describe the geometric evolution of the D_2 shear zones, indicate exclusively counterclockwise deviations during sinistral shearing in all three Domains (A to C; Figures S1d to f, and S1g). The mean strike of the C'_{sin}, sub-parallel to the PaF, NGF and SGF, is constant in all domains, indicating a similar, late-stage deformation field related to the Dolomites Indenter (Figures 6k to 6o). As the sinistral shear zones (C_{sin}) in Domains A to C reactivate the AP_2 axial plane foliation, we argue that they are kinematically linked to the D_2 folds and can be interpreted as part of the transpressive zone (Woodcock & Fischer, 1986; Dewey et al., 1998). This transpressive zone initiated during non-cylindrical folding during indentation and progressed by the reactivation of the $S2_2$ as slip planes during sinistral transpression. The switch in the rotational sense of the structures from opposing directions during non-cylindric folding in Domain C compared to Domains A and B into a uniform rotation sense during shearing in all three Domains supports the two-stage evolution within a constant deformation field.

6.4 Corner Effect, Partitioning, and Decoupling

The sinistral transpressive zone of the western TW established a structural connection between the GB and the SEMP with a kinematic continuity between NNE-ward indentation and eastward extrusion. Indentation induced a transpressive zone with upright folding and hinge-parallel stretching that transitioned into deformation governed by strike-slip shear zones. Outside the transpressive zone, conjugate sinistral and dextral strike-slip faults formed in Domain D along the NNE-facing indenter margin, and extensional shear zones formed in Domain E. Partitioning of NNE-SSW shortening caused a divergence of material flow away from the indenter salient within Domains D and E (cf. Ježek et al., 2002; Reiter et al., 2011).

Kinematically, the BM, JF, and OSZ (Figure 2b) decouple the Ötztal Basement from the western TW by transtensional to extensional deformation west of the transpressive zone. East of the indenter salient conjugate shear zones, i.e., the sinistral AhSZ, DAV, SpSZ and the dextral PGF, Iseltal, and Mölltal faults (Figure 1a) and other small-scale, conjugate faults in Domain D decouple the eastward extruding wedge from the transpressive zone. Hence, the transpressive zone is not part of the eastward extruding wedge, instead it comprises a restraining-bend structural junction between the GB and the SEMP (Figure 9b).

Analog-material and numerical experiments showed that within sinistral transpressive zones, transpressive fold axes initiate parallel to the maximum instantaneous stretching axis and with increasing strain, rotate clockwise and stay parallel to the long axis of the strain ellipse (Frehner, 2016; Ratschbacher et al., 1991a, 1991b; Rosenberg et al., 2004, 2007). The mean orientation of fold axes in the western TW, especially in Domain A, form an angle of ~44° to the GB, suggesting—at first glance—a rather juvenile transpressive structure, where transpressional folds only initiated and started to rotate clockwise towards the indenter margin (Fossen et al., 2013; Frehner, 2016; James & Watkinson, 1994; Tikoff & Peterson, 1998; Treagus & Treagus, 1981). However, the western TW combines transpression due to the connection of two fault zones (GB and SEMP) and the indentation imposed by the Dolomites Indenter. Numerical indentation models (Ježek et al., 2002) show that the deformation pattern in front of an indenter changes little through time, supporting the interpretation of the western TW as a rather mature sinistral transpressive zone that has clear borders in Domains D and E and connects the GB to the SEMP (Ježek et al., 2002).

6.4.1 Decoupling to the West Rocks north of the GB (Figure 1a; Ötztal Basement) were shortened little because of two geometric aspects. First, the angle of 10 to 25° between the N20°E convergence direction and the N30°E strike of the PaF, SGF, and NGF caused a rather oblique deformation field west of the indenter margin compared to the nearly orthogonal shortening in the northern margin of the indenter (the PGF; Figure 9b). Second, the Dolomites Indenter experienced a net eastward movement, which promoted extension in front of the indenter salient. The FA_2 and AP_2 in Domain C strike NE, subparallel to the northwestern margin of the Dolomites Indenter, and rotated counterclockwise during ongoing shortening, indicated by consistently positive dihedral angles $_1$ to $_4$ (Figure S1). The FA_2 and AP_2 in Domains A and B strike ENE and rotated clockwise during ongoing shortening indicated by exclusively negative dihedral angles $_1$ to $_4$ (Figure S1). We argue that this opposing rotation of the material planes/lines NW and NE of the indenter salient caused additional, about convergence-perpendicular extension, necking the D_2 folds (Figure 9b, stereoplots of the D_2 folds). The S_{2b} foliation is restricted to the west-plunging dome axis and the BM (Domain E). Together with the westward increasing steepness of the L_2 stretching lineation within the transpressive zone, it likely is a structural expression of this local extension. The S_{2b} foliation pre-dates the top-west extensional shear zones/bands (C_{nor}, C'_{nor}), that detach and decouple the Ötztal Basement from the transpressive zone. The OSZ (Ebner et al., 2004; Lammerer & Weger, 1998), structures observed at St. Jodok (Figure 8), and partly the JF (Müller et al., 2001; Viola et al., 2001), are transtensive, transferring sinistral displacement of the western TW into east-west extension along the BM (Figure 2b). Extensional shear zones within the TW in the area of Steinach (Figures 2b and 2c) dip NNW (Figure 8a), tracing the BM in a convex arc northeast-ward (Fügenschuh et al., 1997; Töchterle et al., 2011). Therefore, the ENE-striking normal shear zones in the area of St. Jodok separate the thick BM in the south from the brittle SF in the north (Behrmann, 1988; Fügenschuh et al., 1997; Reiser, 2010; Reiter et al., 2018; Schmidegg, 1953). Finally, the NNE-SSW shortening caused a component of eastward motion of the indenter, promoting maximum east-west extension in front of the indenter tip (Rosenberg et al., 2004, 2007). Hence, Domain E marks a decoupling zone between the shortened western TW and the Ötztal Basement (Figure 9b). The BM are coupled with and the SF together with syn- and antithetic faults in its hanging wall are decoupled from the transpressive zone of the western TW (Figure 9b). Thus, how to explain the extension along the SF? We speculate that it is part of a late-stage releasing band connecting the sinistral shear along the IF in the north with that along JF and PaF in the south; these would involve up to a few kms of late brittle normal faulting along the BF.

6.4.2 Decoupling to the East The AhSZ bounds the central TW in the west that lacks high-amplitude folds, subvertical foliations, and transcurrent shear zones (Figures 2a to 2e). Accordingly, the exhumation level is less deep than in the western TW and large areas expose rocks of the structurally high units. North of the PGF (Figure 1a), the convergence in Domain D was mainly accommodated by upright D_2 folds; their axial planes (AP_2) and the rarely developed S_{2a} have an angle of ~20° to the PGF and the latter fade out eastward (Figure 5n). The folds are overprinted by conjugate sinistral and dextral shear/fault zones implying NNE-SSW shortening and eastward material transfer away from the indenter salient (Figure 9b). Domain D, bound by the AhSZ in the north and the PGF in the south, forms the western tip of an eastward extruding wedge (Ratschbacher et al., 1991b).

The ENE-striking transpressive zone of the western TW (Domain A) turns into a NE-strike in Domain B. There, the number of D_2 folds is reduced to two major antiforms, indicating less localized shortening. Several NE-striking sinistral shear zones delimit the transpressive zone to the east from the central TW, where it enters the SEMP with a sudden change in strike (Figures 2b, 2d, 2e; Cole et al., 2007; Rosenberg & Schneider, 2008). We argue that Domain B marks the area where the distributed transpressive deformation expressed by non-cylindric folding and sinistral shearing of the western TW was transferred into more localized sinistral shear zones south of Mittersill (e.g., RSZ, Figure 2b; Cole et al., 2007) and ultimately to the brittle-ductile SEMP (Frost et al., 2011). The fault/shear zones south and east of the western TW that connect to the SEMP and the PGF decouple the extruding central and eastern TW from the stationary western TW (Linzer et al., 2002; Peresson & Decker, 1997). Based on the following observations, we interpret that shortening inside the western TW is at maximum and gradual decreases eastward, and strike-slip motion and extension is minimum in the western TW and gradually increases eastward. First, the location of the western TW—at the tip of the indenter—accommodated maximum shortening and minimum lateral translation. Second, east of the western TW, shortening is localized along the SEMP and PGF, given the large displacements of both faults east of the western TW. Third, the SEMP and numerous conjugate strike-slip faults south and east of the TW nucleate east of the western TW. Forth, the SEMP shows a succession from transpression in the west to transtension in the east along strike.

6.5 Proto-SEMP Hypothesis

In accordance with the results of the analogue-material models (Ratschbacher et al., 1991a, 1991b; Rosenberg et al., 2007), we propose that the N70°E-striking SEMP had a more northerly initial strike and nucleated northeast of the indenter tip, i.e., it never was connected to the GB in the first place (Figures 9b and S4). We present two approaches to restore its orientation to the time of early indentation (Proto-SEMP). The first approach (Proto-$SEMP_1$) is a counterclockwise back-rotation of the present-day western SEMP around a vertical rotation pole close to Liezen (Figure 1a), using the 55-km NNE-SSW shortening and 13-km eastward extension suggested in this study for the western TW. In this restauration, the Proto-$SEMP_1$ had an initial N50°E strike, subparallel to the present-day strike of the Meran-Mauls Basement, and rotated 20° clockwise together with the sub-parallel IF and MMzF (Figures 1a and S4). Palinspastic restorations of Fodor (1995) and Linzer et al. (1995) also imply a N50°E strike of the Proto-SEMP. The Northern Calcareous Alps in between rotated counterclockwise along antithetic Riedel faults, deduced from paleomagnetic analyses of intramontane basins interpreted as domino-block rotation (Haubold et al., 1999; Márton et al., 2000).

The second approach uses the results of paleostress analysis along the western SEMP; these yielded six deformational events, two (D_3 and D_5) involved mostly strike-slip deformation, four mainly thrusting (Wang & Neubauer, 1999). Against the authors' interpretation, we kept the orientation of the principal stress axes constant and rotated the present-day SEMP 55° counterclockwise towards a Proto-$SEMP_2$ orientation of N15°E (Figure 9b), using the rotations derived by Wang & Neubauer (1999); we consider this rotation value an extreme. Both approaches support our hypothesis of a clockwise rotating SEMP during indentation under a stable convergence direction (Figures 9c and S4).

6.6 Wrench Zone Hypothesis

The TW consists of upright folds, delimited by conjugate transpressive shear zones (Ratschbacher et al., 1991a, b; Rosenberg et al., 2004; 2007), forming an arcuate culmination in front of the Dolomites Indenter. This arcuate dome of the

TW with a triangular crustal block south of it (Figure 1a) is consistent with the majority of indentation models (Schueller & Davy, 2008, for a review), which show localized shortening and conjugate shear in front of a triangle pointing away from the indenter margin. However, the western TW accumulated more deformation as the central and eastern TW, indicating a different evolution in the late stage. We defined the Domains A to C as a mature sinistral transpressive zone, connecting the initially separated GB and the SEMP via a restraining bend (Figure 9b). The western TW forms the western margin of the stable triangle in front of the Dolomites Indenter. In an early stage of indentation, the western TW developed as a right step-over between the independently existing GB and the Proto-SEMP with localized high-strain shortening accommodated by upright folds (Figure S4); it evolved over time into a zone dominated by sinistral wrenching. We argue that this transpressive zone together with the GB and the SEMP constitutes a sinistral wrench zone translating Dolomites indentation into lateral extrusion. By that, it decouples the Ötztal Basement in the west, experiencing normal shear/faulting along the Brenner Fault and sinistral transtension along the OSZ and the JF, and the central and eastern TW in the east, experiencing eastward extrusion along conjugate shear zones, e.g., the PGF, SEMP and minor strike-slip faults in between (Ratschbacher et al., 1991a, 1991b; Rosenberg et al., 2007).

7 Conclusions

The western Tauern Window shows a structural evolution distinct from the central and eastern Tauern Window. Tight, upright folds of high-amplitude, subvertical axial plane foliations, and sinistral shear zones indicate absorption of orogen-perpendicular shortening. The western Tauern Window constitutes a right step-over connecting the sinistral transpressive Giudicarie Belt, subparallel to the indentation direction of the Dolomites Indenter, with the sinistral SEMP Fault, a major fault zone related to the eastward lateral extrusion of the central and eastern Eastern Alps. The ~70 km indentation by the Dolomites Indenter has been manifested within the western Tauern Window by upright folds and sinistral shear zones, accommodating 55 +6/-9 km of shortening, and 15 +9/-6 km hinge parallel stretch and likewise 15 +9/-6 km sinistral shear zones, resulting in 13 +7/-5 km of east-west extension. Farther east, the SEMP Fault has accommodated ~56 km of eastward lateral extrusion. At the salient of the Dolomites Indenter, the western Tauern Window forms a relatively stationary structural divide, decoupling the western Eastern Alps along the top-west, normal-slip Brenner Fault from the central and eastern Eastern Alps that extrude eastward. In the central Tauern Window, north-south shortening decreases in comparison to the western Tauern Window, as seen from the preservation of higher tectonostratigraphic units, the lower amplitude of folds, and the lack of axial plane foliations. In turn, the amount of lateral extrusion increases, as indicated by the increasing abundance of conjugated strike-slip shear/fault zones within the Austroalpine nappes south and east of the Tauern Window. The structures and the inferred displacements within the western Tauern Window are consistent with exhumation dominated by erosional denudation during transpressive folding. We interpret the western Tauern Window as a transpressive, right step-over between the sinistral Giudicarie Belt and a sub-parallel Proto-SEMP, which was pinned by the West-European Platform at the southern salient of the Bohemian massif. During indentation, the western Proto-SEMP progressively rotated clockwise around a vertical axis close to Liezen, attaining its present day orientation.

8 Acknowledgments and Data

This study was funded by the DFG grant Ro2177/4. We acknowledge family Schwärzer, especially M. Schwärzer, G. Fankhauser and R. Emberger for field support and accommodation. For helpful discussion, we thank A. Bertrand, S. Favaro, S. Garcia, D. Rutte, and R. Schuster. For critical and constructive reviews of the manuscript in an early stage, we thank M. R. Handy, H. Pomella, and S. M. Schmid. Reviews by C. Teyssier and three anonymous reviewers caused a substantial refocusing of the manuscript.

This data set contains 6965 structural data from 1774 outcrops in the western Tauern Window, collected during July to August, 2007, June to September, 2008, June to September, 2009, July to October, 2010, using a Breithaupt "GEKOM" Stratum Compass, provided by the Freie Universität Berlin, Germany. The raw data, plotted in the lower hemisphere and equal area plots of Figures 5a to 5o, 6a to 6o, and 7a to 7o are given in the Supporting Information Dataset S1. The Supplementary Information Figures 1a to g, 2, and 3 contains the different dihedral angles between the mean values of the respective structural elements of the Domains A to C. The georeferenced raw data are available in the open access research data base OpARA of the Technische Universität Dresden and Technische Universität Bergakademie Freiberg.

9 References

Angel F., & R. Staber (1950), Geologische Karte des Ankogel-Hochalm-Gebiets, 1:50.000. *In: Angel, F., and R. Staber, Wien (Freytag & Berndt).*

Axen, G. J., J. M. Bartley, & J. Selverstone (1995), Structural expression of a rolling hinge in the footwall of the Brenner Line normal fault, eastern Alps. *Tectonics*, *14*, 1380–1392, doi:10.1029/95TC02406.

Barnes, J. D., J. Selverstone, & Z. D. Sharp (2004), Interaction between serpentinite devolatization, metasomatism and strike-slip strain localization during deep-crustal shearing in the Eastern Alps. *Journal of Metamorphic Geology*, *22*, 283–300.

Baroň, I., L. Plan, L. Sokol, B. Grasemann, R. Melichar, I. Mitrovic, & J. Stemberk, J. (2019), Present-day kinematic behaviour of active faults in the Eastern Alps. *Tectonophysics*, *752*, 1–23. https://doi.org/10.1016/j.tecto.2018.12.024

Becker, B. (1993), The structural evolution of the Radstadt Thrust System, Eastern Alps, Austria – Kinematics, Thrust Geometries, Strain Analysis -. *Tübinger Geowissenschaftliche Arbeiten, A14, 92pp.*

Behrmann, J. H. (1988), Crustal scale extension in a convergent orogen: The Sterzing-Steinach mylonite zone in the eastern Alps. *Geodinamica Acta*, *2*, 63–73.

Behrmann, J. H., & W. Frisch (1990), Sinistral ductile shearing associated with metamorphic decompression in the Tauern Window, Eastern Alps. *Jahrbuch der Geologischen Bundesanstalt Austria*, *133*, 135–146.

Bergmeister, K. (2010). Brenner Basistunnel: Aktueller Stand. *Tunnel*, *1.*

Bertrand, A., C. L. Rosenberg, & S. Garcia (2015), Fault slip analysis and late exhumation of the Tauern Window, Eastern Alps. *Tectonophysics*, *649*, 1–17.

Bertrand, A., C. L. Rosenberg, A. Rabaute, F. Herman, & B. Fügenschuh (2017), Exhumation mechanisms of the Tauern Window (Eastern Alps) inferred from apatite and zircon fission track thermochronology. *Tectonics*, *36*, 207–228.

Berryman, E. J., M. Kutzschbach, R. B. Trumbull, A. Meixner, V. van Hinsberg, S. Kasemann, & G. Franz (2017). Tourmaline as a petrogenetic indicator in the Pfitsch Formation, western Tauern window, eastern Alps. *Lithos*, *284*, 138-155.

Bigi, G., D. Cosentino, M. Parotto, & R. Sartori (1992), Structural model of Italy, 1:500000. *CNR, Progetto Finalizzato Geodinamica.*

Bistacchi, A., M. Massiron, & L. Menegon (2010), Three-dimensional characterization of a crustal-scale fault zone: The Pusteria and Sprechenstein fault system (Eastern Alps). *Journal of Structural Geology*, *32*(12), 2022–2041.

Bokelmann, G., E. Qorbani, & I. Bianchi (2013), Seismic anisotropy and large-scale deformation of the Eastern Alps. *Earth and Planetary Science Letters*, 383, 1-6.

Borradaile, G. J. (1978), Transected folds: a study illustrated with examples from Canada and Scotland. *Geological Society of America Bulletin*, *89*(4), 481-493.

Bousquet, R., S.M. Schmid, G. Zeilinger, R. Oberhänsli, C.L. Rosenberg, G. Molli, C. Robert, M. Wiederkehr, & P. Rossi (2012a). *Tectonic framework of the Alps*, 1:100,000: CCGM/CGMW. http://geodynalp.org.

Bousquet, R., R. Oberhänsli, S.M. Schmid, A. Berger, M. Wiederkehr, C. Robert, C.L. Rosenberg, F. Koller, G. Molli, & G. Zeilinger (2012b). *Metamorphic framework of the Alps*, 1:100,000: CCGM/CGMW. http://geodynalp.org.

Brandner, R., A. Töchterle, & F. Reiter (2008), Überblick zu den Ergebnissen der geologischen Vorerkundung für den Brenner-Basistunnel. *Geo.Alp*, *5*, 165–174.

Brandner, R. (2013). Alpenprofil. Institute for Geology. Innsbruck: University of Innsbruck. https://doi.org/10.13140/RG.2.2.20466.81603

Burg, J. P., & Y. Podladchikov (1999), Lithospheric scale folding: numerical modelling and application to the Himalayan syntaxes. *International Journal of Earth Sciences*, *88*, 190–200.

Caporali, A., & S. Martin (2000), First results from GPS measurements on present day alpine kinematics. *Journal of Geodynamics*, *30*, 275–283.

Chopin, F., K. Schulmann, E. Skrzypek, J. Lehmann, J. R. Dujardin, J. E. Martelat, & P. Pitra (2012). Crustal influx, indentation, ductile thinning and gravity redistribution in a continental wedge: building a Moldanubian mantled gneiss dome with underthrust Saxothuringian material (European Variscan belt). *Tectonics*, *31*, doi:10.1029/2011TC002951

Cole, J., B. Hacker, L. Ratschbacher, J. Dolan, G. Seward, E. Frost, & W. Frank (2007), Localized ductile shear below the seismogenic zone: Structural analysis of an exhumed strike-slip fault, Austrian Alps. *Journal of Geophysical Research*, *112*, doi:10.1029/2007JB004975.

Cornelius, H. P. (1940), Zur Auffassung der Ostalpen im Sinne der Deckenlehre. *Zeitschrift der Deutschen Gesellschaft für Geowissenschaft*, *92*, 271–312.

Critelli, S. & E. Garzanti (1994), Provenance of the lower Tertiary Murree redbeds (Hazara-Kashmir Syntaxis, Pakistan) and initial rising of the Himalayas. *Sedimentary Geology*, *89*, 265–284.

De Vecchi, G., & P. Baggio (1982), The Pennine zone of the Vizze region in the western Tauern Window (Italian Eastern Alps). *Bollettino della Societa Geologica italiana*, *101*, 89–116.

Dewey, J.F., R.E. Holdsworth, & R.A. Strachan (1998), Transpression and transtension zones. *Geological Society (London) Special Publications*, *135*, 1–14, doi: 10.1144/GSL.SP.1998.135.01.01.

Ebner, M., K. Decker, & B. Grasemann (2004), Normal versus strike-slip faulting–deformation mechanisms during exhumation in the footwall of the Brenner normal fault (Tyrol, Austria), ISSN 1608–8166, PanGeo Austria 2004, abstract volume.

Elliott, D. (1976), A Discussion on natural strain and geological structure-The energy balance and deformation mechanisms of thrust sheets. Philosophical Transactions of the Royal Society of London. Series A, *Mathematical and Physical Sciences, 283*(1312), 289-312.

Exner, C. (1956), Geologische Karte der Umgebung von Gastein, 1:50.000, Wien: Geologische Bundesanstalt–Austria.

Exner, C. (1962a), Sonnblicklamelle und Mölltallinie. *Jahrbuch der Geologischen Bundesanstalt Austria*, *105*, 272–286.

Exner, C. (1962b), Geologische Karte der Sonnblickgruppe, 1:50.000, Geologische Bundesanstalt, Wien.

Exner, C. (1979), Geologische Karte des Salzachtales zwischen Taxenbach und Lend, 1:25.000. In: Exner, C., Geologie des Salzachtales zwischen Taxenbach und Lend. *Jahrbuch der Geologischen Bundesanstalt Austria*, *122*, p. 73.

Exner, C. (1980), Geologie der Hohen Tauern bei Gmünd in Kärnten. *Jahrbuch der Geologischen Bundesanstalt Austria*, *123*, 343–410.

Exner, C. (1983), Geologische Karte der Hafnergruppe, 1:25.000. *Mitteilungen der Gesellschaft der Geologie- und Bergbaustudenten Österreichs*, *29*, 1983.

Exner, C. (1989), Geologie des mittleren Lungaus. *Jahrbuch der Geologischen Bundesanstalt Austria*, *132*, 7–103.

Favaro, S., M. R. Handy, A. Scharf, & R. Schuster (2017), Changing patterns of exhumation and denudation in front of an advancing crustal indenter, Tauern Window (Eastern Alps). *Tectonics*, *36*(6), 1053–1071.

Fodor, L. (1995), From transpression to transtension: Oligocene-Miocene structural evolution of the Vienna basin and the East Alpine-Western Carpathian junction. *Tectonophysics*, *242*, 151–182.

Fossen, H., C. Teyssier, & D. L. Whitney (2013), Transtensional folding. *Journal of Structural Geology*, *56*, 89–102.

Fossen, H., & B. Tikoff (1993), The deformation matrix for simultaneous simple shearing, pure shearing and volume change, and its application to transpression-transtension tectonics. *Journal of Structural Geology*, 15, 413–422.

Frank, W. & G. Pestal (2008), Geologische Karte – Umgebung von Wagrain, Nachruf auf C. Exner, 1:25.000. *Jahrbuch der Geologischen Bundesanstalt Austria*, p. 148.

Frank, W., C. Miller, G. Pestal, H. P. Cornelius, G. Fuchs, G. Grundmann, L. Hoke, G. Malecki, F. Popp, O. Schmidegg, & H. P. Steyrer (1987), Geological map sheet 152 Matrei 1:50.000. Wien: Geologische Bundesanstalt–Austria.

Frehner, M. (2016), 3D fold growth in transpression. *Tectonophysics*, *693*, 183–196.

Frisch, W. (1976), Ein Modell zur alpidischen Evolution und Orogenese des Tauernfensters. *Geologische Rundschau*, *65*(1), 375–393.

Frisch, W., I. Dunkl, & J. Kuhlemann (2000), Postcollisional orogen-parallel large-scale extension in the Eastern Alps. *Tectonophysics*, *327*, 239–265.

Frisch, W., J. Kuhlemann, I. Dunkl, & A. Brügel (1998), Palinspastic reconstruction and topographic evolution of the Eastern Alps during late Tertiary tectonic extrusion. *Tectonophysics*, *297*(1–4), 1–15.

Froitzheim, N. (1992), Formation of recumbent folds during synorogenic crustal extension (Austroalpine nappes, Switzerland). *Geology*, *20*, 923–926, doi:10.1130/0091-7613.

Frost, E., J. Dolan, C. Sammis, B. Hacker, J. Cole, & L. Ratschbacher (2009), Progressive strain localization in a major strike-slip fault exhumed from midseismogenic depths: Structural observations from the Salzach-Ennstal-Mariazell-Puchberg fault system, Austria. *Journal of Geophysical Research*, *114*, B04406, doi:10.1029/2008JB005763.

Frost, E., J. Dolan, L. Ratschbacher, B. Hacker, & G. Seward (2011), Direct observation of fault zone structure at the brittle-ductile transition along the Salzach-Ennstal-Mariazell-Puchberg fault system, Austrian Alps. *Journal of Geophysical Research*, *116*, B02422, doi:10.1029/2010JB007719.

Fügenschuh, B., D. Seward, & N. S. Mancktelow (1997), Exhumation in a convergent orogen: the western Tauern Window. *Terra Nova*, *9*, 213–217.

Fügenschuh B., N. S. Mancktelow, & S. M. Schmid (2012), Comment on ''Estimating displacement along the Brenner Fault and orogenparallel extension in the Eastern Alps'' by Rosenberg and Garcia. *International Journal of Earth Sciences*, *101*, 1451–1455, doi: 10.1007/s00531-011-0725-4

Genser, J. & F. Neubauer (1989), Low angle normal faults at the eastern margin of the Tauern window (Eastern Alps). *Mitteilungen der österreichischen geologischen Gesellschaft*, *81*, 233–243.

Giese, J. (2004), Geologie der südwestlichen Grenze des Tauernfensters (Mühlwalder Kamm, Italien) und die Analyse von Quarztexturen und Mikrogefügen in L-Tektoniten, Diploma-Thesis, Freie Universität Berlin, p. 134.

Glodny, J., U. Ring, A. Kühn, P. Gleissner, & G. Franz (2005), Crystallization and very rapid exhumation of the youngest Alpine eclogites (Tauern Window, Eastern Alps) from Rb/Sr mineral assemblage analysis. *Contributions to Mineralogy and Petrology*, *149*(6), 699–712.

Grad, M., E. Brückl, M. Majdanski, M. Behm, A. Guterch, & CELEBRATION 2000 and ALP 2002 Working Groups (2009), Crustal structure of the Eastern Alps and their foreland: Seismic model beneath the CEL10/Alp04 profile and tectonic implications. *Geophysical Journal International*, *177*, 279–295. https://doi.org/10.1111/j.1365-246X.2008.04074.x

Groß, P., M. R. Handy, T. John, G. Pestal, & J. Pleuger (2020), Crustal-scale sheath folding at HP conditions in an exhumed Alpine subduction zone (Tauern Window, Eastern Alps). *Tectonics*, *39*(2), e2019TC005942.

Grundmann, G. & G. Morteani (1985), The young uplift and thermal history of the central Eastern Alps (Austria/Italy), evidence from apatite fission track ages. *Jahrbuch der Geologischen Bundesanstalt Austria*, *128*, 197–216.

Haubold, H., R. Scholger, W. Frisch, H. Summesberger, & H. J. Mauritsch (1999), Reconstruction of the geodynamic evolution of the Northern Calcareous Alps by means of paleomagnetism. *Physics and Chemistry of the Earth Part A-Solid Earth and Geodesy*, *24*, 697–703.

Hetényi, G., J. Plomerová, I. Bianchi, H. K. Exnerová, G. Bokelmann, M. R. Handy, V. Babuška & AlpArray-EASI Working Group (2018), From mountain summits to roots: Crustal structure of the Eastern Alps and Bohemian Massif along longitude 13.3 E. *Tectonophysics, 744*, 239–255.

Höck, V., G. Pestal, P. Brandmeier, E. Clar, H. P. Cornelius, W. Frank, H. Matl, P. Neumayr, K. Petrakakis, T. Stadlmann, & H.P. Steyrer (1994), Geological map sheet 153 Großglockner 1:50.000. Wien: Geologische Bundesanstalt–Austria.

James, A. I. & A. J. Watkinson (1994), Initiation of folding and boudinage in wrench shear and transpression. *Journal of Structural Geology*, *16*, 883–893.

Ježek, J., K. Schulmann, & A.B. Thompson (2002), Strain partitioning in front of an obliquely convergent indenter. *EGU Stephan Mueller Special Publications*, *1*, 93–104.

Karl, F., O. Schmidegg, H.P. Cornelius, A. Bianchi, & G.V. Dal Piaz (1979), Geological map sheet 151 Krimml 1:50.000. Wien: Geologische Bundesanstalt–Austria.

Kästle, E. D., C. L. Rosenberg, L. Boschi, N. Bellahsen, T. Meier, & A. El-Sharkawy (2020), Slab break-offs in the Alpine subduction zone. *International Journal of Earth Sciences*, *109*, 587–603.

Kitzig, C.M. (2010), Structural analyses and dating of deformation of the Ahrntal fault, Diploma-Thesis, Freie Universität Berlin, p. 114.

Kufner, S.K., B. Schurr, C. Sippl, X. Yuan, L. Ratschbacher, A. Akbar, A. Ischuk, S. Murodkulov, F. Schneider, J. Mechie, & F. Tilmann (2016), Deep India meets deep Asia: Lithospheric indentation, delamination and break-off under Pamir and Hindu Kush (Central Asia). *Earth and Planetary Science Letters*, *435*, 171–184.

Kurz, W., R. Handler, & C. Bertoldi (2008), Tracing the exhumation of the Eclogite Zone (Tauern Window, Eastern Alps) by ^{40}Ar/^{39}Ar dating of white mica in eclogites. *Swiss Journal of Geosciences*, doi:10.1007/s00015-008-1281-1.

Lammerer, B. & M. Weger (1998), Footwall uplift in an orogenic wedge: the Tauern Window in the Eastern Alps of Europe. *Tectonophysics*, *285*, 213–230.

Lammerer, B., H. Gebrande, E. Lüschen, & P. Veselá (2008), A crustal-scale cross-section through the Tauern Window (eastern Alps) from geophysical and geological data. In: Siegesmund, S., B. Fügenschuh, N. Froitzheim (Eds) Tectonic Aspects of the Alpine-Dinaride-Carpathian System. *Geological Society*

(London) Special Publications, *298*(1), 219–229.

Laubscher, H. (1988), Material balance in Alpine orogeny. *Geological Society of American Bulletin*, *100*(9), 1313–1328.

Laubscher, H. P. (1990), The problem of the deep structure of the Southern Alps: 3-D material balance considerations and regional consequences, *Tectonophysics*, *176*, 103–121.

Le Breton, E., M. R. Handy, G. Molli, & K. Ustaszewski (2017). Post-20 Ma motion of the Adriatic Plate: New constraints from surrounding orogens and implications for crust-mantle decoupling. *Tectonics*, *36*, 3135–3154.

Lichtenheld, T. (2004), Diplomkartierung zwischen Nevesstausee und Weissenbachtal Südtirol, Italien, Diploma-Mapping, Freie Universität Berlin, p. 75.

Linzer, H. G., L. Ratschbacher, & W. Frisch (1995), Transpressional collision structures in the upper crust: the fold-thrust belt of the Northern Calcareous Alps. *Tectonophysics*, *242*, 41–61.

Linzer, H. G., F. Moser, F. Nemes, L. Ratschbacher, & B. Sperner (1997), Build-up and dismembering of the eastern Northern Calcareous Alps. *Tectonophys*ics, 272, 97–124.

Linzer, H. G., K. Decker, H. Peresson, R. Dell'Mour, & W. Frisch (2002), Balancing lateral orogenic float of the Eastern Alps. *Tectonophysics*, *354*, 211–237.

Lippitsch, R., E. Kissling, & J. Ansorge. (2003). Upper mantle structure beneath the Alpine orogen from high-resolution teleseismic tomography. *Journal of Geophysical Research: Solid Earth*, *108*(B8), 1–15.

Luth, S. W., E. Willingshofer, M. ter Borgh, D. Sokoutis, J. van Otterloo, & A. Versteeg (2013), Kinematic analysis and analogue modelling of the Passeier- and Jaufen faults: implications for crustal indentation in the Eastern Alps. *International Journal of Earth Sciences, 102*, 1071–1090.

Luth, S. W. & E. Willingshofer (2008), Mapping of the post-collisional cooling history of the Eastern Alps. *Swiss Journal of Geosciences*, *101*, 207–223.

Mancktelow, N. S., & G. Pennacchioni (2005), The control of precursor brittle fracture and fluid–rock interaction on the development of single and paired ductile shear zones. *Journal of Structural Geology*, *27*(4), 645–661.

Martin, S., G. Bigazzi, M. Zattin, G. Viola, & M. L. Balestrieri (1998), Neogene kinematics of the Giudicarie fault (Central-Eastern Alps, Italy): new apatite fission-track data. *Terra Nova*, *10*, 217–221.

Márton, E., J. Kuhlemann, W. Frisch, & I. Dunkl (2000), Miocene rotations in the Eastern Alps—palaeomagnetic results from intramontane basin sediments. *Tectonophysics*, *323*(3–4), 163–182.

Mitterbauer, U., M. Behm, E. Brückl, R. Lippitsch, A. Guterch, G. R. Keller, E. Koslovskay, E.-M. Rumpfhuber & F. Šumanovac (2011). Shape and origin of the East-Alpine slab constrained by the ALPASS teleseismic model. *Tectonophysics*, *510*(1–2), 195-206.

Molinaro, M., J. C. Guezou, P. Leturmy, S. A. Eshraghi, & D. F. de Lamotte (2004), The origin of changes in structural style across the Bandar Abbas syntaxis, SE Zagros (Iran), *Marine and Petroleum Geology*, *21*, 735–752.

Moser, M. (2006), Geological map sheet 177 St. Jacob in Defereggen 1:50.000. Wien: Geologische Bundesanstalt–Austria.

Most, P. (2003), Late Alpine cooling histories of tectonic blocks along the central part of the Transalp-Traverse (Inntal – Gadertal): constraints from geochronology, PhD-thesis Eberhardt-Karls-Universität Tübingen, 151.

Müller, W., G. Prosser, N.S. Mancktelow, I.M. Villa, S.P. Kelley, G. Viola, & F. Oberli (2001), Geochronological constraints on the evolution of the Periadriatic Fault System (Alps). *International Journal of Earth Sciences*, *90*, 623–653.

Nagel, T. J., D. Herwartz, S. Rexroth, C. Münker, N. Froitzheim, & W. Kurz (2013), Lu-Hf dating, petrography, and tectonic implications of the youngest Alpine eclogites (Tauern Window, Austria). *Lithos*, *170–171*, 179–190.

Neubauer F., J. Genser, W. Kurz, & X. Wang (1999), Exhumation of the Tauern Window, Eastern Alps. *Physics and Chemistry of the Earth, 24*(8), 675–680.

Nussbaum, C. 2000, Neogene tectonics and thermal maturity of sediments of the easternmost Southern Alps (Friuli Area, Italy), PhD Thesis, Institut de Géologie Université de Neuchâtel

Ortner, H., F. Reiter, & R. Brandner (2006). Kinematics of the Inntal shear zone–sub-Tauern ramp fault system and the interpretation of the TRANSALP seismic section, Eastern Alps, Austria. *Tectonophysics*, *414*(1–4), 241–258.

Passchier, C. W., & R. A. Trouw (2005), Microtectonics. Springer Science & Business Media.

Pennacchioni, G., & N. S. Mancktelow (2007), Nucleation and initial growth of a shear zone network within compositionally and structurally heterogeneous granitoids under amphibolite facies conditions. *Journal of Structural Geology*, *29*(11), 1757–1780.

Peresson, H. & K. Decker (1997), The Tertiary dynamics of the northern Eastern Alps (Austria): changing palaeostresses in a collisional plate boundary. *Tectonophysics*, *272*(2), 125–157.

Picotti, V., G. Prosser, & A. Castellarin (1995), Structures and kinematics of the Giudicarie–Val Trompia fold and thrust belt (Central Southern Alps Northern Italy). *Memorie di Scienze Geologiche*, *47*, 95–109.

Polinski, R. K., & G. H. Eisbacher (1992), Deformation partitioning during polyphase oblique convergence in the Karawanken Mountains, southeastern Alps. *Journal of Structural Geology*, *14*(10), 1203–1213.

Pomella, H., U. Klötzli, R. Scholger, M. Stipp, & B. Fügenschuh (2011), The Northern Giudicarie and the Meran-Mauls fault (Alps, Northern Italy) in the light of new paleomagnetic and geochronological data from boudinaged Eo-/Oligocene tonalities. *International Journal of Earth Sciences*, *100*(8), 1827–1850.

Pomella, H., M. Stipp, & B. Fügenschuh (2012), Thermochronological record of thrusting and strike-slip faulting along the Giudicarie fault system (Alps, Northern Italy). *Tectonophysics*, *579*, 118–130.

Qorbani, E., G. Bokelmann, I. Kovács, & G. Falus (2015), Anisotropic structure of the Pannonian basin: Reprocessing SKS splitting data for the CBP project stations. In EGU General Assembly Conference Abstracts (Vol. 16, p. 5166).

Ramsay, J. G., & M. I. Huber (1987). *The techniques of modern structural geology: Folds and fractures* (Vol. 2). Academic press.

Ratschbacher, L., O. Merle, P. Davy, & P. Cobbold (1991a), Lateral extrusion in the eastern Alps: Part 1. Boundary conditions and experiments scaled for gravity. *Tectonics*, *10*, 245–256.

Ratschbacher, L., W. Frisch, H.G. Linzer, & O. Merle (1991b), Lateral extrusion in the Eastern Alps, part 2: structural analysis. *Tectonics*, *10*(2), 257–271.

Reicherter, K., R. Fimmel, & W. Frisch (1993), Sinistral strike-slip faults in the central Tauern window (Eastern Alps, Austria). *Jahrbuch der Geologischen Bundesanstalt Austria*, *136*, 495–502.

Reinecker, J., & W. A. Lenhardt (1999), Present-day stress field and deformation in eastern Austria. *International Journal of Earth Sciences*, *88*(3), 532–550.

Reiser, M. (2010), Hydrological characterisation of Lake Obernberg, Brenner pass area, Tyrol. *Austrian Journal of Earth Sciences*, *103*, 43–57.

Reiter, K., N. Kukowski, & L. Ratschbacher (2011), The interaction of two indenters in analogue experiments and implications for curved fold-and-thrust belts. *Earth and Planetary Science Letters*, *302*(1), 132-146.

Reiter, F., C. Freudenthaler, H. Hausmann, H. Ortner, W. Lenhardt, & R. Brandner (2018), Active seismotectonic deformation in front of the Dolomites indenter, Eastern Alps. *Tectonics*, *37*, 4625–4654.

Rey, P. F., C. Teyssier, S. C. Kruckenberg, & D. L. Whitney (2011), Viscous collision in channel explains double domes in metamorphic core complexes. *Geology*, *39*, 387–390.

Robin, P. Y. F. & A. R. Cruden (1994), Strain and vorticity patterns in ideally ductile transpression zones. *Journal of Structural Geology*, *16*, 447–466.

Röller, K. & C. Trepmann (2008), Stereo32 Version 0.09. http://www.ruhr-uni-bochum.de/hardrock/downloads.htm2008.

Rockenschaub, M., & A. Nowotny (2009), Geological map sheet 148 Brenner 1: 50.000. Wien: Geologische Bundesanstalt–Austria.

Rockenschaub, M., & A. Nowotny (2011), Geological map sheet 175 Sterzing 1:50.000. Wien: Geologische Bundesanstalt–Austria.

Rosenberg, C. L. & A. Berger (2009), On the causes and modes of exhumation and lateral growth of the Alps. *Tectonics*, *28*, doi:10.1029/2008TC002442

Rosenberg, C. L. & S. Garcia (2011), Estimating displacement along the Brenner Fault and orogen-parallel extension in the Eastern Alps. *International Journal of Earth Sciences*, *100*, 1129–1145.

Rosenberg, C. L. & S. Garcia (2012), Reply to the comment of Fügenschuh et al. on the paper 'Estimating displacement along the Brenner Fault and orogen-parallel extension in the Eastern Alps' by Rosenberg and Garcia, Int J Earth Sci (Geol Rundsch) (2011) 100:1129–1145. *International Journal of Earth Sciences*, *101*, 1457–1464, doi:10.1007/s00531-011-0726-3.

Rosenberg, C. L. & S. Schneider (2008), The western termination of the SEMP Fault (eastern Alps) and its bearing on the exhumation of the Tauern Window, In: Siegesmund, S., B. Fügenschuh, N. Froitzheim (Eds) Tectonic Aspects of the Alpine-Dinaride-Carpathian System. *Geological Society (London) Special Publications*, *298*, 197–218.

Rosenberg, C. L., J. P. Brun, & D. Gapais (2004), An indentation model of the Eastern Alps and the origin of the Tauern Window. *Geology*, *32*, 997–1000.

Rosenberg, C. L., J. P. Brun, F. Cagnard, & D. Gapais (2007), Oblique indentation in the Eastern Alps: Insights from laboratory experiments. *Tectonics*, *26*, doi:10.1029/2006TC001960.

Rosenberg, C. L., A. Berger, N. Bellahsen, & R. Bousquet (2015), Relating orogen width to shortening, erosion, and exhumation during Alpine collision. *Tectonics, 34*, 1306–1328.

Rosenberg, C. L., S. Schneider, A. Scharf, A. Bertrand, K. Hammerschmidt, A. Rabaute, & J. P. Brun, (2018). Relating collisional kinematics to exhumation processes in the Eastern Alps. *Earth-Science Reviews*, *176*, 311–344.

Sanderson, D. J. & W. R. D. Marchini (1984), Transpression. *Journal of Structural Geology*, *6*, 449–458.

Scharf, A., M. R. Handy, S. Favaro, S. M. Schmid, & A. Bertrand (2013a), Modes of orogen-parallel stretching and extensional exhumation in response to microplate indentation and roll- back subduction (Tauern Window, Eastern Alps). *International Journal of Earth Sciences*, doi:10.1007/s00531-013-0894-4.

Scharf, A., M. R. Handy, Ziemann, M. A., & S. M. Schmid (2013b), Peak-temperature patterns of polyphase metamorphism resulting from accretion, subduction and collision (eastern Tauern Window, European Alps) – A study with Raman microspectroscopy on carbonaceous material (RSCM). *Journal of Metamorphic Geology*, *31*(8), 863–880, doi)10.1111/jmg.12048.

Schmid, S. M., A. Scharf, M. R. Handy, & C. L. Rosenberg (2013), The Tauern Window (Eastern Alps. Austria): a new tectonic map, with cross-sections and a tectonometamorphic synthesis. *Swiss Journal of Geosciences*, *106*, 1–32.

Schmidegg, O. (1953), Die Silltalstörung und das Tonvorkommen bei der Stefansbrücke. *Verhandlungen der geologischen Bundesanstalt*, 135–138.

Schmidt, J., B. R. Hacker, L. Ratschbacher, K. Stübner, M. Stearns, A. Kylander-Clark, A., & V. Minaev (2011), Cenozoic deep crust in the Pamir. *Earth and Planetary Science Letters*, *312*, 411–421.

Schneider, S., N. Bungies, F. Frütsch, C. M. Kitzig, C. L. Rosenberg, M. Spanka, C. von Nicolai, & M. Wanner, (2009), Extent and significance of sinistral shear along the southwestern border of the Tauern Window, Eastern Alps (Italy/Austria), In EGU General Assembly Conference Abstracts, 11, 11429.

Schneider, S., K. Hammerschmidt, & C. L. Rosenberg (2013), Dating the longevity of ductile shear zones: Insight from $^{40}Ar/^{39}Ar$ in situ analyses. *Earth and Planetary Science Letters*, *369*, 43–58.

Schneider, S., K. Hammerschmidt, C. L. Rosenberg, A. Gerdes, D. Frei, & A. Bertrand (2015), U–Pb ages of apatite in the western Tauern Window (Eastern Alps): tracing the onset of collision-related exhumation in the European plate. *Earth and Planetary Science Letters*, *418*, 53–65.

Schönborn, G. (1992), Alpine tectonics and kinematic models of the central Southern Alps. *Memorie di Scienze Geologiche*, *44*, 229–393.

Schueller, S., & P. Davy (2008), Gravity influenced brittle-ductile deformation and growth faulting in the lithosphere during collision: Results from laboratory experiments. *Journal of Geophysical Research: Solid Earth*, *113*(B12), 1978–2012.

Selverstone, J. (1985), Petrologic constraints on imbrication, metamorphism, and uplift in the SW Tauern Window, Eastern Alps. *Tectonics*, *4*(7), 687–704.

Selverstone, J. (1988), Evidence for E-W crustal extension in the Eastern Alps: implications for the unroofing history of the Tauern Window. *Tectonics*, *7*, 87–105.

Selverstone, J. (1993), Micro- to macroscale interactions between deformational and metamorphic processes, Tauern Window, Eastern Alps. *Schweizerische Mineralogische und Petrographische Mitteilungen*, *73*, 229–239.

Selverstone, J. & F. S. Spear (1985), Metamorphic P–T paths from pelitic schists and greenstones from the south-west Tauern Window, Eastern Alps. *Journal* *of Metamorphic Geology*, *3*(4), 439–465.

Selverstone, J., G. Morteani, & J. M. Staude (1991), Fluid channeling during ductile shearing: transformation of granodiorite into aluminous schist in the Tauern Window, Eastern Alps. *Journal of Metamorphic Geology*, *9*, 419–431.

Selverstone, J., G. J. Axen, & J. M. Bartley (1995), Fluid inclusion constraints on the kinematics of footwall uplift beneath the Brenner Line normal fault, eastern Alps. *Tectonics*, *14*(2), 264–278.

Spada, M., I. Bianchi, E. Kissling, N. P. Agostinetti, & S. Wiemer (2013), Combining controlled-source seismology and receiver function information to derive 3-D Moho topography for Italy. *Geophysical Journal International*, *194*(2), 1050–1068.

Spear F. S. & G. Franz (1986), P-T evolution of metasediments from the Eclogite Zone, south-central Tauern Window, Austria. *Lithos*, *19*(3), 219–234.

Spiess, R. (1995), The Passeier- Jaufen Line: A tectonic boundary between Variscan and an eo-Alpine Meran-Mauls basement. *Schweizerische Mineralogische und Petrographische Mitteilungen*, *75*, 413–425.

Spiess R., M. Marini, W. Frank, B. Marcolongo, & G. Cavazzini (2001), The kinematics of the Southern Passeier fault: radiometric and petrographic constraints. *Schweizerische Mineralogische und Petrographische Mitteilungen*, *81*, 197–212.

Steffen, K. J., & J. Selverstone (2006), Retrieval of P–T information from shear zones: thermobarometric consequences of changes in plagioclase deformation mechanisms. *Contributions to Mineralogy and Petrology*, *151*(5), 600.

Steffen, K. J., J. Selverstone, & A. Brearley (2001), Episodic weakening and strengthening during synmetamorphic deformation in a deep crustal shear zone in the Alps. *Geological Society (London) Special Publications*, *186*, 141–156.

Tikoff, B., & H. Fossen (1993), Simultaneous pure and simple shear: the unifying deformation matrix. *Tectonophysics*, *217*, 267–283.

Tikoff, B., & K. Peterson (1998), Physical experiments of transpressional folding. *Journal of Structural Geology*, *20*, 661–672.

Tikoff, B., & C. Teyssier (1994), Strain modeling of displacement-field partitioning in transpressional orogens. *Journal of Structural Geology*, *16*, 1575–1588.

Töchterle, A., R. Brandner, & F. Reiter (2011), Strain partitioning on major fault zones in the northwestern Tauern Window—insights from the investigations of the Brenner base tunnel. *Austrian Journal of Earth Sciences*, *104*, 15–35.

Treagus, J. E. & S. H. Treagus (1981), Folds and the strain ellipsoid: a general model. *Journal of Structural Geology*, *3*, 1–17.

Van Gelder, I. E., E. Willingshofer, P. A. M. Andriessen, R. Schuster, & D. Sokoutis (2020), Cooling and vertical motions of crustal wedges prior to, during, and after lateral extrusion in the Eastern Alps: New field kinematic and fission track data from the Mur-Mürz Fault System. *Tectonics*, *39*(3), e2019TC005754.

Viola, G., N. S. Mancktelow, & D. Seward (2001), Late Oligocene-Neogene evolution of Europe-Adria collision: New structural and geochronological evidence from the Giudicarie fault system (Italian Eastern Alps). *Tectonics*, *20*, 999–1020, doi:10.1029/2001TC900021.

Wang, X. & F. Neubauer (1998), Orogen-parallel strike-slip faults bordering metamorphic core complexes: the Salzach-Enns fault zone in the Eastern Alps, Austria. *Journal of Structural Geology*, *20*, 799–818.

Werling, E. (1992), Tonale-, Pejo- und Judicarienlinie. Kinematik, Mikrostrukturen und Metamorphose von Tektoniten aus räumlich interferierenden aber verschiedenaltrigen Verwerfungszonen, PhD Thesis, ETH Zürich, p. 276.

Woodcock, N.H, & M. Fischer (1986), Strike-slip duplexes. *Journal of Structural Geology*, *8*, 725–735.

Wolff, R., R. Hetzel, I. Dunkl, A. A. Anczkiewicz, & H. Pomella (2020), Fast cooling of normal-fault footwalls: Rapid fault slip or thermal relaxation? *Geology*, *48*(4), 333–337.

Wollnik, S. (2012), Änderungen der Mikrostrukturen und der Zusammensetzung entlang eines Verformungsgradienten in Gneisen aus dem Ahrntal (Tauernfenster), mit besonderem Augenmerk auf granulares Fließen, Diploma-Thesis, Freie Universistät Berlin, p. 66.

Zhao L., A. Paul, M.G. Malusà, X. Xu, T. Zheng, S. Solarino, S. Guillot, S. Schwartz, T. Dumont, S. Salimbeni, C. Aubert, S. Pondrelli, Q. Wang, and R. Zhu (2016a), Continuity of the Alpine slab unraveled by high-resolution P wave tomography. *Journal of Geophysical Research: Solid Earth 121*(12):8720–8737

10 Figure Captions

Figure 1a. Simplified tectonostratigraphic map of the Tauern Window and surrounding units modified after (Bousquet et al., 2012b). **b.** to **d.** Structural sections of the western, central, and eastern sub-dome of the Tauern Window simplified after Brander (2013) and Schmid et al. (2013).

Figure 2a. Foliation map of the Tauern Window shows the main foliation (undifferentiated). Compiled literature and new data (see paragraph 2 for references). **b.** to **e.** Close ups of the western Tauern Window based on (Bigi et al., 1994) showing **b.** Traces of the macro-scale sinistral shear zones; **c.** Outcrops of this study, definition of the five structural Domains (A to E), and traces of the structural sections (Figure 4); **d.** Interpreted traces of the S_{2a} axial-plane (solid lines) and the S_{2b} foliations (dashed lines); **e.** Interpreted traces of the F_2 upright folds and the tectonostratigraphic units.

Figure 3. Field photographs along the Vals valley from north to south. **a.** Folded S_1 upright, tight folds, Width of the photo is approximately 4 m; **b.** Rootless S_1 folds and newly formed sub-vertical S_{2a} axial-plane foliation; **c.** S_{2a} axial-plane foliation and localized sinistral shear zones (C_{sin}), having an additional north-side-up component; **d.** Top view on sub-vertical S_{2a} axial-plane foliation and localized sinistral shear bands C'_{sin}.

Figure 4. SE-trending structural cross section running from Rosskopf to Onsberg (see Figure 2a for trace). Lithological units based on the Geologische Karte 1:50.000, Blatt 175 Sterzing.

Figure 5. Stereoplots of contoured data in ten contouring intervals, number of data, maximum, minimum, mean densities ( ), cosine exponent, and mean values are given in the bottom-left columns. **a.** to **e.** S_1 foliation, great circles indicate -circles. **f.** to **j.** D_2 fold axes (FA_2). **k.** to **o.** D_2 axial planes (AP_2).

Figure 6. Stereoplots of contoured data in ten contouring intervals, number of data, maximum, minimum, mean densities ( ), cosine exponent, and mean values are given in the bottom-left columns and the lower right corner. **a.** to **e.** S_{2a} axial-plane foliations and L_2 lineations, great circles indicate S_{2a} mean values. **f.** to **j.** Sinistral shear zones (C_{sin}) and stretching lineations (L_{sin}) , great circles indicate C_{sin} mean values. **k.** to **o.** Sinistral shear bands (C'_{sin}), great circles indicate C'_{sin} mean values.

Figure 7. Stereoplots of contoured data in ten contouring intervals, number of data, maximum, minimum, mean densities ( ), cosine exponent, and mean values are given in the bottom-left columns and the lower right corners. **a., e., k., j.** Dextral shear zones (C_{dex}) and stretching lineations (L_{dex}), great circles indicate C_{dex} mean values. **b., f., l., i.** Dextral shear bands (C'_{dex}), great circles indicate C'_{dex} mean values. **c., g., m.** Extensional shear zones (C_{nor}) and stretching lineations (L_{nor}), great circles indicate C_{nor} mean values. **d., h., n.** Extensional shear bands (C'_{nor}), great circles indicate C'_{nor} mean values. o. Composite foliations (S_{2b}), great circles indicate S_{2b} mean value.

Figure 8. a. Sketch of a key outcrop near St. Jodok (outcrop length ~100 m) and stereoplots; from left to right: S_1 foliations, AP_2 axial planes, C_{nor} extensional shear zones, and AP_3 collapse folds. **b.** to **d.** South-verging, tight D_2 folds (F_2) are sheared by normal-sense shear zones along their limbs. Collapse folds (F_3) and tension gashes overprint steep F_2 folds.

Figure 9. a. Block model of the western Tauern Window. Structural map and sections are based on Brandner (2013) and Schmid et al. (2013). Map is displaced and view is parallel to the wrench zone (~NE) to illustrate the along strike variation of the sinistral shear zones (red lines). **b.** Structural summary of the wrench zone highlighted in red. Mean great circles and mean vectors based on data shown in Figures 5, 6, and 7. Sectors with upper-right-to-lower-left stripes indicate the assumed N20°E ($\pm$ 10°) convergence direction of the Dolomites Indenter with respect to the major faults forming the wrench zone (GF, MMF, and Proto-SEMP). Sectors with upper-left-to-lower-right stripes indicate the conver-

gence vector of the respective shear zone boundary (-20°), in which transpression is wrench-dominated. For the MMF and the western TW, the convergence angles are 35° and 40°, respectively, indicating pure-shear-dominated transpression (Tikoff and Peterson, 1998). For the GF, the Proto-$SEMP_1$, and the Proto-$SEMP_2$, the convergence vectors are towards N10°E, N30°E and N15°E, respectively, indicating mostly wrench-dominated transpression (Tikoff and Peterson, 1998). **c.** Structural reinterpretation of the deformation stages of Wang and Neubauer (1998), left: Wang and Neubauer's (1998) interpretation of counterclockwise rotation of principle stress axes around a fixed SEMP, right: reinterpretation in this study assumes a fixed (~N) direction of principle stresses and a ~55° clockwise rotation of the SEMP into the Proto-SEMP orientation.

Supporting Table 1: raw data of structural measurements

Domain A			Domain B			Domain C			Domain D			Domain E		
338	64	S_1	350	30	S_1	161	58	S_1	350	42	S_1	49	55	S_0
165	75	S_1	352	36	S_1	132	70	S_1	357	43	S_1	62	64	S_0
249	46	S_1	303	54	S_1	153	60	S_1	342	44	S_1	43	51	S_0
315	65	S_1	304	57	S_1	163	65	S_1	326	24	S_1	186	88	S_1
0	53	S_1	330	60	S_1	337	81	S_1	120	78	S_1	238	22	S_1
353	30	S_1	322	54	S_1	343	70	S_1	124	81	S_1	243	37	S_1
346	35	S_1	39	34	S_1	345	70	S_1	144	54	S_1	326	45	S_1
325	36	S_1	173	20	S_1	347	35	S_1	142	45	S_1	174	19	S_1
350	42	S_1	338	13	S_1	323	60	S_1	142	44	S_1	357	45	S_1
11	48	S_1	336	41	S_1	319	60	S_1	151	60	S_1	180	48	S_1
359	58	S_1	188	39	S_1	335	63	S_1	143	64	S_1	169	63	S_1
0	54	S_1	21	56	S_1	327	62	S_1	150	84	S_1	169	58	S_1
347	64	S_1	16	55	S_1	311	54	S_1	124	38	S_1	192	74	S_1
169	35	S_1	25	38	S_1	306	69	S_1	119	36	S_1	181	60	S_1
162	84	S_1	20	42	S_1	329	57	S_1	229	35	S_1	349	74	S_1
143	39	S_1	24	54	S_1	355	52	S_1	116	33	S_1	351	79	S_1
107	14	S_1	22	52	S_1	343	47	S_1	127	57	S_1	191	40	S_1
241	70	S_1	146	66	S_1	359	39	S_1	357	49	S_1	186	44	S_1
183	78	S_1	124	61	S_1	359	39	S_1	152	10	S_1	320	47	S_1
181	62	S_1	133	24	S_1	346	53	S_1	147	39	S_1	315	64	S_1
178	57	S_1	183	24	S_1	242	54	S_1	68	44	S_1	315	40	S_1
352	88	S_1	192	26	S_1	317	68	S_1	75	44	S_1	344	57	S_1
151	75	S_1	173	88	S_1	315	64	S_1	32	48	S_1	330	45	S_1
171	69	S_1	351	87	S_1	336	64	S_1	38	42	S_1	334	71	S_1
182	65	S_1	157	72	S_1	331	46	S_1	115	9	S_1	330	64	S_1
181	71	S_1	136	36	S_1	148	64	S_1	116	4	S_1	324	67	S_1
170	71	S_1	154	30	S_1	141	51	S_1	45	72	S_1	50	6	S_1
339	67	S_1	134	84	S_1	129	50	S_1	63	48	S_1	355	79	S_1
327	52	S_1	152	55	S_1	139	50	S_1	34	66	S_1	45	30	S_1
168	79	S_1	313	66	S_1	288	50	S_1	3	38	S_1	277	47	S_1
193	35	S_1	19	74	S_1	281	59	S_1	9	23	S_1	336	38	S_1
352	62	S_1	21	74	S_1	275	74	S_1	256	76	S_1	338	49	S_1
330	70	S_1	198	78	S_1	355	30	S_1	288	77	S_1	332	25	S_1
340	60	S_1	38	87	S_1	331	27	S_1	281	67	S_1	315	33	S_1
351	89	S_1	33	53	S_1	105	75	S_1	284	60	S_1	316	30	S_1
177	87	S_1	4	58	S_1	332	74	S_1	130	56	S_1	335	64	S_1
325	73	S_1	21	75	S_1	326	48	S_1	112	57	S_1	335	63	S_1
347	87	S_1	17	74	S_1	302	38	S_1	115	57	S_1	337	76	S_1
343	79	S_1	349	69	S_1	265	21	S_1	144	63	S_1	328	68	S_1
318	65	S_1	11	73	S_1	260	21	S_1	124	35	S_1	336	32	S_1
310	61	S_1	29	28	S_1	268	67	S_1	163	41	S_1	335	35	S_1
165	78	S_1	1	36	S_1	305	35	S_1	139	37	S_1	300	19	S_1
331	45	S_1	24	45	S_1	297	43	S_1	130	76	S_1	57	9	S_1
148	57	S_1	25	43	S_1	323	68	S_1	144	44	S_1	359	20	S_1
321	55	S_1	20	70	S_1	320	68	S_1	142	48	S_1	355	54	S_1

Supporting Table 1: raw data of structural measurements

Domain A			Domain B			Domain C			Domain D			Domain E		
325	37	S_1	8	48	S_1	325	70	S_1	153	44	S_1	330	56	S_1
320	56	S_1	341	74	S_1	136	52	S_1	148	48	S_1	334	60	S_1
337	80	S_1	22	40	S_1	123	63	S_1	98	36	S_1	328	52	S_1
330	40	S_1	10	51	S_1	322	58	S_1	163	25	S_1	332	48	S_1
355	61	S_1	30	40	S_1	322	55	S_1	139	64	S_1	333	49	S_1
339	34	S_1	24	51	S_1	321	46	S_1	85	32	S_1	280	33	S_1
351	74	S_1	21	45	S_1	322	53	S_1	129	85	S_1	284	33	S_1
172	65	S_1	11	55	S_1	342	34	S_1	356	42	S_1	315	46	S_1
2	75	S_1	181	33	S_1	2	32	S_1	3	45	S_1	309	41	S_1
158	72	S_1	194	45	S_1	356	34	S_1	168	54	S_1	297	35	S_1
166	76	S_1	209	45	S_1	324	72	S_1	185	64	S_1	257	33	S_1
155	57	S_1	196	42	S_1	338	60	S_1	187	51	S_1	290	35	S_1
154	50	S_1	142	52	S_1	312	47	S_1	181	59	S_1	288	35	S_1
316	62	S_1	353	62	S_1	313	41	S_1	184	65	S_1	56	48	S_1
153	73	S_1	168	68	S_1	328	49	S_1	156	65	S_1	62	57	S_1
334	65	S_1	131	72	S_1	321	54	S_1	163	60	S_1	57	49	S_1
315	72	S_1	340	32	S_1	328	44	S_1	160	45	S_1	79	49	S_1
331	64	S_1	114	15	S_1	316	38	S_1	181	40	S_1	72	53	S_1
34	36	S_1	11	13	S_1	342	53	S_1	171	85	S_1	106	62	S_1
11	44	S_1	304	30	S_1	334	57	S_1	185	76	S_1	120	67	S_1
4	50	S_1	329	22	S_1	359	28	S_1	181	71	S_1	58	60	S_1
159	81	S_1	331	54	S_1	359	25	S_1	156	86	S_1	85	61	S_1
158	71	S_1	2	65	S_1	325	65	S_1	347	88	S_1	101	68	S_1
168	67	S_1	143	68	S_1	332	49	S_1	170	79	S_1	97	68	S_1
167	68	S_1	129	67	S_1	296	39	S_1	27	65	S_1	157	75	S_1
351	86	S_1	153	55	S_1	316	33	S_1	22	65	S_1	157	62	S_1
175	79	S_1	157	56	S_1	82	20	S_1	14	76	S_1	120	24	S_1
175	81	S_1	137	79	S_1	194	28	S_1	0	56	S_1	149	75	S_1
172	90	S_1	132	80	S_1	223	28	S_1	2	74	S_1	170	52	S_1
346	79	S_1	129	76	S_1	348	35	S_1	9	74	S_1	162	86	S_1
325	69	S_1	130	77	S_1	346	38	S_1	165	78	S_1	264	59	S_1
341	80	S_1	129	69	S_1	344	48	S_1	165	85	S_1	247	75	S_1
180	40	S_1	30	19	S_1	5	30	S_1	140	82	S_1	191	88	S_1
168	83	S_1	42	30	S_1	345	35	S_1	135	79	S_1	218	43	S_1
168	60	S_1	30	22	S_1	335	32	S_1	154	84	S_1	283	45	S_1
175	41	S_1	48	23	S_1	348	35	S_1	163	83	S_1	176	85	S_1
170	71	S_1	31	40	S_1	340	44	S_1	350	83	S_1	211	36	S_1
170	65	S_1	33	36	S_1	338	61	S_1	350	81	S_1	198	73	S_1
160	35	S_1	59	37	S_1	167	64	S_1	334	65	S_1	235	49	S_1
148	35	S_1	58	34	S_1	177	40	S_1	334	73	S_1	184	79	S_1
145	55	S_1	48	29	S_1	191	28	S_1	320	54	S_1	168	76	S_1
230	34	S_1	52	35	S_1	211	27	S_1	355	45	S_1	164	41	S_1
150	38	S_1	64	48	S_1	264	33	S_1	315	49	S_1	175	55	S_1
150	56	S_1	59	29	S_1	303	68	S_1	352	39	S_1	198	41	S_1
175	67	S_1	85	23	S_1	288	87	S_1	10	49	S_1	188	35	S_1

Supporting Table 1: raw data of structural measurements

Domain A			Domain B			Domain C			Domain D			Domain E		
73	35	S_1	73	27	S_1	277	74	S_1	358	45	S_1	104	87	S_1
252	62	S_1	96	26	S_1	324	50	S_1	353	42	S_1	9	63	S_1
315	34	S_1	28	43	S_1	21	25	S_1	334	52	S_1	19	70	S_1
346	59	S_1	71	39	S_1	19	23	S_1	354	79	S_1	350	52	S_1
322	48	S_1	288	68	S_1	25	25	S_1	355	78	S_1	17	58	S_1
325	60	S_1	300	48	S_1	58	15	S_1	16	48	S_1	281	32	S_1
342	75	S_1	148	26	S_1	267	4	S_1	342	44	S_1	317	42	S_1
351	40	S_1	338	81	S_1	292	35	S_1	11	66	S_1	309	33	S_1
358	58	S_1	39	35	S_1	273	42	S_1	338	56	S_1	175	82	S_1
328	62	S_1	20	38	S_1	7	20	S_1	349	70	S_1	173	88	S_1
332	55	S_1	142	26	S_1	97	53	S_1	351	81	S_1	173	79	S_1
340	60	S_1	339	21	S_1	289	38	S_1	11	83	S_1	176	37	S_1
340	72	S_1	316	24	S_1	247	47	S_1	359	84	S_1	348	24	S_1
340	84	S_1	106	55	S_1	277	47	S_1	338	63	S_1	347	31	S_1
342	70	S_1	108	61	S_1	310	63	S_1	320	70	S_1	206	60	S_1
170	89	S_1	64	35	S_1	272	52	S_1	9	35	S_1	240	35	S_1
254	32	S_1	75	39	S_1	251	64	S_1	62	45	S_1	228	38	S_1
336	38	S_1	329	82	S_2	270	19	S_1	46	39	S_1	339	60	S_1
342	38	S_1	330	67	S_2	113	87	S_1	33	34	S_1	351	86	S_1
159	75	S_1	178	62	S_2	272	67	S_1	47	32	S_1	191	69	S_1
150	60	S_1	216	65	S_2	279	37	S_1	24	43	S_1	325	31	S_1
335	38	S_1	185	75	S_2	291	69	S_1	45	37	S_1	167	72	S_1
328	37	S_1	192	33	S_2	268	45	S_1	44	34	S_1	338	22	S_1
1	58	S_1	180	56	S_2	266	45	S_1	5	42	S_1	350	47	S_1
357	54	S_1	184	77	S_2	304	58	S_1	69	34	S_1	170	85	S_1
346	53	S_1	189	80	S_2	282	40	S_1	24	43	S_1	336	55	S_1
326	45	S_1	216	56	S_2	306	52	S_1	179	49	S_1	198	42	S_1
340	35	S_1	3	82	S_2	312	53	S_1	165	50	S_1	190	88	S_1
339	69	S_1	10	84	S_2	337	65	S_1	225	66	S_1	0	52	S_1
331	35	S_1	220	80	S_2	311	82	S_1	168	66	S_1	215	45	S_1
147	42	S_1	211	86	S_2	286	79	S_1	164	30	S_1	216	49	S_1
165	59	S_1	135	86	S_2	321	65	S_1	135	24	S_1	246	25	S_1
165	59	S_1	325	68	S_2	326	85	S_1	175	48	S_1	203	33	S_1
322	48	S_1	312	69	S_2	321	56	S_1	189	27	S_1	202	39	S_1
328	46	S_1	359	79	S_2	0	55	S_1	177	42	S_1	204	29	S_1
340	46	S_1	186	88	S_2	321	41	S_1	20	8	S_1	247	22	S_1
350	49	S_1	346	85	S_2	328	48	S_1	208	33	S_1	250	28	S_1
325	68	S_1	346	86	S_2	348	57	S_1	225	32	S_1	197	14	S_1
18	89	S_1	351	85	S_2	348	66	S_1	346	18	S_1	202	26	S_1
10	61	S_1	151	60	S_2	331	82	S_1	354	38	S_1	246	18	S_1
171	85	S_1	159	63	S_2	65	53	S_1	220	36	S_1	232	28	S_1
162	83	S_1	148	62	S_2	354	64	S_1	194	52	S_1	235	29	S_1
10	61	S_1	155	67	S_2	349	54	S_1	177	28	S_1	251	22	S_1
11	41	S_1	157	65	S_2	348	49	S_1	207	43	S_1	263	28	S_1
5	48	S_1	153	67	S_2	14	47	S_1	214	27	S_1	257	41	S_1

Domain A			Domain B			Domain C			Domain D			Domain E		
31	17	S_1	355	74	S_2	342	80	S_1	192	77	S_1	240	35	S_1
344	57	S_1	360	73	S_2	347	65	S_1	207	77	S_1	253	49	S_1
355	69	S_1	138	80	S_2	162	59	S_1	3	74	S_1	266	59	S_1
332	67	S_1	150	72	S_2	162	49	S_1	167	44	S_1	310	48	S_1
336	79	S_1	135	73	S_2	308	48	S_1	193	60	S_1	316	52	S_1
335	88	S_1	168	78	S_2	304	45	S_1	159	52	S_1	293	47	S_1
157	64	S_1	157	84	S_2	34	28	S_1	168	64	S_1	265	35	S_1
155	62	S_1	329	83	S_2	48	30	S_1	171	66	S_1	317	30	S_1
155	62	S_1	329	89	S_2	123	66	S_1	351	53	S_1	335	33	S_1
162	46	S_1	317	84	S_2	137	67	S_1	305	55	S_1	274	25	S_1
166	52	S_1	318	82	S_2	120	11	S_1	311	20	S_1	267	27	S_1
170	52	S_1	122	79	S_2	356	28	S_1	340	42	S_1	239	15	S_1
120	49	S_1	131	70	S_2	179	10	S_1	347	45	S_1	205	24	S_1
144	35	S_1	131	72	S_2	348	45	S_1	188	86	S_1	191	28	S_1
131	43	S_1	145	62	S_2	11	26	S_1	3	88	S_1	191	21	S_1
165	82	S_1	346	74	S_2	32	25	S_1	0	84	S_1	208	9	S_1
45	19	S_1	348	71	S_2	341	40	S_1	342	43	S_1	172	25	S_1
35	23	S_1	344	71	S_2	345	35	S_1	359	81	S_1	202	19	S_1
340	35	S_1	342	75	S_2	353	45	S_1	174	65	S_1	229	21	S_1
176	82	S_1	339	65	S_2	356	38	S_1	183	75	S_1	219	30	S_1
115	82	S_1	339	72	S_2	351	30	S_1	151	34	S_1	335	20	S_1
191	5	S_1	353	68	S_2	324	28	S_1	172	58	S_1	326	32	S_1
240	10	S_1	355	68	S_2	302	35	S_1	158	30	S_1	329	18	S_1
342	72	S_1	358	68	S_2	106	25	S_1	174	46	S_1	195	63	S_1
348	78	S_1	6	72	S_2	120	51	S_1	169	70	S_1	184	81	S_1
166	78	S_1	1	77	S_2	233	83	S_1	168	67	S_1	329	34	S_1
324	83	S_1	346	85	S_2	264	28	S_1	174	64	S_1	186	27	S_1
177	64	S_1	342	81	S_2	325	30	S_1	178	80	S_1	13	89	S_1
152	69	S_1	350	84	S_2	344	22	S_1	170	64	S_1	22	46	S_1
185	87	S_1	160	65	S_2	296	31	S_1	170	67	S_1	4	64	S_1
264	34	S_1	322	83	S_2	334	81	S_1	165	43	S_1	33	43	S_1
284	45	S_1	151	68	S_2	246	77	S_1	154	55	S_1	9	67	S_1
153	75	S_1	336	64	S_2	263	63	S_1	162	57	S_1	182	72	S_1
152	88	S_1	174	48	S_2	277	82	S_1	168	55	S_1	178	46	S_1
350	87	S_1	168	50	S_2	278	81	S_1	171	61	S_1	186	72	S_1
336	90	S_1	188	58	S_2	186	28	S_1	166	67	S_1	330	55	S_1
336	90	S_1	181	47	S_2	154	62	S_1	180	56	S_1	337	47	S_1
355	38	S_1	112	60	S_2	172	47	S_1	172	70	S_1	169	39	S_1
347	60	S_1	114	57	S_2	322	52	S_1	142	15	S_1	220	34	S_1
349	87	S_1	94	30	S_2	324	50	S_1	175	65	S_1	344	36	S_1
355	85	S_1	97	63	S_2	304	440	S_1	161	41	S_1	320	22	S_1
6	56	S_1	105	70	S_2	336	87	S_1	172	40	S_1	15	25	S_1
2	55	S_1	259	37	S_2	353	85	S_1	155	24	S_1	354	35	S_1
355	76	S_1	285	51	S_2	315	48	S_1	135	19	S_1	337	44	S_1
5	84	S_1	125	46	S_2	334	62	S_1	175	35	S_1	24	28	S_1

Domain A			Domain B			Domain C			Domain D			Domain E		
172	87	S_1	91	45	S_2	297	34	S_1	170	38	S_1	5	40	S_1
145	62	S_1	316	65	S_2	304	25	S_1	165	68	S_1	334	59	S_1
116	46	S_1	109	63	S_2	329	48	S_1	164	67	S_1	330	21	S_1
349	58	S_1	119	63	S_2	356	45	S_1	164	63	S_1	334	28	S_1
33	27	S_1	119	67	S_2	345	47	S_1	167	72	S_1	355	81	S_2
112	24	S_1	128	80	S_2	323	60	S_1	172	78	S_1	343	90	S_2
21	29	S_1	132	71	S_2	321	48	S_1	205	33	S_1	342	88	S_2
340	70	S_1	131	80	S_2	328	62	S_1	206	30	S_1	342	87	S_2
332	70	S_1	139	72	S_2	303	60	S_1	190	37	S_1	357	78	S_2
354	86	S_1	133	72	S_2	308	56	S_1	190	45	S_1	353	75	S_2
357	72	S_1	132	69	S_2	300	85	S_1	161	34	S_1	359	60	S_2
349	88	S_1	137	84	S_2	309	70	S_1	174	45	S_1	345	46	S_2
346	65	S_1	136	86	S_2	269	58	S_1	166	35	S_1	144	80	S_2
8	57	S_1	138	74	S_2	328	60	S_1	173	35	S_1	155	72	S_2
324	43	S_1	133	80	S_2	314	59	S_1	188	40	S_1	325	86	S_2
329	9	S_1	150	90	S_2	309	26	S_1	196	37	S_1	309	73	S_2
312	42	S_1	158	87	S_2	325	37	S_1	19	24	S_1	333	85	S_2
145	81	S_1	148	76	S_2	332	48	S_1	14	30	S_1	318	83	S_2
153	88	S_1	142	78	S_2	331	49	S_1	10	20	S_1	16	69	S_2
5	86	S_1	148	78	S_2	272	22	S_1	106	27	S_1	15	79	S_2
165	35	S_1	158	68	S_2	247	21	S_1	13	67	S_1	21	80	S_2
146	27	S_1	150	82	S_2	303	51	S_1	357	59	S_1	22	76	S_2
146	20	S_1	146	84	S_2	316	54	S_1	18	80	S_1	348	63	S_2
347	53	S_1	150	82	S_2	331	39	S_1	11	81	S_1	349	74	S_2
335	69	S_1	142	82	S_2	327	38	S_1	167	36	S_1	358	67	S_2
329	65	S_1	288	58	S_2	339	55	S_1	162	22	S_1	344	46	S_2
338	57	S_1	290	73	S_2	340	54	S_1	180	54	S_1	351	59	S_2
335	50	S_1	134	71	S_2	292	75	S_1	199	56	S_1	353	70	S_2
280	32	S_1	293	76	S_2	304	86	S_1	210	45	S_1	332	79	S_2
344	54	S_1	121	90	S_2	251	37	S_1	191	45	S_1	345	71	S_2
351	64	S_1	310	67	S_2	259	39	S_1	224	38	S_1	330	45	S_2
334	55	S_1	133	80	S_2	152	26	S_1	134	23	S_1	334	71	S_2
340	60	S_1	129	63	S_2	161	24	S_1	121	24	S_1	330	64	S_2
342	72	S_1	120	64	S_2	98	35	S_1	194	38	S_1	324	67	S_2
332	65	S_1	162	82	S_2	93	31	S_1	203	53	S_1	330	64	S_2
341	72	S_1	153	75	S_2	130	83	S_1	200	58	S_1	330	64	S_2
12	55	S_1	162	82	S_2	134	64	S_1	136	78	S_1	319	67	S_2
10	58	S_1	153	75	S_2	291	48	S_1	150	58	S_1	330	69	S_2
5	64	S_1	356	39	S_2	291	40	S_1	147	63	S_1	323	63	S_2
253	8	S_1	334	62	S_2	301	46	S_1	144	69	S_1	319	81	S_2
215	18	S_1	45	30	S_2	240	34	S_1	160	67	S_1	342	40	S_2
160	65	S_1	33	33	S_2	256	35	S_1	203	55	S_1	332	35	S_2
170	90	S_1	347	46	S_2	155	72	S_1	192	64	S_1	332	49	S_2
156	60	S_1	333	37	S_2	141	45	S_1	216	35	S_1	333	53	S_2
150	80	S_1	150	80	S_2	157	54	S_1	170	65	S_1	352	37	S_2

Supporting Table 1: raw data of structural measurements

Domain A			Domain B			Domain C			Domain D			Domain E		
334	74	S_1	161	85	S_2	308	50	S_1	186	55	S_1	342	48	S_2
173	25	S_1	145	88	S_2	306	54	S_1	196	37	S_1	345	49	S_2
115	3	S_1	161	78	S_2	306	46	S_1	296	39	S_1	352	52	S_2
80	42	S_1	149	62	S_2	341	67	S_1	186	73	S_1	354	52	S_2
350	84	S_1	332	82	S_2	331	58	S_1	214	51	S_1	359	52	S_2
145	45	S_1	326	86	S_2	333	61	S_1	198	13	S_1	6	45	S_2
120	52	S_1	345	77	S_2	331	50	S_1	196	14	S_1	328	52	S_2
348	57	S_1	28	73	S_2	322	72	S_1	2	40	S_1	340	73	S_2
194	83	S_1	30	88	S_2	318	48	S_1	58	45	S_1	44	54	S_2
40	72	S_1	271	20	S_2	176	65	S_1	290	15	S_1	355	46	S_2
7	61	S_1	159	30	S_2	188	69	S_1	113	18	S_1	343	48	S_2
347	67	S_1	135	36	S_2	299	56	S_1	172	63	S_1	331	50	S_2
347	37	S_1	258	85	C_{dex}	304	56	S_1	179	43	S_1	358	51	S_2
356	39	S_1	38	77	C_{dex}	302	60	S_1	182	80	S_1	325	40	S_2
172	55	S_1	22	72	C_{dex}	338	47	S_1	168	46	S_1	5	61	S_2
184	57	S_1	356	39	C_{rev}	333	45	S_1	174	53	S_1	324	65	S_2
358	70	S_1	352	45	C_{rev}	310	41	S_1	172	65	S_1	10	43	S_2
344	65	S_1	11	66	C_{rev}	228	21	S_1	186	71	S_1	342	84	S_2
350	55	S_1	194	74	C_{rev}	300	6	S_1	189	80	S_1	333	57	S_2
355	68	S_1	131	73	C_{sin}	301	50	S_1	343	46	S_1	152	70	S_2
6	45	S_1	124	72	C_{sin}	288	58	S_1	0	52	S_1	168	71	S_2
2	37	S_1	140	70	C_{sin}	280	43	S_1	145	35	S_1	332	85	S_2
332	34	S_1	296	75	C_{sin}	174	21	S_1	32	22	S_1	143	80	S_2
337	37	S_1	304	85	C_{sin}	325	25	S_1	172	33	S_1	308	88	S_2
346	67	S_1	112	82	C_{sin}	269	18	S_1	121	42	S_1	343	66	S_2
334	54	S_1	210	78	C_{sin}	177	23	S_1	139	28	S_1	343	52	S_2
172	84	S_1	11	63	C_{sin}	291	37	S_1	182	24	S_1	244	90	S_2
355	86	S_1	39	78	C_{sin}	200	24	S_1	146	36	S_1	244	90	S_2
334	35	S_1	5	65	C_{sin}	281	49	S_1	172	54	S_1	337	72	S_2
341	54	S_1	186	80	C_{sin}	273	48	S_1	178	43	S_1	348	87	S_2
342	50	S_1	17	86	C_{sin}	333	54	S_1	149	38	S_1	331	70	S_2
352	60	S_1	139	79	C_{sin}	325	42	S_1	206	46	S_1	334	86	S_2
356	72	S_1	135	85	C_{sin}	303	33	S_1	178	87	S_1	329	42	S_2
348	70	S_1	129	72	C_{sin}	16	29	S_1	187	82	S_1	327	54	S_2
324	27	S_1	323	86	C_{sin}	309	49	S_1	9	68	S_1	343	53	S_2
329	26	S_1	125	60	C_{sin}	19	90	S_1	359	62	S_1	340	57	S_2
331	44	S_1	152	61	C_{sin}	2	70	S_1	342	72	S_1	318	51	S_2
349	59	S_1	162	70	C_{sin}	318	52	S_1	341	42	S_1	176	40	S_2
342	70	S_1	126	74	C_{sin}	343	74	S_1	327	60	S_1	156	68	S_2
345	55	S_1	128	79	C_{sin}	314	56	S_1	280	34	S_1	170	47	S_2
340	56	S_1	126	82	C_{sin}	344	38	S_1	10	66	S_1	292	90	S_2
346	35	S_1	137	90	C_{sin}	276	48	S_1	37	30	S_1	140	80	S_2
344	50	S_1	135	84	C_{sin}	326	46	S_1	353	78	S_1	134	80	S_2
345	23	S_1	137	75	C_{sin}	317	48	S_1	339	84	S_1	300	82	S_2
149	37	S_1	122	78	C_{sin}	334	81	S_1	338	49	S_1	334	36	S_2

Domain A			Domain B			Domain C			Domain D			Domain E		
5	71	S_1	118	70	C_{sin}	353	81	S_1	118	18	S_1	339	21	S_2
338	40	S_1	122	70	C_{sin}	5	67	S_1	146	54	S_1	264	79	S_2
310	62	S_1	330	85	C_{sin}	24	77	S_1	158	82	S_1	273	76	S_2
345	60	S_1	335	88	C_{sin}	343	54	S_1	152	65	S_1	167	85	S_2
331	73	S_1	350	87	C_{sin}	189	46	S_1	163	68	S_1	166	78	S_2
320	75	S_1	348	85	C_{sin}	289	29	S_1	328	86	S_1	357	67	S_2
350	81	S_1	126	60	C_{sin}	202	58	S_1	156	80	S_1	11	64	S_2
295	45	S_1	311	78	C_{sin}	231	32	S_1	156	32	S_1	285	10	S_3
338	55	S_1	296	75	C_{sin}	207	20	S_1	158	30	S_1	220	28	S_3
353	80	S_1	304	85	C_{sin}	258	52	S_1	140	24	S_1	306	7	S_3
153	76	S_1	112	82	C_{sin}	340	52	S_1	121	20	S_1	353	19	S_3
130	68	S_1	291	65	C_{sin}	2	44	S_1	144	23	S_1	100	36	S_3
143	62	S_1	164	66	C_{sin}	173	5	S_1	188	23	S_1	319	16	S_3
136	70	S_1	298	68	C_{sin}	67	29	S_1	337	85	S_1	289	45	S_3
144	75	S_1	320	85	C_{sin}	305	21	S_1	357	82	S_1	248	46	S_3
138	66	S_1	178	82	C_{sin}	173	15	S_1	1	84	S_1	277	53	S_3
140	74	S_1	191	78	C_{sin}	81	54	S_1	168	30	S_1	197	30	S_3
142	79	S_1	181	74	C_{sin}	214	35	S_1	137	28	S_1	308	59	S_3
137	40	S_1	192	84	C_{sin}	44	20	S_1	168	35	S_1	226	19	S_3
161	51	S_1	30	53	C_{sin}	24	16	S_1	178	42	S_1	253	32	S_3
154	69	S_1	321	78	C_{sin}	4	20	S_1	190	56	S_1	263	30	S_3
316	33	S_1	317	90	C_{sin}	26	56	S_1	175	62	S_1	315	28	S_3
144	84	S_1	322	82	C_{sin}	48	31	S_1	174	30	S_1	300	30	S_3
140	75	S_1	157	51	C'_{dex}	78	79	S_1	112	36	S_1	339	60	S_3
141	56	S_1	4	79	C'_{dex}	65	79	S_1	66	45	S_1	335	50	S_3
176	48	S_1	174	73	C'_{dex}	52	37	S_1	30	39	S_1	266	18	S_3
170	67	S_1	96	46	C'_{nor}	33	46	S_1	118	25	S_1	284	27	S_3
299	50	S_1	133	43	C'_{nor}	15	39	S_1	170	65	S_1	338	18	S_3
289	52	S_1	102	49	C'_{nor}	340	53	S_1	357	68	S_1	344	16	S_3
262	24	S_1	83	55	C'_{nor}	257	39	S_1	152	63	S_1	118	20	S_3
238	15	S_1	66	51	C'_{nor}	337	44	S_1	17	72	S_1	286	24	S_3
183	39	S_1	68	25	C'_{nor}	347	42	S_1	174	85	S_1	286	26	S_3
312	67	S_1	60	54	C'_{nor}	341	50	S_1	148	78	S_1	333	39	S_3
310	67	S_1	80	45	C'_{nor}	335	65	S_1	170	66	S_1	357	65	S_3
324	80	S_1	91	71	C'_{nor}	331	58	S_1	338	84	S_1	341	56	S_3
326	78	S_1	141	67	C'_{nor}	326	67	S_1	176	84	S_1	259	59	S_3
288	59	S_1	99	74	C'_{nor}	331	45	S_1	333	79	S_1	294	54	S_3
308	66	S_1	64	50	C'_{nor}	321	40	S_1	178	22	S_1	280	47	S_3
176	56	S_1	139	45	C'_{sin}	338	40	S_1	320	24	S_1	285	57	S_3
164	62	S_1	119	86	C'_{sin}	356	45	S_1	114	40	S_1	305	55	S_3
145	66	S_1	113	75	C'_{sin}	320	43	S_1	113	24	S_1	110	25	S_3
153	66	S_1	97	81	C'_{sin}	353	51	S_1	6	14	S_1	87	32	S_3
170	53	S_1	129	74	C'_{sin}	338	41	S_1	143	37	S_1	292	38	S_3
169	57	S_1	132	90	C'_{sin}	308	34	S_1	307	36	S_1	100	23	S_3
140	62	S_1	316	82	C'_{sin}	329	33	S_1	148	73	S_1	305	30	S_3

Domain A			Domain B			Domain C			Domain D			Domain E		
140	67	S_1	320	88	C'_{sin}	358	36	S_1	138	68	S_1	311	28	S_3
183	63	S_1	141	78	C'_{sin}	11	26	S_1	336	68	S_1	336	38	S_3
301	87	S_1	149	80	C'_{sin}	16	36	S_1	333	71	S_1	316	36	S_3
321	61	S_1	101	76	C'_{sin}	329	9	S_1	328	61	S_1	336	31	S_3
166	39	S_1	102	80	C'_{sin}	307	14	S_1	81	10	S_1	262	28	S_3
164	70	S_1	104	80	C'_{sin}	65	24	S_1	321	32	S_1	216	35	S_3
153	70	S_1	124	83	C'_{sin}	350	28	S_1	174	20	S_1	14	25	S_3
168	56	S_1	108	82	C'_{sin}	288	25	S_1	307	38	S_1	326	36	S_3
244	22	S_1	296	84	C'_{sin}	294	39	S_1	311	47	S_1	326	46	S_3
150	77	S_1	110	85	C'_{sin}	338	40	S_1	353	69	S_1	314	40	S_3
287	23	S_1	106	81	C'_{sin}	335	39	S_1	216	58	S_1	285	32	S_3
164	24	S_1	33	17	AP_1	328	30	S_1	298	30	S_1	287	28	S_3
58	33	S_1	6	30	AP_1	18	30	S_1	181	26	S_1	293	41	S_3
319	44	S_1	31	41	AP_1	21	20	S_1	174	41	S_1	283	44	S_3
326	51	S_1	31	40	AP_1	324	27	S_1	166	50	S_1	282	38	S_3
354	21	S_1	33	36	AP_1	341	33	S_1	109	28	S_1	292	39	S_3
225	14	S_1	59	37	AP_1	332	50	S_1	136	31	S_1	282	37	S_3
57	21	S_1	58	34	AP_1	339	39	S_1	77	22	S_1	286	32	S_3
289	17	S_1	48	29	AP_1	296	41	S_1	154	47	S_1	309	30	S_3
130	27	S_1	52	35	AP_1	312	40	S_1	185	48	S_1	325	30	S_3
193	18	S_1	64	48	AP_1	315	37	S_1	121	55	S_1	298	26	S_3
154	4	S_1	59	29	AP_1	323	33	S_1	128	34	S_1	301	27	S_3
255	20	S_1	85	23	AP_1	304	40	S_1	112	32	S_1	285	29	S_3
226	19	S_1	73	27	AP_1	313	38	S_1	125	30	S_1	204	14	S_3
339	19	S_1	96	26	AP_1	322	58	S_1	140	41	S_1	214	7	S_3
215	21	S_1	28	43	AP_1	315	70	S_1	166	22	S_1	259	12	S_3
337	42	S_1	71	39	AP_1	316	59	S_1	163	34	S_1	317	11	S_3
305	15	S_1	320	76	AP_2	308	40	S_1	218	32	S_1	160	17	S_3
294	10	S_1	30	53	AP_2	301	56	S_1	188	26	S_1	230	45	S_3
311	31	S_1	209	72	AP_2	304	49	S_1	172	35	S_1	6	41	S_3
172	23	S_1	205	61	AP_2	306	55	S_1	166	62	S_1	262	13	S_3
181	35	S_1	214	66	AP_2	329	68	S_1	218	30	S_1	209	34	S_3
335	50	S_1	216	56	AP_2	331	58	S_1	206	25	S_1	0	0	S_3
44	21	S_1	202	62	AP_2	325	59	S_1	192	10	S_1	270	27	S_3
326	36	S_1	234	36	AP_2	313	77	S_1	357	43	S_1	269	24	S_3
168	38	S_1	259	78	AP_2	335	52	S_1	276	35	S_1	254	11	S_3
208	11	S_1	268	82	AP_2	323	63	S_1	285	38	S_1	256	6	S_3
244	11	S_1	191	82	AP_2	325	71	S_1	301	55	S_1	323	21	S_3
336	26	S_1	356	82	AP_2	328	79	S_1	222	66	S_1	236	20	S_3
321	44	S_1	171	85	AP_2	333	68	S_1	198	75	S_1	292	34	S_3
289	23	S_1	180	90	AP_2	347	48	S_1	359	61	S_1	300	33	S_3
127	25	S_1	166	82	AP_2	347	48	S_1	348	36	S_1	309	48	S_3
131	16	S_1	344	80	AP_2	334	71	S_1	352	67	S_1	53	11	S_3
190	3	S_1	167	86	AP_2	337	60	S_1	357	42	S_1	299	25	S_3
146	39	S_1	167	87	AP_2	341	64	S_1	348	63	S_1	96	15	S_3

Supporting Table 1: raw data of structural measurements

Domain A			Domain B			Domain C			Domain D			Domain E		
201	10	S_1	352	47	AP_2	335	77	S_1	354	60	S_1	300	30	S_3
188	44	S_1	355	48	AP_2	344	69	S_1	350	57	S_1	286	34	S_3
166	58	S_1	346	76	AP_2	326	57	S_1	159	24	S_1	281	40	S_3
183	42	S_1	11	45	AP_2	153	62	S_1	168	18	S_1	267	47	S_3
178	79	S_1	349	66	AP_2	154	42	S_1	164	23	S_1	273	34	S_3
158	51	S_1	92	74	AP_2	161	39	S_1	148	25	S_1	300	37	S_3
209	34	S_1	83	70	AP_2	150	62	S_1	176	25	S_1	302	40	S_3
186	42	S_1	315	75	AP_2	357	88	S_1	166	9	S_1	320	58	S_3
165	55	S_1	296	58	AP_2	199	60	S_1	170	37	S_1	320	52	S_3
152	79	S_1	272	22	AP_2	196	53	S_1	130	11	S_1	323	56	S_3
147	82	S_1	204	30	AP_2	198	66	S_1	254	15	S_1	299	40	S_3
149	58	S_1	153	50	AP_2	169	90	S_1	258	6	S_1	320	40	S_3
174	48	S_1	125	16	AP_2	325	47	S_1	136	45	S_1	306	29	S_3
151	45	S_1	251	50	AP_2	307	51	S_1	120	36	S_1	251	41	S_3
173	53	S_1	234	58	AP_2	303	47	S_1	116	28	S_1	222	62	S_3
152	59	S_1	109	81	AP_2	28	15	S_1	172	56	S_1	286	27	S_3
172	37	S_1	225	80	AP_2	296	29	S_1	156	75	S_1	314	14	S_3
147	26	S_1	345	35	AP_2	156	51	S_1	170	65	S_1	255	26	S_3
165	38	S_1	227	47	AP_2	126	45	S_1	153	57	S_1	2	26	S_3
269	19	S_1	291	48	AP_2	139	44	S_1	172	49	S_1	338	39	S_3
131	17	S_1	311	62	AP_2	103	40	S_1	188	52	S_1	330	21	S_3
311	16	S_1	249	43	AP_2	327	67	S_1	148	26	S_1	296	50	S_3
212	45	S_1	312	70	AP_2	116	72	S_1	162	25	S_1	268	35	S_3
194	63	S_1	185	25	AP_2	91	38	S_1	173	49	S_1	254	7	S_3
333	74	S_1	280	15	AP_2	110	25	S_1	183	63	S_1	307	23	S_3
338	66	S_1	148	24	AP_2	141	35	S_1	190	42	S_1	281	23	S_3
331	15	S_1	160	90	AP_2	153	45	S_1	157	55	S_1	265	23	S_3
0	0	S_1	350	80	AP_2	148	51	S_1	172	50	S_1	78	8	S_3
349	37	S_1	162	82	AP_2	325	78	S_1	171	60	S_1	66	10	S_3
342	24	S_1	271	20	AP_2	180	58	S_1	166	39	S_1	91	2	S_3
263	16	S_1	159	30	AP_2	137	54	S_1	178	40	S_1	231	19	S_3
332	62	S_1	135	36	AP_2	128	58	S_1	174	38	S_1	285	12	S_3
347	45	S_1	28	73	AP_2	129	33	S_1	211	27	S_1	288	22	S_3
317	30	S_1	30	88	AP_2	101	41	S_1	185	19	S_1	2	67	AP_1
312	63	S_1	152	68	AP_2	250	27	S_1	203	44	S_1	6	64	AP_1
316	63	S_1	163	82	AP_2	247	16	S_1	183	63	S_1	17	67	AP_1
302	57	S_1	159	51	AP_2	50	52	S_1	200	67	S_1	62	22	AP_1
117	30	S_1	332	82	AP_2	72	55	S_1	194	22	S_1	188	40	AP_1
156	55	S_1	326	86	AP_2	331	15	S_1	323	33	S_1	220	14	AP_1
146	65	S_1	345	77	AP_2	266	24	S_1	302	21	S_1	244	18	AP_1
194	25	S_1	100	9	FA_1	265	35	S_1	273	23	S_1	256	25	AP_1
300	29	S_1	132	3	FA_1	355	25	S_1	158	30	S_1	280	28	AP_1
324	42	S_1	328	22	FA_1	47	26	S_1	168	27	S_1	291	24	AP_1
244	8	S_1	124	4	FA_1	69	22	S_1	243	21	S_1	300	30	AP_1
324	58	S_1	312	3	FA_1	52	24	S_1	165	44	S_1	320	45	AP_1

Domain A			Domain B			Domain C			Domain D			Domain E		
323	54	S_1	310	3	FA_1	69	32	S_1	203	17	S_1	321	57	AP_1
289	40	S_1	272	42	FA_2	63	13	S_1	230	13	S_1	332	40	AP_1
304	45	S_1	262	24	FA_2	359	49	S_1	212	58	S_1	335	38	AP_1
334	80	S_1	280	23	FA_2	328	54	S_1	207	68	S_1	336	34	AP_1
342	82	S_1	278	22	FA_2	337	54	S_1	200	83	S_1	337	45	AP_1
319	72	S_1	288	12	FA_2	340	46	S_1	238	64	S_1	354	40	AP_1
342	35	S_1	288	8	FA_2	341	38	S_1	234	62	S_1	357	67	AP_1
327	50	S_1	320	30	FA_2	341	58	S_1	211	70	S_1	357	59	AP_1
315	36	S_1	283	2	FA_2	336	64	S_1	216	76	S_1	341	78	AP_2
340	52	S_1	72	40	FA_2	328	68	S_1	200	81	S_1	342	84	AP_2
332	56	S_1	85	19	FA_2	99	66	S_1	210	70	S_1	0	25	AP_2
334	46	S_1	83	22	FA_2	101	67	S_1	222	68	S_1	0	63	AP_2
190	21	S_1	53	42	FA_2	115	66	S_1	217	68	S_1	2	76	AP_2
307	37	S_1	83	47	FA_2	54	87	S_1	222	76	S_1	2	88	AP_2
328	48	S_1	73	32	FA_2	232	75	S_1	210	65	S_1	2	79	AP_2
352	62	S_1	53	24	FA_2	11	67	S_1	198	66	S_1	2	67	AP_2
349	60	S_1	67	40	FA_2	32	69	S_1	168	50	S_1	2	67	AP_2
354	61	S_1	74	42	FA_2	23	65	S_1	167	71	S_1	3	67	AP_2
346	56	S_1	55	45	FA_2	16	62	S_1	172	84	S_1	3	50	AP_2
346	60	S_1	349	43	FA_2	44	60	S_1	169	62	S_1	5	55	AP_2
193	14	S_1	359	37	FA_2	34	65	S_1	188	73	S_1	5	77	AP_2
188	16	S_1	36	33	FA_2	37	58	S_1	180	78	S_1	5	44	AP_2
191	13	S_1	21	39	FA_2	297	72	S_1	171	66	S_1	6	44	AP_2
335	67	S_1	114	20	FA_2	344	66	S_1	202	75	S_1	6	56	AP_2
335	77	S_1	121	20	FA_2	322	82	S_1	188	64	S_1	7	87	AP_2
330	88	S_1	125	16	FA_2	288	42	S_1	189	54	S_1	7	58	AP_2
2	33	S_1	44	44	FA_2	309	47	S_1	192	64	S_1	8	59	AP_2
32	17	S_1	22	0	FA_2	304	74	S_1	204	80	S_1	8	18	AP_2
30	14	S_1	235	60	FA_2	310	45	S_1	217	81	S_1	10	54	AP_2
6	44	S_1	225	15	FA_2	319	50	S_1	16	78	S_1	10	64	AP_2
256	36	S_1	202	10	FA_2	334	50	S_1	45	72	S_1	11	53	AP_2
12	45	S_1	208	5	FA_2	326	47	S_1	158	14	S_1	12	34	AP_2
11	66	S_1	256	17	FA_2	348	60	S_1	162	57	S_1	12	33	AP_2
9	48	S_1	71	70	FA_2	314	58	S_1	173	62	S_1	12	65	AP_2
316	40	S_1	210	48	FA_2	337	68	S_1	182	59	S_1	13	48	AP_2
313	38	S_1	240	20	FA_2	150	82	S_1	121	88	S_1	14	45	AP_2
321	26	S_1	98	26	FA_2	198	42	S_1	62	58	S_1	16	57	AP_2
325	36	S_1	110	21	FA_2	111	72	S_1	60	63	S_1	16	50	AP_2
158	72	S_1	300	10	L_1	150	60	S_1	61	57	S_1	17	50	AP_2
156	79	S_1	297	22	L_1	144	70	S_1	89	65	S_1	18	65	AP_2
137	27	S_1	253	17	L_1	308	72	S_1	61	723	S_1	19	52	AP_2
216	34	S_1	231	16	L_2	162	82	S_1	100	73	S_1	21	57	AP_2
353	25	S_1	108	6	L_2	188	77	S_1	103	64	S_1	21	17	AP_2
357	28	S_1	284	34	L_2	171	58	S_1	100	74	S_1	21	87	AP_2
344	62	S_1	114	13	L_2	157	41	S_1	155	80	S_1	22	76	AP_2

Supporting Table 1: raw data of structural measurements

Domain A			Domain B			Domain C			Domain D			Domain E		
358	63	S_1	282	40	L_2	152	46	S_1	5	45	S_1	26	80	AP_2
178	38	S_1	278	4	L_2	160	47	S_1	346	31	S_1	28	67	AP_2
181	46	S_1	226	4	L_2	156	38	S_1	353	54	S_1	29	54	AP_2
154	15	S_1	232	8	L_2	135	40	S_1	357	45	S_1	30	46	AP_2
183	37	S_1	268	8	L_2	195	24	S_1	342	54	S_1	32	62	AP_2
183	34	S_1	277	7	L_2	185	15	S_1	9	18	S_1	34	42	AP_2
168	33	S_1	275	11	L_2	195	18	S_1	0	42	S_1	34	50	AP_2
161	32	S_1	253	27	L_2	315	45	S_1	336	17	S_1	41	47	AP_2
121	21	S_1	246	2	L_2	333	52	S_1	4	35	S_1	42	87	AP_2
147	14	S_1	226	29	L_2	308	78	S_1	344	22	S_1	61	88	AP_2
165	16	S_1	228	21	L_2	318	78	S_1	358	34	S_1	70	64	AP_2
146	22	S_1	255	13	L_2	320	72	S_1	346	48	S_1	74	83	AP_2
164	33	S_1	235	23	L_2	17	31	S_1	337	14	S_1	92	53	AP_2
352	54	S_1	238	22	L_2	34	42	S_1	325	55	S_1	95	74	AP_2
350	73	S_1	270	13	L_2	57	35	S_1	312	53	S_1	154	58	AP_2
354	72	S_1	268	10	L_2	80	60	S_1	336	72	S_1	160	71	AP_2
358	54	S_1	32	24	L_2	6	28	S_1	322	64	S_1	175	82	AP_2
11	48	S_1	20	22	L_2	335	38	S_1	39	80	S_1	187	75	AP_2
338	68	S_1	36	17	L_2	112	38	S_1	72	65	S_1	190	52	AP_2
348	36	S_1	61	11	L_2	150	50	S_1	42	75	S_1	219	70	AP_2
351	73	S_1	235	7	L_2	22	49	S_1	296	80	S_1	221	40	AP_2
351	63	S_1	58	2	L_2	22	62	S_1	148	82	S_1	229	49	AP_2
337	63	S_1	43	8	L_2	44	40	S_1	137	79	S_1	239	85	AP_2
347	54	S_1	48	9	L_2	349	12	S_1	138	86	S_1	246	78	AP_2
350	57	S_1	47	13	L_2	291	35	S_1	288	80	S_1	257	68	AP_2
355	62	S_1	46	12	L_2	193	24	S_1	332	86	S_1	258	68	AP_2
351	62	S_1	53	13	L_2	198	24	S_1	103	84	S_1	289	19	AP_2
349	70	S_1	72	3	L_2	185	21	S_1	137	90	S_1	304	22	AP_2
349	67	S_1	58	30	L_2	160	28	S_1	150	80	S_1	309	14	AP_2
349	71	S_1	40	0	L_{sin}	192	16	S_1	100	81	S_1	313	44	AP_2
359	75	S_1	38	3	L_{sin}	164	39	S_1	102	81	S_1	317	90	AP_2
0	83	S_1	210	4	L_{sin}	160	26	S_1	158	82	S_1	318	56	AP_2
355	90	S_1	36	5	L_{sin}	228	10	S_1	119	73	S_1	327	46	AP_2
350	60	S_1	34	7	L_{sin}	245	9	S_1	128	66	S_1	333	23	AP_2
350	61	S_1	35	0	L_{sin}	266	13	S_1	109	65	S_1	334	90	AP_2
359	69	S_1	59	4	L_{sin}	281	31	S_1	138	61	S_1	335	38	AP_2
349	60	S_1	249	2	L_{sin}	256	36	S_1	91	87	S_1	337	20	AP_2
350	50	S_1	58	15	L_{sin}	348	54	S_1	276	80	S_1	338	35	AP_2
219	9	S_1	58	15	L_{nor}	342	36	S_1	138	82	S_1	339	90	AP_2
226	26	S_1	220	23	L_{dex}	322	36	S_1	257	85	S_1	340	35	AP_2
195	30	S_1	227	12	L_{dex}	294	55	S_1	233	81	S_1	342	60	AP_2
194	53	S_1				296	50	S_1	147	82	S_1	342	47	AP_2
198	48	S_1				291	56	S_1	113	81	S_1	342	28	AP_2
194	51	S_1				316	41	S_1	134	80	S_1	343	65	AP_2
192	53	S_1				298	41	S_1	190	80	S_1	344	83	AP_2

Supporting Table 1: raw data of structural measurements

Domain A			Domain A			Domain C			Domain D			Domain E		
56	61	S_1	139	65	S_2	313	39	S_1	186	78	S_1	344	25	AP_2
56	64	S_1	346	65	S_2	331	37	S_1	142	68	S_1	345	55	AP_2
60	84	S_1	342	68	S_2	326	33	S_1	130	78	S_1	345	49	AP_2
277	39	S_1	8	74	S_2	325	37	S_1	115	49	S_1	345	19	AP_2
351	77	S_1	317	75	S_2	312	55	S_1	6	41	S_1	346	86	AP_2
351	78	S_1	320	72	S_2	303	54	S_1	0	45	S_1	346	60	AP_2
359	72	S_1	102	52	S_2	309	45	S_1	330	38	S_1	346	58	AP_2
8	74	S_1	128	75	S_2	312	53	S_1	328	38	S_1	346	38	AP_2
6	67	S_1	319	82	S_2	318	58	S_1	10	33	S_1	347	61	AP_2
0	70	S_1	342	90	S_2	312	48	S_1	3	26	S_1	347	52	AP_2
2	71	S_1	342	72	S_2	310	86	S_1	1	41	S_1	348	64	AP_2
186	72	S_1	357	78	S_2	139	84	S_1	342	45	S_1	349	84	AP_2
351	80	S_1	189	63	S_2	144	87	S_1	2	58	S_1	350	50	AP_2
357	78	S_1	173	53	S_2	324	90	S_1	356	52	S_1	351	61	AP_2
156	42	S_1	199	52	S_2	148	88	S_1	334	30	S_1	351	76	AP_2
159	37	S_1	9	73	S_2	200	23	S_1	353	30	S_1	352	47	AP_2
156	78	S_1	352	71	S_2	172	28	S_1	105	38	S_1	352	66	AP_2
159	76	S_1	351	57	S_2	181	24	S_1	121	45	S_1	353	50	AP_2
152	45	S_1	354	61	S_2	189	18	S_1	116	33	S_1	353	70	AP_2
146	30	S_1	345	80	S_2	184	12	S_1	359	53	S_1	353	79	AP_2
150	32	S_1	324	83	S_2	205	60	S_1	16	56	S_1	353	19	AP_2
156	82	S_1	139	82	S_2	202	61	S_1	8	62	S_1	353	53	AP_2
153	83	S_1	156	60	S_2	196	65	S_1	2	73	S_1	353	51	AP_2
142	38	S_1	159	80	S_2	197	50	S_1	2	62	S_1	355	57	AP_2
152	45	S_1	13	50	S_2	184	72	S_1	353	47	S_1	355	58	AP_2
146	60	S_1	22	52	S_2	210	68	S_1	355	50	S_1	356	65	AP_2
142	58	S_1	11	43	S_2	204	50	S_1	345	51	S_1	357	60	AP_2
139	51	S_1	351	50	S_2	218	42	S_1	353	48	S_1	358	26	AP_2
150	69	S_1	331	48	S_2	206	65	S_1	354	46	S_1	359	87	AP_2
181	35	S_1	342	58	S_2	195	50	S_1	163	90	S_1	359	65	AP_2
162	82	S_1	347	58	S_2	202	51	S_1	166	75	S_1	359	38	AP_2
157	82	S_1	345	45	S_2	196	55	S_1	165	67	S_1	348	61	AP_2
162	76	S_1	34	63	S_2	196	45	S_1	157	60	S_1	351	78	AP_2
345	84	S_1	342	80	S_2	20	88	S_1	142	67	S_1	355	72	AP_2
321	78	S_1	356	87	S_2	197	88	S_1	143	72	S_1	359	49	AP_2
336	72	S_1	176	85	S_2	183	51	S_1	2	61	S_2	350	32	AP_3
352	66	S_1	174	81	S_2	210	65	S_1	23	79	S_2	343	40	AP_3
16	57	S_1	168	81	S_2	198	72	S_1	22	82	S_2	3	20	AP_3
9	58	S_1	176	84	S_2	327	23	S_1	124	68	S_2	3	21	AP_3
152	60	S_1	6	83	S_2	17	33	S_1	311	86	S_2	4	64	AP_3
169	55	S_1	355	86	S_2	149	60	S_1	133	88	S_2	6	30	AP_3
352	56	S_1	359	86	S_2	301	31	S_1	136	60	S_2	10	64	AP_3
350	50	S_1	178	88	S_2	159	90	S_1	356	88	S_2	15	78	AP_3
351	74	S_1	170	84	S_2	167	56	S_1	331	89	S_2	17	87	AP_3
345	75	S_1	176	86	S_2	194	39	S_1	166	52	S_2	21	20	AP_3

Supporting Table 1: raw data of structural measurements

Domain A			Domain A			Domain C			Domain D			Domain E		
347	67	S_1	182	77	S_2	198	54	S_1	177	70	S_2	28	38	AP_3
338	54	S_1	180	77	S_2	202	23	S_1	173	59	S_2	34	85	AP_3
341	65	S_1	178	69	S_2	192	35	S_1	178	62	S_2	34	31	AP_3
341	52	S_1	173	88	S_2	308	30	S_1	194	70	S_2	56	23	AP_3
340	55	S_1	347	87	S_2	341	46	S_1	192	77	S_2	70	90	AP_3
331	74	S_1	350	90	S_2	343	45	S_1	196	80	S_2	164	53	AP_3
345	85	S_1	13	87	S_2	342	45	S_1	194	84	S_2	166	75	AP_3
352	66	S_1	359	87	S_2	157	45	S_1	188	83	S_2	172	67	AP_3
336	62	S_1	180	89	S_2	347	60	S_1	188	85	S_2	179	72	AP_3
342	50	S_1	1	86	S_2	348	60	S_1	186	89	S_2	191	70	AP_3
233	36	S_1	179	89	S_2	351	54	S_1	188	82	S_2	195	8	AP_3
154	65	S_1	5	87	S_2	219	40	S_1	180	74	S_2	196	82	AP_3
153	50	S_1	190	88	S_2	235	33	S_1	172	78	S_2	200	80	AP_3
56	25	S_1	7	87	S_2	220	46	S_1	170	75	S_2	207	71	AP_3
74	45	S_1	359	86	S_2	239	18	S_1	174	80	S_2	213	4	AP_3
30	34	S_1	5	86	S_2	208	30	S_1	191	64	S_2	218	57	AP_3
98	25	S_1	3	88	S_2	234	11	S_1	207	66	S_2	222	62	AP_3
88	41	S_1	0	83	S_2	218	18	S_1	202	63	S_2	229	28	AP_3
312	35	S_1	186	83	S_2	27	60	S_1	212	72	S_2	236	76	AP_3
316	41	S_1	181	86	S_2	219	37	S_1	176	60	S_2	251	18	AP_3
329	75	S_1	352	86	S_2	191	18	S_1	205	55	S_2	256	88	AP_3
324	69	S_1	355	83	S_2	153	25	S_1	194	62	S_2	257	72	AP_3
212	24	S_1	1	85	S_2	198	23	S_1	185	54	S_2	264	24	AP_3
165	38	S_1	358	82	S_2	181	26	S_1	188	63	S_2	281	25	AP_3
328	54	S_1	356	87	S_2	309	25	S_1	161	73	S_2	284	26	AP_3
332	54	S_1	5	88	S_2	288	74	S_1	175	82	S_2	303	20	AP_3
329	76	S_1	173	88	S_2	268	78	S_1	170	84	S_2	313	23	AP_3
334	64	S_1	180	90	S_2	108	82	S_1	343	85	S_2	337	34	AP_3
330	61	S_1	2	87	S_2	280	71	S_1	149	88	S_2	351	54	AP_3
351	50	S_1	151	85	S_2	122	86	S_1	157	83	S_2	353	13	AP_3
355	51	S_1	149	86	S_2	109	75	S_1	328	86	S_2	1	57	AP_3
331	59	S_1	151	88	S_2	113	72	S_1	340	82	S_2	351	55	AP_3
328	56	S_1	142	75	S_2	114	69	S_1	159	81	S_2	353	49	AP_3
328	70	S_1	148	64	S_2	261	41	S_1	162	71	S_2	355	56	AP_3
341	45	S_1	150	70	S_2	240	20	S_1	147	90	S_2	207	16	AP_3
342	49	S_1	1	78	S_2	254	31	S_1	145	80	S_2	345	64	AP_3
316	80	S_1	159	82	S_2	298	17	S_1	149	75	S_2	15	90	C_{dex}
326	74	S_1	160	75	S_2	357	36	S_1	5	62	S_2	10	88	C_{dex}
321	81	S_1	168	65	S_2	307	12	S_1	38	48	S_2	38	54	C_{dex}
197	41	S_1	134	73	S_2	3	19	S_1	15	52	S_2	45	59	C_{dex}
195	30	S_1	152	90	S_2	22	21	S_1	38	46	S_2	32	65	C_{dex}
169	24	S_1	338	80	S_2	10	26	S_1	9	39	S_2	357	69	C_{dex}
171	27	S_1	165	84	S_2	19	21	S_1	16	46	S_2	25	75	C_{dex}
151	75	S_1	311	13	S_3	41	29	S_1	338	39	S_2	176	82	C_{dex}
151	73	S_1	339	59	S_3	346	32	S_1	18	62	S_2	240	29	C_{nor}

Domain A			Domain A			Domain C			Domain D			Domain E		
170	90	S_1	339	59	S_3	330	24	S_1	344	51	S_2	236	34	C_{nor}
169	89	S_1	324	28	S_3	334	32	S_1	345	56	S_2	299	58	C_{nor}
157	63	S_1	322	30	S_3	304	66	S_1	14	52	S_2	290	55	C_{nor}
149	75	S_1	347	48	S_3	94	78	S_1	19	49	S_2	313	55	C_{nor}
177	34	S_1	357	67	C_{dex}	301	65	S_1	49	30	S_2	304	56	C_{nor}
157	60	S_1	333	85	C_{dex}	297	67	S_1	325	53	S_2	283	49	C_{nor}
169	38	S_1	350	85	C_{dex}	319	59	S_1	10	57	S_2	276	44	C_{nor}
179	39	S_1	183	88	C_{dex}	316	64	S_1	330	45	S_2	211	32	C_{nor}
168	64	S_1	130	90	C_{dex}	316	65	S_1	10	46	S_2	221	36	C_{nor}
164	65	S_1	341	85	C_{dex}	294	45	S_1	30	51	S_2	205	48	C_{nor}
166	69	S_1	161	81	C_{dex}	285	47	S_1	330	69	S_2	235	38	C_{nor}
292	27	S_1	161	78	C_{dex}	275	52	S_1	353	75	S_2	207	22	C_{nor}
315	42	S_1	188	58	C_{dex}	281	48	S_1	25	50	S_2	213	25	C_{nor}
317	37	S_1	196	63	C_{dex}	291	62	S_1	326	55	S_2	169	43	C_{nor}
326	42	S_1	8	76	C_{dex}	332	61	S_1	339	81	S_2	192	24	C_{nor}
328	67	S_1	12	60	C_{dex}	332	68	S_1	30	69	S_2	177	38	C_{nor}
336	64	S_1	11	83	C_{dex}	328	67	S_1	16	63	S_2	57	29	C_{nor}
137	48	S_1	7	78	C_{dex}	310	65	S_1	27	70	S_2	82	48	C_{nor}
119	64	S_1	22	88	C_{dex}	311	42	S_1	179	78	S_2	244	18	C_{nor}
140	62	S_1	185	87	C_{dex}	310	54	S_1	19	70	S_2	1	53	C_{nor}
174	75	S_1	188	65	C_{dex}	314	65	S_1	4	75	S_2	25	16	C_{nor}
166	84	S_1	195	73	C_{dex}	337	77	S_1	186	86	S_2	348	38	C_{nor}
136	58	S_1	199	69	C_{dex}	299	61	S_1	355	79	S_2	81	36	C_{nor}
196	84	S_1	182	63	C_{dex}	316	78	S_1	352	90	S_2	108	27	C_{nor}
27	89	S_1	333	76	C_{dex}	322	55	S_1	180	87	S_2	84	30	C_{nor}
151	69	S_1	174	67	C_{dex}	324	61	S_1	18	76	S_2	98	42	C_{nor}
134	66	S_1	5	74	C_{dex}	308	54	S_1	159	35	S_2	140	32	C_{nor}
177	50	S_1	102	58	C_{dex}	313	37	S_1	170	49	S_2	176	22	C_{nor}
169	67	S_1	1	78	C_{dex}	321	62	S_1	177	35	S_2	188	17	C_{nor}
164	47	S_1	1	83	C_{dex}	311	56	S_1	158	38	S_2	56	19	C_{nor}
159	61	S_1	341	79	C_{dex}	321	59	S_1	134	24	S_2	291	42	C_{nor}
356	80	S_1	4	88	C_{dex}	307	62	S_1	128	38	S_2	290	40	C_{nor}
23	44	S_1	355	87	C_{dex}	315	40	S_1	43	43	S_2	171	13	C_{nor}
40	46	S_1	7	77	C_{dex}	303	39	S_1	36	36	S_2	300	34	C_{nor}
321	66	S_1	183	87	C_{dex}	291	49	S_1	38	35	S_2	259	34	C_{nor}
329	70	S_1	339	63	C_{dex}	307	59	S_1	23	44	S_2	296	52	C_{nor}
273	22	S_1	343	55	C_{dex}	299	52	S_1	189	54	C_{dex}	271	61	C_{nor}
302	20	S_1	162	82	C_{dex}	306	72	S_1	185	43	C_{dex}	307	42	C_{nor}
188	39	S_1	354	83	C_{dex}	307	70	S_1	182	48	C_{dex}	354	68	C_{nor}
196	40	S_1	321	57	C_{dex}	318	43	S_1	185	63	C_{dex}	325	72	C_{nor}
198	40	S_1	329	69	C_{dex}	337	47	S_1	183	65	C_{dex}	290	58	C_{nor}
195	48	S_1	9	67	C_{dex}	308	41	S_1	356	88	C_{dex}	319	26	C_{nor}
222	26	S_1	356	72	C_{dex}	315	48	S_1	174	90	C_{dex}	331	20	C_{nor}
195	36	S_1	182	80	C_{dex}	281	64	S_1	349	88	C_{dex}	265	58	C_{nor}
168	38	S_1	192	72	C_{dex}	54	64	S_1	0	84	C_{dex}	264	65	C_{nor}

Supporting Table 1: raw data of structural measurements

Domain A			Domain A			Domain C			Domain D			Domain E		
330	47	S_1	182	85	C_{dex}	319	54	S_1	171	58	C_{dex}	283	31	C_{nor}
332	54	S_1	330	68	C_{dex}	317	50	S_1	152	40	C_{dex}	294	48	C_{nor}
332	50	S_1	5	76	C_{dex}	329	45	S_1	31	58	C_{nor}	226	27	C_{nor}
356	40	S_1	182	83	C_{dex}	315	53	S_1	20	58	C_{nor}	217	38	C_{nor}
8	40	S_1	305	69	C_{dex}	313	55	S_1	7	35	C_{nor}	226	33	C_{nor}
330	57	S_1	136	88	C_{dex}	334	65	S_1	286	65	C_{nor}	226	28	C_{nor}
345	54	S_1	131	87	C_{dex}	332	41	S_1	321	42	C_{rev}	209	38	C_{nor}
11	42	S_1	247	52	C_{dex}	326	53	S_1	331	33	C_{rev}	274	52	C_{nor}
329	30	S_1	4	34	C_{dex}	334	36	S_1	38	46	C_{rev}	278	16	C_{nor}
344	39	S_1	314	65	C_{dex}	239	11	S_1	358	71	C_{sin}	320	50	C_{nor}
4	32	S_1	321	62	C_{dex}	1	26	S_1	163	77	C_{sin}	337	43	C_{nor}
355	32	S_1	339	76	C_{dex}	353	15	S_1	161	90	C_{sin}	231	28	C_{nor}
12	24	S_1	337	57	C_{dex}	274	29	S_1	169	80	C_{sin}	34	48	C_{nor}
342	49	S_1	4	66	C_{dex}	290	61	S_1	160	80	C_{sin}	330	21	C_{nor}
0	77	S_1	12	62	C_{dex}	296	55	S_1	335	83	C_{sin}	269	14	C_{nor}
351	70	S_1	32	30	C_{dex}	220	70	S_1	157	75	C_{sin}	343	74	C_{sin}
353	82	S_1	112	40	C_{dex}	229	68	S_1	145	82	C_{sin}	339	79	C_{sin}
0	75	S_1	357	86	C_{dex}	226	60	S_1	327	82	C_{sin}	346	74	C_{sin}
9	52	S_1	167	83	C_{dex}	316	37	S_1	328	80	C_{sin}	337	88	C_{sin}
346	67	S_1	8	76	C_{dex}	315	36	S_1	318	73	C_{sin}	8	48	C_{sin}
333	86	S_1	350	82	C_{dex}	321	81	S_1	319	66	C_{sin}	3	40	C_{sin}
334	54	S_1	334	77	C_{dex}	314	81	S_1	329	77	C_{sin}	10	56	C_{sin}
353	75	S_1	345	79	C_{dex}	321	89	S_1	327	67	C_{sin}	353	50	C_{sin}
333	47	S_1	340	84	C_{dex}	156	85	S_1	328	83	C_{sin}	353	48	C_{sin}
329	54	S_1	355	83	C_{dex}	119	68	S_1	164	76	C_{sin}	356	64	C_{sin}
147	31	S_1	350	85	C_{dex}	115	65	S_1	351	88	C_{sin}	330	60	C_{sin}
3	77	S_1	142	90	C_{dex}	107	74	S_1	333	77	C_{sin}	322	32	C_{sin}
145	75	S_1	172	88	C_{dex}	138	67	S_1	346	85	C_{sin}	325	41	C_{sin}
180	72	S_1	359	74	C_{dex}	119	62	S_1	130	89	C_{sin}	347	38	C_{sin}
161	73	S_1	324	71	C_{dex}	160	70	S_1	55	27	C_{sin}	278	75	C_{sin}
121	73	S_1	326	75	C_{dex}	195	10	S_1	340	34	C_{sin}	201	42	C_{sin}
340	60	S_1	165	88	C_{dex}	164	17	S_1	324	48	C_{sin}	199	45	C_{sin}
129	68	S_1	174	80	C_{dex}	224	14	S_1	335	50	C_{sin}	308	45	C_{sin}
129	67	S_1	180	88	C_{dex}	184	86	S_1	340	54	C_{sin}	297	58	C_{sin}
322	54	S_1	178	82	C_{dex}	15	72	S_1	352	34	C_{sin}	317	77	C_{sin}
322	44	S_1	338	90	C_{dex}	162	45	S_1	13	26	C_{sin}	301	55	C_{sin}
336	75	S_1	340	88	C_{dex}	331	57	S_1	26	32	C_{sin}	349	46	C_{sin}
330	86	S_1	215	74	C_{dex}	324	51	S_1	356	67	C_{sin}	100	36	C_{sin}
345	43	S_1	216	81	C_{dex}	204	87	S_1	351	58	C_{sin}	111	52	C_{sin}
351	60	S_1	215	52	C_{dex}	203	83	S_1	2	57	C_{sin}	90	61	C_{sin}
150	75	S_1	180	50	C_{dex}	201	88	S_1	352	84	C_{sin}	281	61	C_{sin}
152	75	S_1	133	24	C_{dex}	170	88	S_1	174	88	C_{sin}	46	43	C'_{dex}
152	74	S_1	126	30	C_{dex}	160	80	S_1	350	87	C_{sin}	36	46	C'_{dex}
299	50	S_1	132	32	C_{dex}	149	83	S_1	336	87	C_{sin}	23	60	C'_{dex}
280	44	S_1	229	68	C_{dex}	359	76	S_2	162	87	C_{sin}	52	43	C'_{dex}

Supporting Table 1: raw data of structural measurements

Domain A			Domain A			Domain C			Domain D			Domain E		
295	40	S_1	214	82	C_{dex}	345	70	S_2	358	45	C_{sin}	18	44	C'_{dex}
307	42	S_1	302	73	C_{dex}	349	87	S_2	12	50	C_{sin}	352	68	C'_{dex}
200	62	S_1	337	74	C_{dex}	352	72	S_2	336	68	C_{sin}	337	45	C'_{dex}
213	61	S_1	168	86	C_{dex}	352	58	S_2	333	65	C_{sin}	329	45	C'_{dex}
201	55	S_1	5	75	C_{dex}	335	55	S_2	340	75	C_{sin}	357	50	C'_{dex}
206	58	S_1	5	83	C_{dex}	257	70	S_2	340	68	C_{sin}	349	61	C'_{dex}
355	88	S_1	10	87	C_{dex}	233	78	S_2	38	46	C_{sin}	131	75	C'_{dex}
202	70	S_1	335	90	C_{dex}	228	78	S_2	166	77	C_{sin}	21	52	C'_{dex}
208	64	S_1	27	72	C_{dex}	211	84	S_2	175	77	C_{sin}	21	47	C'_{dex}
330	33	S_1	32	66	C_{dex}	208	86	S_2	42	68	C'_{dex}	17	42	C'_{dex}
144	64	S_1	158	78	C_{dex}	184	86	S_2	36	28	C'_{dex}	15	54	C'_{dex}
168	69	S_1	159	76	C_{dex}	77	72	S_2	22	65	C'_{dex}	10	64	C'_{dex}
218	41	S_1	14	75	C_{dex}	49	55	S_2	333	88	C'_{dex}	2	60	C'_{dex}
133	74	S_1	184	78	C_{dex}	47	54	S_2	173	77	C'_{dex}	352	68	C'_{rev}
21	34	S_1	35	89	C_{dex}	23	86	S_2	154	86	C'_{dex}	337	45	C'_{rev}
31	40	S_1	225	87	C_{dex}	16	87	S_2	336	85	C'_{dex}	329	45	C'_{rev}
159	39	S_1	225	84	C_{dex}	15	58	S_2	337	79	C'_{dex}	305	80	C'_{nor}
161	38	S_1	7	73	C_{dex}	15	70	S_2	165	85	C'_{dex}	293	31	C'_{nor}
11	72	S_1	18	80	C_{dex}	15	80	S_2	175	67	C'_{dex}	359	60	C'_{nor}
358	76	S_1	346	84	C_{dex}	14	50	S_2	191	69	C'_{dex}	356	58	C'_{nor}
156	58	S_1	198	90	C_{dex}	13	75	S_2	5	90	C'_{dex}	338	57	C'_{nor}
332	90	S_1	336	81	C_{dex}	12	65	S_2	352	72	C'_{dex}	337	55	C'_{nor}
4	65	S_1	336	86	C_{dex}	10	54	S_2	12	54	C'_{dex}	333	55	C'_{nor}
191	51	S_1	172	71	C_{dex}	10	81	S_2	148	64	C'_{dex}	314	57	C'_{nor}
62	3	S_1	161	72	C_{dex}	6	66	S_2	157	54	C'_{dex}	303	68	C'_{nor}
350	75	S_1	17	46	C_{dex}	2	86	S_2	149	54	C'_{dex}	281	71	C'_{nor}
8	54	S_1	357	58	C_{dex}	165	52	S_2	41	84	C'_{dex}	278	75	C'_{nor}
1	54	S_1	5	89	C_{dex}	165	88	S_2	28	84	C'_{dex}	344	61	C'_{nor}
16	77	S_1	184	84	C_{dex}	167	76	S_2	80	45	C'_{dex}	312	83	C'_{nor}
165	90	S_1	329	69	C_{dex}	170	77	S_2	20	52	C'_{dex}	305	54	C'_{nor}
342	67	S_1	339	65	C_{dex}	176	83	S_2	50	67	C'_{dex}	304	49	C'_{nor}
330	83	S_1	356	80	C_{dex}	246	25	S_2	46	53	C'_{dex}	299	70	C'_{nor}
163	81	S_1	341	85	C_{dex}	239	29	S_2	70	84	C'_{dex}	298	58	C'_{nor}
176	87	S_1	20	75	C_{dex}	226	24	S_2	50	75	C'_{dex}	291	45	C'_{nor}
183	83	S_1	20	56	C_{dex}	226	25	S_2	163	88	C'_{dex}	283	55	C'_{nor}
187	87	S_1	14	68	C_{dex}	210	20	S_2	165	84	C'_{dex}	276	43	C'_{nor}
342	67	S_1	208	89	C_{dex}	203	29	S_2	188	85	C'_{dex}	273	40	C'_{nor}
333	78	S_1	208	80	C_{dex}	199	42	S_2	163	89	C'_{dex}	267	44	C'_{nor}
325	42	S_1	210	88	C_{dex}	193	29	S_2	172	87	C'_{dex}	233	23	C'_{nor}
163	63	S_1	358	72	C_{dex}	191	49	S_2	174	64	C'_{dex}	322	50	C'_{nor}
172	85	S_1	358	80	C_{dex}	11	48	S_2	178	60	C'_{dex}	318	32	C'_{nor}
176	84	S_1	7	89	C_{dex}	317	46	S_2	177	56	C'_{dex}	317	29	C'_{nor}
351	85	S_1	212	80	C_{dex}	297	46	S_2	175	64	C'_{dex}	311	64	C'_{nor}
349	82	S_1	171	76	C_{dex}	295	40	S_2	185	67	C'_{dex}	299	55	C'_{nor}
165	87	S_1	175	55	C_{dex}	302	38	S_2	195	70	C'_{dex}	295	46	C'_{nor}

Supporting Table 1: raw data of structural measurements

Domain A			Domain A			Domain C			Domain D			Domain E		
325	84	S_1	29	56	C_{dex}	349	59	S_2	202	68	C'_{dex}	289	68	C'_{nor}
166	64	S_1	45	69	C_{dex}	349	65	S_2	39	69	C'_{dex}	284	75	C'_{nor}
145	80	S_1	27	87	C_{dex}	341	67	S_2	40	77	C'_{dex}	284	55	C'_{nor}
318	75	S_2	212	63	C_{dex}	338	66	S_2	24	72	C'_{dex}	282	41	C'_{nor}
330	76	S_2	234	72	C_{dex}	334	64	S_2	212	86	C'_{dex}	282	61	C'_{nor}
357	87	S_2	207	60	C_{dex}	333	50	S_2	187	90	C'_{dex}	280	65	C'_{nor}
359	90	S_2	229	83	C_{dex}	332	54	S_2	6	81	C'_{dex}	276	64	C'_{nor}
170	88	S_2	234	79	C_{dex}	331	60	S_2	16	75	C'_{dex}	274	78	C'_{nor}
331	68	S_2	193	78	C_{dex}	321	55	S_2	29	84	C'_{dex}	270	64	C'_{nor}
356	79	S_2	185	76	C_{dex}	294	76	S_2	31	74	C'_{dex}	268	58	C'_{nor}
356	82	S_2	342	68	C_{dex}	292	21	S_2	192	43	C'_{dex}	266	38	C'_{nor}
330	84	S_2	343	86	C_{dex}	291	51	S_2	196	49	C'_{dex}	266	46	C'_{nor}
343	76	S_2	172	76	C_{dex}	290	48	S_2	234	33	C'_{dex}	265	38	C'_{nor}
188	82	S_2	187	86	C_{dex}	290	75	S_2	247	33	C'_{dex}	264	46	C'_{nor}
344	84	S_2	357	80	C_{dex}	289	55	S_2	263	25	C'_{dex}	264	29	C'_{nor}
337	72	S_2	348	80	C_{dex}	289	64	S_2	210	39	C'_{dex}	264	65	C'_{nor}
340	86	S_2	343	81	C_{dex}	289	24	S_2	198	25	C'_{dex}	263	44	C'_{nor}
345	90	S_2	220	78	C_{dex}	288	23	S_2	187	20	C'_{dex}	260	42	C'_{nor}
168	84	S_2	13	74	C_{dex}	287	72	S_2	189	54	C'_{dex}	260	68	C'_{nor}
172	88	S_2	14	70	C_{dex}	280	75	S_2	185	43	C'_{dex}	259	61	C'_{nor}
333	87	S_2	141	84	C_{dex}	276	63	S_2	182	48	C'_{dex}	259	82	C'_{nor}
324	86	S_2	172	88	C_{dex}	276	77	S_2	185	63	C'_{dex}	256	28	C'_{nor}
335	89	S_2	8	55	C_{dex}	276	64	S_2	183	65	C'_{dex}	250	38	C'_{nor}
351	76	S_2	9	67	C_{dex}	275	68	S_2	24	80	C'_{dex}	250	43	C'_{nor}
350	74	S_2	18	63	C_{dex}	274	53	S_2	32	85	C'_{dex}	250	42	C'_{nor}
337	75	S_2	12	90	C_{dex}	274	64	S_2	32	80	C'_{dex}	250	46	C'_{nor}
310	78	S_2	180	77	C_{dex}	268	23	S_2	31	81	C'_{dex}	246	41	C'_{nor}
354	84	S_2	4	81	C_{dex}	266	38	S_2	32	70	C'_{dex}	244	55	C'_{nor}
325	81	S_2	343	85	C_{dex}	266	24	S_2	220	81	C'_{dex}	238	35	C'_{nor}
327	88	S_2	2	86	C_{dex}	264	34	S_2	237	89	C'_{dex}	235	54	C'_{nor}
338	84	S_2	198	76	C_{dex}	250	39	S_2	40	66	C'_{dex}	216	48	C'_{nor}
340	80	S_2	2	82	C_{dex}	246	44	S_2	179	38	C'_{nor}	212	44	C'_{nor}
344	85	S_2	205	84	C_{dex}	245	30	S_2	178	36	C'_{nor}	211	58	C'_{nor}
166	82	S_2	41	81	C_{dex}	89	84	S_2	124	24	C'_{nor}	201	64	C'_{nor}
165	85	S_2	29	74	C_{dex}	98	84	S_2	254	42	C'_{nor}	116	24	C'_{nor}
358	78	S_2	31	70	C_{dex}	103	44	S_2	244	54	C'_{nor}	267	58	C'_{nor}
338	85	S_2	3	78	C_{dex}	107	87	S_2	224	52	C'_{nor}	259	64	C'_{nor}
0	80	S_2	358	70	C_{dex}	108	49	S_2	223	69	C'_{nor}	247	38	C'_{nor}
345	79	S_2	326	42	C_{nor}	109	85	S_2	96	65	C'_{nor}	239	59	C'_{nor}
335	84	S_2	308	34	C_{nor}	112	72	S_2	349	74	C'_{rev}	232	39	C'_{nor}
340	86	S_2	307	41	C_{nor}	114	71	S_2	348	77	C'_{rev}	184	64	C'_{nor}
350	80	S_2	305	37	C_{nor}	115	75	S_2	44	68	C'_{rev}	220	27	C'_{nor}
345	76	S_2	161	61	C_{nor}	118	68	S_2	51	74	C'_{rev}	201	26	C'_{nor}
335	82	S_2	161	65	C_{nor}	119	85	S_2	41	69	C'_{rev}	323	39	C'_{nor}
344	87	S_2	105	88	C_{nor}	120	82	S_2	40	67	C'_{rev}	319	37	C'_{nor}

Supporting Table 1: raw data of structural measurements

Domain A			Domain A			Domain C			Domain D			Domain E		
0	84	S_2	322	72	C_{nor}	124	55	S_2	0	46	C'_{sin}	318	54	C'_{nor}
358	79	S_2	100	81	C_{nor}	126	86	S_2	7	58	C'_{sin}	314	60	C'_{nor}
163	86	S_2	155	49	C_{nor}	128	90	S_2	301	65	C'_{sin}	304	59	C'_{nor}
169	84	S_2	245	14	C_{nor}	129	55	S_2	106	87	C'_{sin}	283	38	C'_{nor}
167	82	S_2	224	35	C_{nor}	135	89	S_2	107	77	C'_{sin}	42	44	C'_{nor}
352	88	S_2	294	64	C_{nor}	140	78	S_2	28	50	C'_{sin}	37	48	C'_{nor}
340	77	S_2	268	41	C_{nor}	141	75	S_2	101	68	C'_{sin}	40	40	C'_{nor}
355	84	S_2	70	49	C_{nor}	142	85	S_2	107	67	C'_{sin}	24	51	C'_{nor}
358	75	S_2	44	55	C_{nor}	146	88	S_2	337	85	C'_{sin}	19	54	C'_{nor}
155	86	S_2	276	72	C_{nor}	150	86	S_2	346	90	C'_{sin}	94	37	C'_{nor}
344	85	S_2	296	57	C_{nor}	151	72	S_2	74	52	C'_{sin}	76	45	C'_{nor}
160	89	S_2	279	53	C_{nor}	152	79	S_2	141	76	C'_{sin}	45	45	C'_{nor}
6	74	S_2	263	53	C_{nor}	155	87	S_2	129	78	C'_{sin}	46	43	C'_{nor}
175	88	S_2	254	65	C_{nor}	162	87	S_2	137	89	C'_{sin}	36	46	C'_{nor}
337	88	S_2	140	15	C_{nor}	163	86	S_2	300	74	C'_{sin}	23	60	C'_{nor}
167	82	S_2	152	19	C_{nor}	265	88	S_2	132	87	C'_{sin}	52	43	C'_{nor}
355	73	S_2	164	31	C_{nor}	272	72	S_2	128	80	C'_{sin}	18	44	C'_{nor}
338	75	S_2	310	42	C_{nor}	295	40	S_2	291	82	C'_{sin}	157	48	C'_{rev}
336	86	S_2	354	46	C_{nor}	297	76	S_2	298	75	C'_{sin}	83	43	C'_{rev}
345	81	S_2	333	61	C_{nor}	297	46	S_2	283	53	C'_{sin}	332	76	C'_{sin}
2	82	S_2	6	79	C_{nor}	299	85	S_2	284	64	C'_{sin}	327	72	C'_{sin}
335	72	S_2	160	55	C_{nor}	300	64	S_2	308	90	C'_{sin}	327	63	C'_{sin}
342	65	S_2	140	58	C_{nor}	302	38	S_2	309	87	C'_{sin}	321	67	C'_{sin}
341	82	S_2	346	66	C_{nor}	306	83	S_2	127	88	C'_{sin}	317	64	C'_{sin}
351	81	S_2	175	85	C_{nor}	306	80	S_2	131	89	C'_{sin}	316	90	C'_{sin}
349	66	S_2	345	76	C_{nor}	308	73	S_2	133	86	C'_{sin}	314	70	C'_{sin}
346	77	S_2	349	80	C_{nor}	308	34	S_2	302	78	C'_{sin}	314	66	C'_{sin}
358	88	S_2	353	84	C_{nor}	308	81	S_2	303	90	C'_{sin}	312	75	C'_{sin}
342	80	S_2	292	33	C_{nor}	308	70	S_2	342	85	C'_{sin}	308	74	C'_{sin}
134	86	S_2	304	27	C_{nor}	308	80	S_2	2	86	C'_{sin}	304	68	C'_{sin}
0	82	S_2	294	28	C_{nor}	309	88	S_2	346	79	C'_{sin}	304	67	C'_{sin}
347	89	S_2	288	32	C_{nor}	310	66	S_2	148	89	C'_{sin}	301	85	C'_{sin}
355	83	S_2	288	21	C_{nor}	310	86	S_2	76	43	C'_{sin}	300	70	C'_{sin}
3	90	S_2	327	25	C_{nor}	310	78	S_2	317	55	C'_{sin}	298	75	C'_{sin}
334	84	S_2	288	30	C_{nor}	311	88	S_2	327	81	C'_{sin}	288	80	C'_{sin}
341	76	S_2	302	20	C_{nor}	312	72	S_2	341	82	C'_{sin}	286	85	C'_{sin}
315	65	S_2	323	35	C_{nor}	312	86	S_2	326	76	C'_{sin}	286	81	C'_{sin}
357	72	S_2	248	24	C_{nor}	313	72	S_2	305	72	C'_{sin}	178	52	C'_{sin}
335	82	S_2	181	50	C_{nor}	317	52	S_2	298	87	C'_{sin}	175	57	C'_{sin}
166	86	S_2	343	34	C_{rev}	317	46	S_2	144	87	C'_{sin}	174	82	C'_{sin}
167	89	S_2	347	47	C_{rev}	318	62	S_2	148	90	C'_{sin}	165	55	C'_{sin}
351	82	S_2	357	38	C_{rev}	318	74	S_2	139	74	C'_{sin}	147	87	C'_{sin}
175	89	S_2	326	87	C_{rev}	321	71	S_2	288	90	C'_{sin}	139	72	C'_{sin}
162	85	S_2	337	85	C_{rev}	321	80	S_2	125	80	C'_{sin}	139	70	C'_{sin}
337	90	S_2	335	81	C_{rev}	322	73	S_2	103	90	C'_{sin}	135	57	C'_{sin}

Supporting Table 1: raw data of structural measurements

Domain A			Domain A			Domain C			Domain D			Domain E		
166	87	S_2	138	98	C_{rev}	323	78	S_2	136	72	C'_{sin}	118	78	C'_{sin}
336	75	S_2	142	81	C_{rev}	325	78	S_2	137	68	C'_{sin}	114	81	C'_{sin}
162	82	S_2	320	85	C_{rev}	325	78	S_2	126	78	C'_{sin}	105	75	C'_{sin}
170	82	S_2	349	85	C_{rev}	325	71	S_2	305	83	C'_{sin}	96	84	C'_{sin}
355	75	S_2	351	85	C_{rev}	326	77	S_2	307	88	C'_{sin}	87	77	C'_{sin}
358	77	S_2	346	71	C_{rev}	326	86	S_2	304	84	C'_{sin}	40	82	C'_{sin}
342	82	S_2	334	65	C_{rev}	326	88	S_2	326	62	C'_{sin}	32	75	C'_{sin}
324	86	S_2	135	48	C_{rev}	326	75	S_2	318	56	C'_{sin}	5	63	C'_{sin}
337	83	S_2	153	36	C_{rev}	326	86	S_2	302	75	C'_{sin}	2	67	C'_{sin}
156	83	S_2	326	81	C_{rev}	328	80	S_2	310	77	C'_{sin}	273	17	L_1
166	87	S_2	355	85	C_{rev}	329	85	S_2	288	75	C'_{sin}	93	6	L_1
342	89	S_2	353	72	C_{rev}	329	54	S_2	307	70	C'_{sin}	236	9	L_1
345	80	S_2	337	72	C_{rev}	330	90	S_2	274	38	C'_{sin}	62	5	L_1
343	75	S_2	335	75	C_{rev}	330	86	S_2	295	31	C'_{sin}	50	3	L_1
350	90	S_2	304	67	C_{rev}	330	84	S_2	292	31	C'_{sin}	73	35	L_1
348	84	S_2	311	45	C_{rev}	330	89	S_2	291	34	C'_{sin}	222	32	L_1
162	85	S_2	314	45	C_{rev}	332	69	S_2	286	25	C'_{sin}	235	43	L_1
334	78	S_2	334	51	C_{rev}	332	84	S_2	294	30	C'_{sin}	254	35	L_1
155	83	S_2	334	52	C_{rev}	334	69	S_2	296	32	C'_{sin}	253	37	L_1
350	88	S_2	302	55	C_{rev}	334	82	S_2	320	57	C'_{sin}	233	47	L_1
175	84	S_2	303	52	C_{rev}	335	82	S_2	312	57	C'_{sin}	230	46	L_1
165	83	S_2	9	67	C_{rev}	335	79	S_2	330	73	C'_{sin}	289	3	L_1
341	90	S_2	12	63	C_{rev}	337	74	S_2	139	89	C'_{sin}	264	24	L_1
343	75	S_2	18	53	C_{rev}	342	74	S_2	309	80	C'_{sin}	253	34	L_1
155	85	S_2	157	70	C_{sin}	342	87	S_2	328	86	C'_{sin}	254	45	L_1
0	90	S_2	167	63	C_{sin}	150	75	C_{dex}	309	88	C'_{sin}	236	18	L_1
151	88	S_2	343	82	C_{sin}	153	71	C_{dex}	308	90	C'_{sin}	245	24	L_1
152	85	S_2	345	88	C_{sin}	178	68	C_{dex}	344	77	AP_1	239	15	L_1
358	86	S_2	342	72	C_{sin}	156	68	C_{dex}	12	55	AP_1	229	21	L_1
358	90	S_2	354	84	C_{sin}	355	70	C_{dex}	39	45	AP_1	219	30	L_1
0	79	S_2	188	88	C_{sin}	338	68	C_{dex}	32	22	AP_1	279	7	L_1
330	84	S_2	2	90	C_{sin}	131	67	C_{dex}	245	46	AP_1	109	7	L_1
334	81	S_2	139	89	C_{sin}	123	52	C_{dex}	222	50	AP_1	285	47	L_1
334	81	S_2	338	89	C_{sin}	138	30	C_{dex}	322	28	AP_1	97	24	L_1
350	83	S_2	332	89	C_{sin}	141	28	C_{dex}	27	15	AP_1	282	11	L_1
354	89	S_2	333	82	C_{sin}	135	34	C_{dex}	39	22	AP_1	262	12	L_1
150	79	S_2	333	79	C_{sin}	105	76	C_{dex}	42	25	AP_1	252	19	L_1
325	90	S_2	335	81	C_{sin}	288	86	C_{dex}	164	30	AP_1	263	6	L_1
170	84	S_2	145	87	C_{sin}	324	68	C_{dex}	134	39	AP_1	277	39	L_1
154	88	S_2	144	88	C_{sin}	326	60	C_{dex}	341	29	AP_1	274	19	L_1
342	75	S_2	172	79	C_{sin}	319	58	C_{dex}	32	75	AP_2	271	23	L_1
325	88	S_2	152	74	C_{sin}	345	70	C_{dex}	38	73	AP_2	268	10	L_1
170	71	S_2	152	77	C_{sin}	353	73	C_{dex}	175	82	AP_2	285	25	L_1
349	87	S_2	154	84	C_{sin}	36	36	C_{dex}	356	82	AP_2	329	27	L_1
178	77	S_2	148	85	C_{sin}	76	25	C_{dex}	132	78	AP_2	87	1	L_1

Domain A			Domain A			Domain C			Domain D			Domain E		
157	87	S_2	151	85	C_{sin}	5	65	C_{dex}	148	60	AP_2	252	25	L_2
349	80	S_2	137	71	C_{sin}	16	53	C_{dex}	298	70	AP_2	269	7	L_2
342	88	S_2	139	75	C_{sin}	50	42	C_{dex}	319	32	AP_2	102	20	L_2
346	84	S_2	149	80	C_{sin}	34	48	C_{dex}	106	88	AP_2	72	4	L_2
166	84	S_2	148	74	C_{sin}	289	70	C_{nor}	105	81	AP_2	84	7	L_2
158	85	S_2	168	86	C_{sin}	1	64	C_{nor}	124	84	AP_2	276	23	L_2
175	84	S_2	325	81	C_{sin}	359	69	C_{nor}	309	87	AP_2	271	34	L_2
175	56	S_2	329	81	C_{sin}	22	55	C_{nor}	146	77	AP_2	201	53	L_2
333	84	S_2	324	83	C_{sin}	18	45	C_{nor}	145	42	AP_2	184	59	L_2
2	83	S_2	155	77	C_{sin}	19	54	C_{nor}	319	78	AP_2	203	59	L_2
353	80	S_2	170	84	C_{sin}	22	66	C_{nor}	7	47	AP_2	235	22	L_2
315	66	S_2	148	86	C_{sin}	329	75	C_{nor}	15	27	AP_2	238	29	L_2
348	78	S_2	339	84	C_{sin}	317	86	C_{nor}	347	64	AP_2	78	18	L_2
320	71	S_2	340	80	C_{sin}	30	53	C_{nor}	168	85	AP_2	274	1	L_2
356	89	S_2	340	84	C_{sin}	20	45	C_{nor}	166	62	AP_2	260	48	L_2
358	85	S_2	338	64	C_{sin}	305	45	C_{nor}	328	70	AP_2	254	36	L_2
315	64	S_2	339	74	C_{sin}	267	72	C_{nor}	335	78	AP_2	262	18	L_{sin}
8	89	S_2	338	76	C_{sin}	265	75	C_{nor}	157	89	AP_2	254	19	L_{sin}
350	74	S_2	328	62	C_{sin}	13	48	C_{nor}	343	83	AP_2	260	30	L_{sin}
164	85	S_2	345	85	C_{sin}	347	37	C_{nor}	7	84	AP_2	252	44	L_{sin}
337	89	S_2	18	85	C_{sin}	348	65	C_{nor}	171	76	AP_2	212	32	L_{sin}
5	89	S_2	11	85	C_{sin}	350	55	C_{nor}	344	90	AP_2	261	7	L_{nor}
359	80	S_2	9	83	C_{sin}	138	83	C_{rev}	346	81	AP_2	247	16	L_{nor}
180	80	S_2	4	82	C_{sin}	355	77	C_{rev}	194	76	AP_2	240	13	L_{nor}
348	83	S_2	8	79	C_{sin}	108	88	C_{rev}	11	89	AP_2	247	16	L_{nor}
345	80	S_2	6	87	C_{sin}	296	86	C_{rev}	219	85	AP_2	238	10	L_{nor}
165	80	S_2	7	58	C_{sin}	223	73	C_{rev}	203	73	AP_2	268	5	L_{nor}
335	80	S_2	357	43	C_{sin}	308	85	C_{rev}	199	74	AP_2	273	4	L_{nor}
186	78	S_2	26	40	C_{sin}	333	89	C_{rev}	211	74	AP_2	355	32	L_{nor}
350	88	S_2	345	55	C_{sin}	119	77	C_{rev}	189	85	AP_2	261	3	FA_1
355	85	S_2	338	46	C_{sin}	117	80	C_{rev}	330	78	AP_2	276	2	FA_1
344	90	S_2	339	69	C_{sin}	305	87	C_{rev}	169	74	AP_2	270	3	FA_1
335	89	S_2	323	68	C_{sin}	135	82	C_{rev}	343	79	AP_2	270	2	FA_1
161	89	S_2	326	42	C_{sin}	318	88	C_{rev}	352	82	AP_2	276	29	FA_1
350	86	S_2	308	34	C_{sin}	324	86	C_{rev}	6	60	AP_2	284	9	FA_1
167	79	S_2	307	41	C_{sin}	211	90	C_{rev}	13	38	AP_2	254	3	FA_1
149	80	S_2	305	37	C_{sin}	186	70	C_{rev}	352	46	AP_2	86	17	FA_1
146	88	S_2	152	80	C_{sin}	183	66	C_{rev}	358	51	AP_2	269	6	FA_1
158	75	S_2	156	80	C_{sin}	348	75	C_{rev}	182	86	AP_2	255	19	FA_1
144	67	S_2	322	90	C_{sin}	181	85	C_{rev}	164	87	AP_2	257	19	FA_1
355	88	S_2	148	84	C_{sin}	123	68	C_{rev}	179	86	AP_2	267	44	FA_1
159	88	S_2	158	81	C_{sin}	111	84	C_{rev}	61	89	AP_2	272	27	FA_1
152	82	S_2	140	80	C_{sin}	295	15	C_{rev}	208	82	AP_2	260	11	FA_1
165	71	S_2	150	70	C_{sin}	303	31	C_{rev}	196	74	AP_2	247	18	FA_1
336	81	S_2	330	88	C_{sin}	292	81	C_{sin}	170	88	AP_2	285	14	FA_1

Domain A			Domain A			Domain C			Domain D			Domain E		
176	87	S_2	338	70	C_{sin}	304	86	C_{sin}	180	90	AP_2	260	11	FA_1
347	73	S_2	340	90	C_{sin}	296	79	C_{sin}	10	84	AP_2	247	18	FA_1
151	80	S_2	340	75	C_{sin}	335	48	C_{sin}	178	80	AP_2	253	19	FA_2
180	72	S_2	161	82	C_{sin}	318	50	C_{sin}	170	78	AP_2	265	8	FA_2
174	87	S_2	148	87	C_{sin}	327	50	C_{sin}	175	73	AP_2	291	14	FA_2
162	88	S_2	311	73	C_{sin}	334	90	C_{sin}	180	75	AP_2	277	15	FA_2
354	71	S_2	168	68	C_{sin}	315	75	C_{sin}	355	88	AP_2	254	22	FA_2
180	72	S_2	154	67	C_{sin}	157	80	C_{sin}	171	80	AP_2	278	3	FA_2
344	70	S_2	154	72	C_{sin}	164	89	C_{sin}	342	88	AP_2	276	4	FA_2
153	70	S_2	155	73	C_{sin}	140	85	C_{sin}	175	90	AP_2	252	38	FA_2
152	67	S_2	154	78	C_{sin}	274	51	C_{sin}	47	64	AP_2	84	14	FA_2
168	69	S_2	144	80	C_{sin}	250	30	C_{sin}	162	80	AP_2	266	7	FA_2
168	82	S_2	134	88	C_{sin}	279	71	C_{sin}	190	90	AP_2	85	2	FA_2
335	86	S_2	139	87	C_{sin}	306	39	C_{sin}	10	90	AP_2	270	11	FA_2
337	85	S_2	133	77	C_{sin}	293	45	C_{sin}	330	90	AP_2	270	7	FA_2
344	79	S_2	176	77	C_{sin}	287	50	C_{sin}	148	84	AP_2	265	7	FA_2
346	78	S_2	169	82	C_{sin}	251	60	C_{sin}	323	90	AP_2	276	4	FA_2
342	80	S_2	164	75	C_{sin}	88	90	C_{sin}	183	45	AP_2	72	5	FA_2
342	82	S_2	156	73	C_{sin}	260	79	C_{sin}	191	89	AP_2	94	4	FA_2
340	87	S_2	322	86	C_{sin}	266	85	C_{sin}	220	88	AP_2	80	6	FA_2
355	88	S_2	172	90	C_{sin}	264	73	C_{sin}	252	76	AP_2	117	7	FA_2
178	87	S_2	140	81	C_{sin}	268	78	C_{sin}	263	52	AP_2	278	10	FA_2
312	85	S_2	132	80	C_{sin}	262	74	C_{sin}	261	64	AP_2	276	23	FA_2
156	85	S_2	165	85	C_{sin}	132	48	C_{sin}	14	79	AP_2	86	7	FA_2
320	60	S_2	137	75	C_{sin}	133	54	C_{sin}	357	55	AP_2	110	8	FA_2
350	81	S_2	311	85	C_{sin}	146	60	C_{sin}	346	58	AP_2	115	12	FA_2
345	84	S_2	137	68	C_{sin}	119	51	C_{sin}	232	32	AP_2	87	18	FA_2
338	86	S_2	149	72	C_{sin}	121	49	C_{sin}	242	48	AP_2	105	19	FA_2
323	87	S_2	138	73	C_{sin}	334	82	C_{sin}	268	55	AP_2	95	14	FA_2
340	86	S_2	153	62	C_{sin}	325	90	C_{sin}	86	78	AP_4	299	24	FA_2
164	80	S_2	150	49	C_{sin}	337	55	C_{sin}	91	69	AP_4	122	21	FA_2
142	75	S_2	140	76	C_{sin}	346	76	C_{sin}	281	90	AP_4	301	27	FA_2
165	90	S_2	131	77	C_{sin}	331	72	C_{sin}	94	82	AP_4	91	2	FA_2
358	83	S_2	142	84	C_{sin}	342	76	C_{sin}	92	79	AP_4	262	11	FA_2
302	75	S_2	142	77	C_{sin}	334	80	C_{sin}	308	84	AP_4	267	12	FA_2
160	90	S_2	142	75	C_{sin}	158	88	C_{sin}	132	82	AP_4	277	13	FA_2
331	70	S_2	154	83	C_{sin}	311	86	C_{sin}	158	77	AP_4	274	18	FA_2
338	80	S_2	148	83	C_{sin}	326	73	C_{sin}	231	58	AP_4	266	18	FA_2
341	85	S_2	135	72	C_{sin}	314	72	C_{sin}	108	74	AP_4	272	7	FA_2
333	55	S_2	135	65	C_{sin}	318	58	C_{sin}	79	82	AP_4	108	13	FA_2
332	50	S_2	147	90	C_{sin}	155	77	C_{sin}	252	74	AP_4	101	23	FA_2
337	65	S_2	331	88	C_{sin}	130	72	C_{sin}	111	78	AP_4	245	35	FA_2
357	88	S_2	335	70	C_{sin}	142	69	C_{sin}	93	85	AP_4	97	9	FA_2
158	90	S_2	339	74	C_{sin}	266	74	C_{sin}	112	90	AP_4	94	6	FA_2
334	89	S_2	326	80	C_{sin}	260	75	C_{sin}	126	83	AP_4	323	30	FA_2

Domain A			Domain A			Domain C			Domain D			Domain E		
338	83	S_2	148	85	C_{sin}	274	80	C_{sin}	116	88	AP_4	321	25	FA_2
0	85	S_2	336	87	C_{sin}	114	71	C_{sin}	133	88	AP_4	78	23	FA_2
155	86	S_2	159	77	C_{sin}	125	78	C_{sin}	142	84	AP_4	113	17	FA_2
152	87	S_2	174	74	C_{sin}	117	84	C_{sin}	324	65	AP_4	250	5	FA_2
154	90	S_2	159	72	C_{sin}	100	86	C_{sin}	103	82	AP_4	260	28	FA_2
171	69	S_2	354	74	C_{sin}	79	89	C_{sin}	130	32	FA_1	320	52	FA_2
167	65	S_2	345	75	C_{sin}	303	62	C_{sin}	103	32	FA_1	279	22	FA_2
136	81	S_2	185	85	C_{sin}	298	68	C_{sin}	335	38	FA_1	2	9	FA_2
332	86	S_2	0	74	C_{sin}	312	77	C_{sin}	349	36	FA_1	279	21	FA_2
337	87	S_2	2	72	C_{sin}	312	77	C_{sin}	71	14	FA_1	280	21	FA_2
344	68	S_2	4	82	C_{sin}	298	82	C_{sin}	65	11	FA_1	307	43	FA_2
171	56	S_2	164	87	C_{sin}	332	59	C_{sin}	74	20	FA_1	307	18	FA_2
160	61	S_2	151	87	C_{sin}	322	38	C_{sin}	100	20	FA_1	301	26	FA_2
172	69	S_2	149	73	C_{sin}	293	70	C_{sin}	124	1	FA_2	306	33	FA_2
328	82	S_2	151	90	C_{sin}	303	77	C_{sin}	303	7	FA_2	300	38	FA_2
333	82	S_2	144	86	C_{sin}	324	76	C_{sin}	91	46	FA_2	292	16	FA_2
340	82	S_2	325	82	C_{sin}	320	75	C_{sin}	88	50	FA_2	294	30	FA_2
180	90	S_2	330	85	C_{sin}	316	84	C_{sin}	226	1	FA_2	285	17	FA_2
135	88	S_2	331	85	C_{sin}	300	85	C_{sin}	225	2	FA_2	296	17	FA_2
142	56	S_2	349	81	C_{sin}	272	84	C_{sin}	48	25	FA_2	307	22	FA_2
139	74	S_2	324	85	C_{sin}	318	83	C_{sin}	110	29	FA_2	298	26	FA_2
161	76	S_2	342	70	C_{sin}	316	85	C_{sin}	56	18	FA_2	357	28	FA_2
155	71	S_2	341	77	C_{sin}	108	90	C_{sin}	38	21	FA_2	4	9	FA_2
153	62	S_2	336	76	C_{sin}	296	86	C_{sin}	74	28	FA_2	278	17	FA_2
168	68	S_2	343	84	C_{sin}	5	52	C'_{dex}	264	5	FA_2	269	24	FA_2
153	83	S_2	165	86	C_{sin}	29	45	C'_{dex}	254	3	FA_2	271	18	FA_2
349	72	S_2	331	82	C_{sin}	37	60	C'_{dex}	252	7	FA_2	233	44	FA_2
169	82	S_2	322	74	C_{sin}	57	53	C'_{dex}	79	8	FA_2	274	42	FA_2
358	90	S_2	320	72	C_{sin}	226	77	C'_{dex}	167	22	FA_2	269	53	FA_2
1	88	S_2	345	72	C_{sin}	17	83	C'_{dex}	62	73	FA_2	256	9	FA_2
155	89	S_2	344	77	C_{sin}	216	63	C'_{dex}	84	74	FA_2	256	33	FA_2
351	87	S_2	157	83	C_{sin}	195	64	C'_{dex}	281	37	FA_2	240	47	FA_2
347	79	S_2	153	90	C_{sin}	0	80	C'_{dex}	270	38	FA_2	254	35	FA_2
351	83	S_2	334	83	C_{sin}	357	85	C'_{dex}	135	74	FA_2	244	39	FA_2
350	80	S_2	155	83	C_{sin}	349	48	C'_{dex}	146	66	FA_2	206	43	FA_2
355	85	S_2	152	90	C_{sin}	41	55	C'_{dex}	132	74	FA_2	85	12	FA_2
188	58	S_2	156	77	C_{sin}	22	55	C'_{dex}	188	77	FA_2	286	4	FA_2
346	87	S_2	153	78	C_{sin}	258	48	C'_{dex}	260	7	FA_2	294	27	FA_2
355	75	S_2	168	87	C_{sin}	183	78	C'_{dex}	86	10	FA_2	304	22	FA_2
353	79	S_2	158	68	C_{sin}	176	76	C'_{dex}	287	14	FA_2	267	41	FA_2
352	80	S_2	161	67	C_{sin}	208	68	C'_{dex}	118	0	FA_2	263	28	FA_2
3	69	S_2	139	76	C_{sin}	191	70	C'_{dex}	270	10	FA_2	272	13	FA_2
357	75	S_2	131	79	C_{sin}	14	65	C'_{dex}	275	7	FA_2	280	6	FA_2
4	67	S_2	134	65	C_{sin}	7	72	C'_{dex}	265	30	FA_2	287	11	FA_2
3	74	S_2	340	86	C_{sin}	139	74	C'_{dex}	262	27	FA_2	269	5	FA_2

Domain A			Domain A			Domain C			Domain D			Domain E		
6	81	S_2	155	87	C_{sin}	146	81	C'_{dex}	267	20	FA_2	288	32	FA_2
357	71	S_2	335	75	C_{sin}	294	53	C'_{dex}	223	31	FA_2	276	13	FA_2
357	77	S_2	333	76	C_{sin}	292	47	C'_{dex}	247	10	FA_2	270	19	FA_2
353	77	S_2	339	67	C_{sin}	299	45	C'_{dex}	240	15	FA_2	286	6	FA_2
355	80	S_2	333	75	C_{sin}	25	15	C'_{dex}	145	8	FA_2	288	19	FA_2
3	78	S_2	340	80	C_{sin}	345	45	C'_{dex}	244	32	FA_2	276	8	FA_2
356	77	S_2	334	86	C_{sin}	167	69	C'_{dex}	106	16	FA_2	290	5	FA_2
6	64	S_2	155	20	C_{sin}	99	54	C'_{dex}	93	0	FA_2	228	20	FA_2
7	90	S_2	312	82	C_{sin}	151	55	C'_{dex}	100	20	FA_2	283	22	FA_2
7	81	S_2	163	64	C_{sin}	170	53	C'_{dex}	287	14	FA_2	319	55	FA_2
166	88	S_2	333	70	C_{sin}	181	34	C'_{dex}	127	74	FA_2	94	6	FA_2
357	88	S_2	332	61	C_{sin}	182	32	C'_{dex}	132	54	FA_2	269	30	FA_2
358	88	S_2	324	55	C_{sin}	139	68	C'_{dex}	144	64	FA_2	282	25	FA_2
178	84	S_2	326	65	C_{sin}	6	64	C'_{dex}	153	48	FA_2	277	24	FA_2
3	89	S_2	124	66	C_{sin}	350	75	C'_{dex}	96	42	FA_2	244	3	FA_3
161	75	S_2	298	84	C_{sin}	329	77	C'_{dex}	275	22	FA_2	325	10	FA_3
182	84	S_2	294	88	C_{sin}	340	72	C'_{dex}	272	12	FA_2	80	3	FA_3
191	78	S_2	284	76	C_{sin}	4	82	C'_{dex}	262	29	FA_2	259	15	FA_3
176	69	S_2	108	71	C_{sin}	7	88	C'_{dex}	275	10	FA_2	284	7	FA_3
343	74	S_2	88	84	C_{sin}	172	76	C'_{dex}	285	14	FA_2	267	4	FA_3
188	85	S_2	104	74	C_{sin}	350	89	C'_{dex}	87	12	FA_2	244	22	FA_3
194	88	S_2	134	86	C_{sin}	0	65	C'_{dex}	112	7	FA_2	114	14	FA_3
199	72	S_2	281	69	C_{sin}	21	69	C'_{dex}	94	18	FA_2	285	24	FA_3
336	87	S_2	289	69	C_{sin}	354	73	C'_{dex}	99	15	FA_2	274	5	FA_3
152	84	S_2	291	53	C_{sin}	3	67	C'_{dex}	88	10	FA_2	274	13	FA_3
150	80	S_2	340	64	C_{sin}	356	64	C'_{dex}	279	28	FA_2	272	13	FA_3
332	89	S_2	311	45	C_{sin}	347	88	C'_{dex}	250	20	FA_2	282	17	FA_3
140	84	S_2	160	88	C_{sin}	343	78	C'_{dex}	75	25	FA_2	122	12	FA_3
314	80	S_2	134	72	C_{sin}	319	55	C'_{dex}	266	9	FA_2	270	8	FA_3
331	87	S_2	122	65	C_{sin}	320	61	C'_{dex}	285	27	FA_2	260	1	FA_3
142	84	S_2	318	87	C_{sin}	24	27	C'_{dex}	242	51	FA_2	273	24	FA_3
321	78	S_2	308	84	C_{sin}	31	36	C'_{dex}	151	60	FA_4	263	31	FA_3
351	85	S_2	328	90	C_{sin}	45	36	C'_{dex}	69	56	FA_4	267	23	FA_3
353	82	S_2	142	87	C_{sin}	222	58	C'_{dex}	260	87	FA_4	341	28	FA_3
173	89	S_2	315	77	C_{sin}	203	71	C'_{dex}	80	81	FA_4	285	32	FA_3
358	84	S_2	154	63	C_{sin}	325	43	C'_{dex}	76	76	FA_4	319	31	FA_3
355	85	S_2	142	83	C_{sin}	256	44	C'_{dex}	240	54	FA_4	299	30	FA_3
161	86	S_2	159	59	C_{sin}	230	50	C'_{dex}	72	76	FA_4	290	20	FA_3
6	85	S_2	146	68	C_{sin}	200	37	C'_{dex}	214	77	FA_4	321	15	FA_3
6	84	S_2	147	69	C_{sin}	260	55	C'_{dex}	156	85	FA_4	325	13	FA_3
349	84	S_2	94	84	C_{sin}	264	52	C'_{dex}	113	69	FA_4	282	15	FA_3
340	87	S_2	76	65	C_{sin}	255	39	C'_{dex}	155	64	FA_4	280	12	FA_3
160	79	S_2	246	79	C_{sin}	288	79	C'_{dex}	320	60	FA_4	277	7	FA_3
162	76	S_2	286	56	C_{sin}	284	77	C'_{dex}	212	40	FA_4	290	10	FA_3
331	60	S_2	147	72	C_{sin}	274	88	C'_{dex}	62	85	FA_4	279	21	FA_3

Domain A			Domain A			Domain C			Domain D			Domain E		
335	57	S_2	333	83	C_{sin}	357	87	C'_{dex}	259	88	FA_4	291	32	FA_3
341	70	S_2	326	81	C_{sin}	185	86	C'_{dex}	126	83	FA_4	278	12	FA_3
152	86	S_2	307	85	C_{sin}	353	84	C'_{dex}	194	42	FA_4	274	16	FA_3
332	90	S_2	347	43	C_{sin}	164	64	C'_{dex}	286	53	FA_4	294	0	FA_3
144	89	S_2	351	85	C_{sin}	157	72	C'_{dex}	39	14	L_1	300	4	FA_3
140	89	S_2	271	49	C_{sin}	347	86	C'_{dex}	29	6	L_1	286	11	FA_3
147	70	S_2	303	56	C_{sin}	339	87	C'_{dex}	271	8	L_1	286	10	FA_3
0	69	S_2	280	88	C_{sin}	158	82	C'_{dex}	272	9	L_1			
333	80	S_2	101	77	C_{sin}	164	68	C'_{dex}	272	4	L_1			
343	75	S_2	116	80	C_{sin}	171	80	C'_{dex}	111	35	L_1			
333	90	S_2	18	82	C_{sin}	330	84	C'_{dex}	105	37	L_1			
338	81	S_2	17	74	C_{sin}	0	75	C'_{dex}	267	22	L_1			
165	90	S_2	337	47	C_{sin}	17	83	C'_{dex}	246	29	L_1			
162	87	S_2	331	52	C_{sin}	186	89	C'_{dex}	254	14	L_1			
142	74	S_2	314	49	C_{sin}	354	82	C'_{dex}	257	37	L_1			
138	80	S_2	321	36	C_{sin}	8	80	C'_{dex}	247	11	L_1			
326	90	S_2	300	50	C_{sin}	9	70	C'_{dex}	246	20	L_1			
339	89	S_2	295	66	C_{sin}	294	42	C'_{dex}	250	22	L_1			
328	80	S_2	287	68	C_{sin}	311	36	C'_{dex}	257	37	L_1			
160	89	S_2	298	72	C_{sin}	333	55	C'_{dex}	264	28	L_1			
321	87	S_2	288	70	C_{sin}	334	50	C'_{dex}	74	49	L_1			
325	85	S_2	278	69	C_{sin}	27	65	C'_{dex}	106	51	L_1			
335	88	S_2	280	58	C_{sin}	20	70	C'_{dex}	98	39	L_1			
157	80	S_2	307	77	C_{sin}	24	66	C'_{dex}	274	36	L_1			
153	81	S_2	294	74	C_{sin}	5	90	C'_{dex}	74	27	L_1			
330	90	S_2	299	73	C_{sin}	258	58	C'_{dex}	82	11	L_1			
325	77	S_2	299	72	C_{sin}	306	45	C'_{nor}	66	27	L_1			
138	85	S_2	286	78	C_{sin}	317	55	C'_{nor}	73	28	L_1			
336	85	S_2	278	67	C_{sin}	224	52	C'_{nor}	76	18	L_1			
341	80	S_2	110	67	C_{sin}	230	48	C'_{nor}	148	40	L_1			
326	83	S_2	118	67	C_{sin}	295	78	C'_{nor}	90	34	L_1			
326	86	S_2	84	75	C_{sin}	268	70	C'_{nor}	69	24	L_1			
330	83	S_2	133	90	C_{sin}	264	16	C'_{nor}	72	9	L_1			
324	82	S_2	149	82	C_{sin}	321	16	C'_{nor}	73	74	L_1			
324	81	S_2	153	73	C_{sin}	297	36	C'_{nor}	58	74	L_1			
154	82	S_2	155	82	C_{sin}	247	21	C'_{nor}	75	61	L_1			
162	88	S_2	154	76	C_{sin}	151	55	C'_{nor}	284	7	L_1			
351	75	S_2	148	80	C_{sin}	170	53	C'_{nor}	108	2	L_1			
353	71	S_2	110	77	C_{sin}	181	34	C'_{nor}	272	8	L_1			
328	65	S_2	126	84	C_{sin}	182	32	C'_{nor}	97	26	L_2			
348	85	S_2	312	85	C_{sin}	139	68	C'_{nor}	103	23	L_2			
163	72	S_2	304	83	C_{sin}	332	52	C'_{nor}	101	23	L_2			
356	63	S_2	141	75	C_{sin}	329	64	C'_{nor}	92	25	L_2			
181	40	S_2	141	76	C_{sin}	198	43	C'_{nor}	94	28	L_2			
183	43	S_2	149	84	C_{sin}	216	36	C'_{nor}	103	32	L_2			

Domain A			Domain A			Domain C			Domain D			Domain A		
161	88	S_2	263	53	C_{sin}	4	21	C'_{nor}	94	18	L_2	318	32	AP_3
175	73	S_2	254	65	C_{sin}	293	53	C'_{nor}	107	37	L_2	300	22	AP_3
171	79	S_2	304	80	C_{sin}	273	43	C'_{nor}	110	11	L_2	314	29	AP_3
163	45	S_2	149	82	C_{sin}	276	45	C'_{nor}	126	12	L_2	285	45	AP_3
335	80	S_2	121	83	C_{sin}	226	22	C'_{nor}	132	34	L_2	288	33	AP_3
152	50	S_2	129	73	C_{sin}	244	28	C'_{nor}	135	28	L_2	246	52	AP_3
150	89	S_2	307	77	C_{sin}	252	43	C'_{nor}	3	45	L_2	272	45	AP_3
147	77	S_2	287	89	C_{sin}	334	80	C'_{nor}	281	19	L_{sin}	283	41	AP_3
150	86	S_2	304	40	C_{sin}	332	78	C'_{nor}	284	60	L_{sin}	92	60	AP_3
146	71	S_2	304	69	C_{sin}	270	57	C'_{nor}	235	34	L_{sin}	268	69	AP_3
350	75	S_2	271	76	C_{sin}	260	70	C'_{nor}	256	28	L_{sin}	253	65	AP_3
337	63	S_2	308	54	C_{sin}	208	40	C'_{nor}	251	34	L_{sin}	274	72	AP_3
341	62	S_2	306	59	C_{sin}	219	53	C'_{nor}				89	87	AP_3
189	79	S_2	302	76	C_{sin}	228	53	C'_{nor}				310	24	AP_3
349	81	S_2	295	65	C_{sin}	344	70	C'_{nor}				312	24	AP_3
337	61	S_2	304	54	C_{sin}	333	66	C'_{nor}				241	28	AP_3
353	68	S_2	320	66	C_{sin}	283	64	C'_{nor}				236	44	AP_3
329	50	S_2	295	65	C_{sin}	263	38	C'_{nor}				222	49	AP_3
322	68	S_2	311	64	C_{sin}	248	54	C'_{nor}				321	17	AP_3
351	49	S_2	328	62	C_{sin}	250	63	C'_{nor}				314	15	AP_3
335	55	S_2	345	85	C_{sin}	271	38	C'_{nor}				342	25	AP_3
322	45	S_2	156	81	C_{sin}	239	45	C'_{nor}				338	35	AP_3
326	70	S_2	140	76	C_{sin}	264	74	C'_{nor}				302	10	AP_3
134	87	S_2	348	52	C_{sin}	9	70	C'_{nor}				37	30	FA_1
326	83	S_2	348	42	C_{sin}	305	65	C'_{nor}				51	22	FA_1
333	74	S_2	297	80	C_{sin}	239	75	C'_{nor}				78	37	FA_1
154	88	S_2	132	83	C_{sin}	247	63	C'_{nor}				86	24	FA_1
144	67	S_2	143	80	C_{sin}	267	67	C'_{nor}				242	7	FA_1
329	70	S_2	309	87	C_{sin}	266	61	C'_{nor}				224	31	FA_1
331	85	S_2	324	85	C_{sin}	257	61	C'_{nor}				242	28	FA_1
162	85	S_2	153	89	C_{sin}	24	66	C'_{nor}				224	31	FA_1
330	80	S_2	156	90	C_{sin}	5	90	C'_{nor}				250	10	FA_1
344	66	S_2	146	85	C_{sin}	258	58	C'_{nor}				254	14	FA_1
331	90	S_2	149	84	C_{sin}	117	72	C'_{rev}				274	2	FA_1
338	86	S_2	340	81	C_{sin}	118	69	C'_{rev}				277	11	FA_1
149	84	S_2	328	82	C_{sin}	72	42	C'_{rev}				71	4	FA_1
334	89	S_2	336	86	C_{sin}	67	42	C'_{rev}				245	5	FA_1
160	85	S_2	342	85	C_{sin}	301	60	C'_{rev}				85	7	FA_1
150	81	S_2	113	70	C_{sin}	307	57	C'_{rev}				74	4	FA_1
332	69	S_2	100	80	C_{sin}	303	50	C'_{rev}				96	7	FA_1
349	84	S_2	333	85	C_{sin}	320	30	C'_{rev}				92	5	FA_1
347	82	S_2	327	88	C_{sin}	325	75	C'_{rev}				254	7	FA_1
166	85	S_2	286	55	C_{sin}	304	70	C'_{rev}				259	0	FA_1
173	83	S_2	328	82	C_{sin}	292	65	C'_{rev}				110	24	FA_1
351	68	S_2	331	90	C_{sin}	271	51	C'_{rev}				102	18	FA_1

Domain A			Domain A			Domain C			Domain A			Domain A		
166	86	S_2	154	73	C_{sin}	68	77	C'_{rev}	71	59	L_2	100	15	FA_1
350	88	S_2	142	72	C_{sin}	58	64	C'_{rev}	74	69	L_2	69	7	FA_2
355	80	S_2	332	76	C_{sin}	201	69	C'_{rev}	73	67	L_2	251	3	FA_2
329	71	S_2	312	82	C_{sin}	224	77	C'_{rev}	70	24	L_2	227	26	FA_2
329	61	S_2	313	84	C_{sin}	205	70	C'_{rev}	64	48	L_2	240	14	FA_2
328	72	S_2	148	65	C_{sin}	184	73	C'_{rev}	72	41	L_2	255	4	FA_2
357	73	S_2	139	58	C_{sin}	240	90	C'_{rev}	68	46	L_2	249	2	FA_2
355	77	S_2	163	72	C_{sin}	306	88	C'_{rev}	84	45	L_2	72	16	FA_2
344	62	S_2	166	65	C_{sin}	305	75	C'_{rev}	90	36	L_2	84	24	FA_2
340	78	S_2	343	86	C_{sin}	294	42	C'_{rev}	90	34	L_2	250	5	FA_2
175	75	S_2	158	80	C_{sin}	311	36	C'_{rev}	93	51	L_2	78	6	FA_2
183	85	S_2	346	89	C_{sin}	333	55	C'_{rev}	79	55	L_2	228	8	FA_2
7	67	S_2	167	88	C_{sin}	334	50	C'_{rev}	98	57	L_2	81	12	FA_2
2	59	S_2	339	86	C_{sin}	27	65	C'_{rev}	275	45	L_2	264	24	FA_2
334	60	S_2	345	86	C_{sin}	20	70	C'_{rev}	270	35	L_2	254	30	FA_2
348	64	S_2	139	80	C_{sin}	18	67	C'_{sin}	256	23	L_2	254	16	FA_2
0	59	S_2	148	70	C_{sin}	119	72	C'_{sin}	254	46	L_2	256	19	FA_2
332	87	S_2	130	67	C_{sin}	114	71	C'_{sin}	262	62	L_2	255	16	FA_2
341	81	S_2	146	55	C_{sin}	126	85	C'_{sin}	96	34	L_2	93	29	FA_2
332	80	S_2	152	75	C_{sin}	113	77	C'_{sin}	68	39	L_2	93	30	FA_2
332	85	S_2	155	87	C_{sin}	277	89	C'_{sin}	89	45	L_2	251	5	FA_2
0	70	S_2	147	74	C_{sin}	298	85	C'_{sin}	96	47	L_2	71	1	FA_2
359	71	S_2	313	77	C_{sin}	316	55	C'_{sin}	50	45	L_2	63	10	FA_2
344	52	S_2	310	74	C_{sin}	122	75	C'_{sin}	52	43	L_2	72	20	FA_2
347	56	S_2	314	72	C_{sin}	306	78	C'_{sin}	58	40	L_2	74	20	FA_2
1	70	S_2	304	90	C_{sin}	324	70	C'_{sin}	54	30	L_2	65	26	FA_2
358	65	S_2	301	80	C_{sin}	254	82	C'_{sin}	78	35	L_2	72	20	FA_2
181	84	S_2	289	89	C_{sin}	270	69	C'_{sin}	64	29	L_2	69	28	FA_2
337	86	S_2	111	88	C_{sin}	257	70	C'_{sin}	60	52	L_2	14	66	FA_2
343	65	S_2	334	81	C_{sin}	292	77	C'_{sin}	72	5	L_2	16	50	FA_2
184	71	S_2	331	77	C_{sin}	124	70	C'_{sin}	12	64	L_2	66	20	FA_2
1	89	S_2	161	86	C_{sin}	117	76	C'_{sin}	251	47	L_2	85	13	FA_2
167	82	S_2	316	90	C_{sin}	302	90	C'_{sin}	237	39	L_2	272	32	FA_2
169	88	S_2	315	84	C_{sin}	300	72	C'_{sin}	225	37	L_2	253	5	FA_2
9	90	S_2	321	66	C_{sin}	274	77	C'_{sin}	233	38	L_2	245	12	FA_2
171	75	S_2	122	78	C_{sin}	77	88	C'_{sin}	249	25	L_2	245	15	FA_2
178	82	S_2	315	86	C_{sin}	261	87	C'_{sin}	247	25	L_2	79	5	FA_2
191	86	S_2	150	90	C_{sin}	126	80	C'_{sin}	242	19	L_2	69	4	FA_2
8	84	S_2	140	84	C_{sin}	123	84	C'_{sin}	243	22	L_2	76	0	FA_2
188	83	S_2	321	83	C_{sin}	136	81	C'_{sin}	244	24	L_2	234	10	FA_2
345	69	S_2	305	78	C_{sin}	121	79	C'_{sin}	247	24	L_2	242	9	FA_2
341	75	S_2	304	77	C_{sin}	283	83	C'_{sin}	31	43	L_2	269	24	FA_2
178	79	S_2	349	67	C_{sin}	284	57	C'_{sin}	51	29	L_2	244	22	FA_2
178	83	S_2	352	62	C_{sin}	260	77	C'_{sin}	50	16	L_2	244	11	FA_2
336	64	S_2	145	75	C_{sin}	265	77	C'_{sin}	242	26	L_2	222	59	FA_2

Domain A			Domain A			Domain C			Domain A			Domain A		
334	72	S_2	140	77	C_{sin}	110	45	C'_{sin}	243	25	L_2	240	80	FA_2
342	82	S_2	310	42	C_{sin}	112	44	C'_{sin}	247	52	L_2	257	1	FA_2
357	58	S_2	295	72	C_{sin}	106	89	C'_{sin}	248	47	L_2	256	2	FA_2
351	81	S_2	139	84	C_{sin}	105	90	C'_{sin}	93	28	L_2	244	3	FA_2
346	77	S_2	329	84	C_{sin}	237	83	C'_{sin}	97	27	L_2	90	11	FA_2
346	67	S_2	332	85	C_{sin}	149	74	C'_{sin}	98	38	L_2	240	9	FA_2
335	90	S_2	332	89	C_{sin}	105	76	C'_{sin}	234	38	L_2	55	3	FA_2
334	90	S_2	246	78	C_{sin}	108	75	C'_{sin}	231	46	L_2	62	1	FA_2
334	78	S_2	264	85	C_{sin}	107	74	C'_{sin}	237	18	L_2	40	14	FA_2
333	76	S_2	312	62	C_{sin}	100	86	C'_{sin}	234	20	L_2	219	11	FA_2
339	80	S_2	347	66	C_{sin}	301	84	C'_{sin}	235	17	L_2	218	19	FA_2
349	73	S_2	349	63	C_{sin}	277	65	C'_{sin}	39	15	L_2	225	26	FA_2
342	55	S_2	110	74	C_{sin}	275	72	C'_{sin}	55	10	L_2	70	15	FA_2
349	80	S_2	307	88	C_{sin}	90	85	C'_{sin}	62	3	L_2	70	21	FA_2
334	50	S_2	303	78	C_{sin}	86	73	C'_{sin}	61	9	L_2	239	22	FA_2
345	69	S_2	91	72	C_{sin}	306	68	C'_{sin}	81	34	L_2	75	16	FA_2
324	78	S_2	320	75	C_{sin}	306	80	C'_{sin}	67	22	L_2	56	1	FA_2
161	78	S_2	305	90	C_{sin}	233	90	C'_{sin}	74	22	L_2	237	5	FA_2
335	88	S_2	308	87	C_{sin}	42	89	C'_{sin}	88	23	L_2	265	20	FA_2
159	82	S_2	342	68	C_{sin}	246	85	C'_{sin}	94	38	L_2	254	5	FA_2
159	74	S_2	141	88	C_{sin}	225	78	C'_{sin}	152	74	L_2	266	2	FA_2
339	87	S_2	332	84	C_{sin}	306	82	C'_{sin}	86	59	L_2	265	4	FA_2
333	80	S_2	167	88	C_{sin}	309	90	C'_{sin}	55	27	L_2	257	17	FA_2
342	72	S_2	329	84	C_{sin}	129	86	C'_{sin}	87	27	L_2	264	21	FA_2
339	71	S_2	335	82	C_{sin}	280	58	C'_{sin}	56	36	L_2	260	7	FA_2
344	79	S_2	129	83	C_{sin}	271	68	C'_{sin}	62	32	L_2	263	11	FA_2
349	89	S_2	134	85	C_{sin}	106	81	C'_{sin}	88	25	L_2	281	54	FA_2
334	69	S_2	167	86	C_{sin}	116	84	C'_{sin}	84	28	L_2	285	3	FA_2
338	74	S_2	171	86	C_{sin}	114	81	C'_{sin}	83	48	L_2	84	26	FA_2
336	85	S_2	134	40	C_{sin}	99	75	C'_{sin}	77	33	L_2	95	17	FA_2
329	80	S_2	132	60	C_{sin}	115	77	C'_{sin}	85	12	L_2	88	32	FA_2
330	85	S_2	155	75	C_{sin}	298	88	C'_{sin}	82	8	L_2	89	31	FA_2
299	69	S_2	325	79	C_{sin}	310	80	C'_{sin}	168	77	L_2	90	35	FA_2
332	76	S_2	149	83	C_{sin}	118	85	C'_{sin}	222	58	L_2	90	12	FA_2
332	77	S_2	328	86	C_{sin}	305	87	C'_{sin}	232	42	L_2	89	18	FA_2
346	88	S_2	149	86	C_{sin}	141	78	C'_{sin}	107	63	L_2	263	33	FA_2
336	88	S_2	313	81	C_{sin}	82	68	C'_{sin}	73	53	L_2	245	20	FA_2
152	70	S_2	165	82	C_{sin}	93	80	C'_{sin}	81	31	L_2	112	5	FA_2
153	81	S_2	356	88	C_{sin}	289	70	C'_{sin}	83	28	L_2	111	1	FA_2
160	81	S_2	166	70	C_{sin}	98	86	C'_{sin}	84	46	L_2	102	32	FA_2
150	83	S_2	165	71	C_{sin}	90	89	C'_{sin}	89	44	L_2	94	23	FA_2
156	80	S_2	345	82	C_{sin}	96	80	C'_{sin}	246	42	L_2	84	18	FA_2
156	81	S_2	346	78	C_{sin}	291	81	C'_{sin}	243	58	L_2	86	22	FA_2
146	82	S_2	350	87	C_{sin}	286	87	C'_{sin}	240	52	L_2	281	5	FA_2
322	88	S_2	343	73	C_{sin}	315	77	C'_{sin}	246	56	L_2	340	14	FA_2

Supporting Table 1: raw data of structural measurements

Domain A			Domain A			Domain C			Domain A			Domain A		
333	80	S_2	353	80	C_{sin}	308	82	C'_{sin}	235	52	L_2	330	24	FA_2
3387	80	S_2	0	80	C_{sin}	319	87	C'_{sin}	250	49	L_2	329	32	FA_2
159	75	S_2	181	89	C_{sin}	274	77	C'_{sin}	252	55	L_2	285	10	FA_2
160	74	S_2	170	86	C_{sin}	283	79	C'_{sin}	263	56	L_2	270	1	FA_2
325	84	S_2	161	68	C_{sin}	247	63	C'_{sin}	253	56	L_2	71	10	FA_2
326	87	S_2	116	64	C_{sin}	267	67	C'_{sin}	262	55	L_2	70	16	FA_2
157	79	S_2	127	78	C_{sin}	266	61	C'_{sin}	237	55	L_2	94	23	FA_2
157	66	S_2	119	52	C_{sin}	257	61	C'_{sin}	239	54	L_2	89	29	FA_2
295	65	S_2	285	82	C_{sin}	306	88	C'_{sin}	247	36	L_2	77	34	FA_2
298	67	S_2	125	62	C_{sin}	305	75	C'_{sin}	242	47	L_2	287	8	FA_2
144	83	S_2	112	65	C_{sin}	147	20	AP_1	269	75	L_2	284	2	FA_2
331	90	S_2	314	80	C_{sin}	195	56	AP_1	248	63	L_2	91	5	FA_2
335	90	S_2	318	67	C_{sin}	204	54	AP_1	241	61	L_2	96	15	FA_2
144	69	S_2	306	66	C_{sin}	286	44	AP_1	75	37	L_2	78	4	FA_2
146	76	S_2	331	71	C_{sin}	305	34	AP_1	91	42	L_2	79	9	FA_2
327	87	S_2	333	84	C_{sin}	306	38	AP_1	75	52	L_2	268	6	FA_2
149	88	S_2	343	88	C_{sin}	37	67	AP_1	75	28	L_2	92	32	FA_2
142	88	S_2	324	84	C_{sin}	123	27	AP_1	252	4	L_2	45	45	FA_2
153	89	S_2	336	83	C_{sin}	172	45	AP_1	251	19	L_2	89	22	FA_2
144	90	S_2	324	80	C_{sin}	210	29	AP_1	250	27	L_2	65	34	FA_2
148	90	S_2	330	60	C_{sin}	153	30	AP_1	68	13	L_2	230	39	FA_2
151	90	S_2	310	90	C_{sin}	140	63	AP_1	65	15	L_2	236	18	FA_2
142	90	S_2	286	89	C_{sin}	97	14	AP_1	53	9	L_2	275	62	FA_2
330	85	S_2	138	88	C_{sin}	73	52	AP_1	59	20	L_2	64	17	FA_2
336	80	S_2	330	52	C_{sin}	70	50	AP_1	59	11	L_2	72	8	FA_2
154	86	S_2	316	56	C_{sin}	291	16	AP_1	47	20	L_2	53	12	FA_2
141	84	S_2	313	67	C_{sin}	265	18	AP_1	15	38	L_2	52	29	FA_2
155	87	S_2	123	55	C_{sin}	303	10	AP_1	40	27	L_2	95	12	FA_2
330	70	S_2	267	83	C_{sin}	216	23	AP_1	34	28	L_2	99	22	FA_2
332	78	S_2	295	81	C_{sin}	197	45	AP_1	81	28	L_2	59	32	FA_2
153	80	S_2	330	51	C_{sin}	89	0	AP_1	81	20	L_2	92	4	FA_2
149	85	S_2	332	84	C_{sin}	228	14	AP_1	89	10	L_2	248	13	FA_3
336	83	S_2	330	82	C_{sin}	279	28	AP_1	68	24	L_2	250	13	FA_3
334	75	S_2	308	60	C_{sin}	274	54	AP_1	78	14	L_2	253	2	FA_3
333	75	S_2	309	66	C_{sin}	22	26	AP_1	75	25	L_2	243	54	FA_3
333	75	S_2	314	51	C_{sin}	33	29	AP_1	85	24	L_2	251	32	FA_3
335	84	S_2	335	62	C_{sin}	334	36	AP_1	77	19	L_2	256	42	FA_3
336	75	S_2	318	58	C_{sin}	239	11	AP_1	68	24	L_2	252	12	FA_3
336	85	S_2	326	64	C_{sin}	1	26	AP_1	71	20	L_2	85	36	FA_3
156	87	S_2	358	46	C_{sin}	353	15	AP_1	69	27	L_2	266	35	FA_3
161	89	S_2	334	39	C_{sin}	274	29	AP_1	71	29	L_2	264	28	FA_3
157	87	S_2	319	81	C_{sin}	308	85	AP_2	80	23	L_2	242	43	FA_3
331	90	S_2	297	69	C_{sin}	300	86	AP_2	67	32	L_2	235	31	FA_3
334	86	S_2	142	78	C_{sin}	351	48	AP_2	78	18	L_2	25	35	FA_3
335	86	S_2	132	86	C_{sin}	24	64	AP_2	76	33	L_2	82	47	FA_3

Domain A			Domain A			Domain C			Domain A			Domain A		
333	88	S_2	154	78	C_{sin}	323	67	AP_2	76	22	L_2	212	52	FA_3
336	89	S_2	151	77	C_{sin}	341	82	AP_2	256	15	L_2	217	60	FA_3
325	70	S_2	128	72	C_{sin}	144	52	AP_2	257	8	L_2	231	59	FA_3
339	82	S_2	132	76	C_{sin}	130	57	AP_2	248	4	L_2	153	85	FA_3
339	82	S_2	139	72	C_{sin}	90	90	AP_2	256	21	L_2	271	17	FA_3
161	88	S_2	124	60	C_{sin}	329	65	AP_2	266	22	L_2	274	15	FA_3
357	79	S_2	121	79	C_{sin}	326	84	AP_2	252	39	L_2	298	18	FA_3
126	47	S_2	115	80	C_{sin}	312	73	AP_2	253	14	L_2	252	4	FA_3
135	58	S_2	127	77	C_{sin}	302	72	AP_2	261	33	L_2	258	11	FA_3
160	69	S_2	118	70	C_{sin}	309	65	AP_2	253	11	L_2	267	8	FA_3
156	73	S_2	303	85	C_{sin}	204	73	AP_2	254	18	L_2	82	11	L_1
135	50	S_2	307	90	C_{sin}	166	69	AP_2	242	8	L_2	285	7	L_1
150	57	S_2	312	90	C_{sin}	171	69	AP_2	263	5	L_2	272	3	L_1
137	78	S_2	309	78	C_{sin}	17	9	AP_2	220	30	L_2	258	18	L_1
139	76	S_2	313	83	C_{sin}	330	15	AP_2	232	10	L_2	259	20	L_1
144	64	S_2	337	67	C_{sin}	95	37	AP_2	237	20	L_2	265	13	L_1
145	57	S_2	344	70	C_{sin}	68	22	AP_2	249	27	L_2	263	20	L_1
132	51	S_2	356	74	C_{sin}	110	74	AP_2	234	4	L_2	65	4	L_1
142	55	S_2	107	61	C_{sin}	93	85	AP_2	229	15	L_2	252	8	L_1
133	68	S_2	300	78	C_{sin}	280	75	AP_2	230	20	L_2	261	11	L_1
137	64	S_2	304	85	C_{sin}	258	86	AP_2	241	8	L_2	239	34	L_1
157	77	S_2	332	67	C_{sin}	266	83	AP_2	243	5	L_2	255	21	L_1
156	72	S_2	322	67	C_{sin}	294	79	AP_2	250	21	L_2	255	32	L_1
344	58	S_2	319	55	C_{sin}	299	72	AP_2	236	17	L_2	260	32	L_1
328	52	S_2	321	71	C_{sin}	284	64	AP_2	229	29	L_2	248	21	L_1
160	88	S_2	323	67	C_{sin}	282	67	AP_2	42	18	L_2	262	19	L_1
336	88	S_2	168	72	C_{sin}	277	45	AP_2	52	10	L_2	261	6	L_1
332	86	S_2	324	48	C_{sin}	317	50	AP_2	232	10	L_2	249	21	L_1
148	86	S_2	309	35	C_{sin}	320	70	AP_2	224	8	L_2	246	2	L_1
0	72	S_2	336	60	C_{sin}	333	52	AP_2	60	7	L_2	254	15	L_1
345	85	S_2	338	65	C_{sin}	333	69	AP_2	51	5	L_2	249	46	L_1
352	64	S_2	342	45	C_{sin}	325	82	AP_2	250	14	L_2	235	41	L_1
21	65	S_2	355	78	C_{sin}	343	90	AP_2	242	9	L_2	221	24	L_1
10	68	S_2	349	82	C_{sin}	131	37	AP_2	236	12	L_2	55	8	L_1
172	60	S_2	353	85	C_{sin}	133	34	AP_2	228	4	L_2	60	4	L_1
173	60	S_2	349	84	C_{sin}	117	60	AP_2	238	6	L_2	254	4	L_1
315	80	S_2	339	86	C_{sin}	243	72	AP_2	90	13	L_2	235	18	L_1
323	73	S_2	353	85	C_{sin}	270	88	AP_2	275	5	L_2	232	11	L_1
326	90	S_2	354	87	C_{sin}	276	76	AP_2	82	16	L_2	83	20	L_1
137	90	S_2	343	84	C_{sin}	90	70	AP_2	82	5	L_2	88	21	L_1
158	84	S_2	342	77	C_{sin}	80	70	AP_2	246	46	L_3	245	6	L_1
160	82	S_2	325	63	C_{sin}	91	70	AP_2	242	44	L_3	255	14	L_1
157	82	S_2	326	57	C_{sin}	345	73	AP_2	242	39	L_3	257	12	L_1
162	87	S_2	339	50	C_{sin}	345	73	AP_2	235	44	L_3	232	2	L_1
159	82	S_2	342	77	C_{sin}	326	87	AP_2	273	3	L_3	208	52	L_1

Domain A			Domain A			Domain C			Domain A			Domain A		
185	83	S_2	329	66	C_{sin}	324	82	AP_2	250	23	L_{dex}	226	25	L_1
340	90	S_2	294	80	C_{sin}	329	80	AP_2	271	16	L_{dex}	232	24	L_1
349	86	S_2	300	68	C_{sin}	146	84	AP_2	261	58	L_{dex}	236	24	L_1
339	86	S_2	286	62	C_{sin}	330	78	AP_2	109	30	L_{dex}	236	28	L_1
340	87	S_2	292	60	C_{sin}	93	80	AP_2	242	24	L_{dex}	264	19	L_1
344	89	S_2	320	87	C_{sin}	321	88	AP_2	216	15	L_{dex}	264	22	L_1
159	83	S_2	145	86	C_{sin}	145	89	AP_2	238	39	L_{dex}	273	32	L_1
340	82	S_2	346	84	C_{sin}	146	87	AP_2	78	45	L_{dex}	251	19	L_1
337	84	S_2	308	86	C_{sin}	37	76	AP_2	78	20	L_{dex}	255	17	L_1
171	80	S_2	351	82	C_{sin}	312	45	AP_2	105	26	L_{dex}	62	4	L_1
169	86	S_2	156	90	C_{sin}	345	52	AP_2	273	11	L_{dex}	241	17	L_1
169	88	S_2	321	86	C_{sin}	260	86	AP_2	21	54	L_{dex}	250	14	L_1
172	85	S_2	331	89	C_{sin}	311	74	AP_2	23	59	L_{dex}	246	10	L_1
164	87	S_2	312	83	C_{sin}	312	72	AP_2	262	30	L_{rev}	248	19	L_1
166	86	S_2	310	80	C_{sin}	308	70	AP_2	268	35	L_{rev}	57	4	L_1
335	84	S_2	316	83	C_{sin}	316	75	AP_2	66	6	L_{rev}	262	20	L_1
338	65	S_2	301	77	C_{sin}	356	86	AP_2	230	25	L_{rev}	89	20	L_1
335	58	S_2	306	79	C_{sin}	180	34	AP_2	49	5	L_{rev}	218	10	L_1
317	63	S_2	317	77	C_{sin}	167	26	AP_2	48	14	L_{rev}	85	28	L_1
326	70	S_2	309	85	C_{sin}	305	78	AP_2	245	10	L_{rev}	265	23	L_1
343	82	S_2	317	86	C_{sin}	321	85	AP_2	265	19	L_{sin}	109	11	L_1
335	80	S_2	313	80	C_{sin}	357	76	AP_2	259	14	L_{sin}	271	5	L_1
332	79	S_2	317	76	C_{sin}	352	62	AP_2	264	17	L_{sin}	76	5	L_1
324	78	S_2	318	70	C_{sin}	218	58	AP_2	260	28	L_{sin}	251	9	L_1
168	66	S_2	288	88	C_{sin}	252	82	AP_2	265	20	L_{sin}	82	8	L_1
161	63	S_2	303	86	C_{sin}	269	73	AP_2	163	64	L_{sin}	264	1	L_1
154	70	S_2	306	88	C_{sin}	267	72	AP_2	247	32	L_{sin}	272	5	L_1
145	65	S_2	304	86	C_{sin}	246	88	AP_2	243	32	L_{sin}	106	3	L_1
180	70	S_2	301	85	C_{sin}	245	90	AP_2	234	17	L_{sin}	72	4	L_1
176	78	S_2	301	90	C_{sin}	75	83	AP_2	236	8	L_{sin}	82	5	L_1
162	86	S_2	125	85	C_{sin}	83	68	AP_2	226	10	L_{sin}	261	7	L_1
323	83	S_2	114	88	C_{sin}	72	73	AP_2	223	3	L_{sin}	258	8	L_1
345	87	S_2	321	90	C_{sin}	284	36	AP_2	252	17	L_{sin}	76	4	L_1
140	87	S_2	140	78	C_{sin}	293	44	AP_2	251	21	L_{sin}	243	3	L_1
133	88	S_2	106	80	C_{sin}	290	40	AP_2	228	18	L_{sin}	70	1	L_1
131	84	S_2	114	69	C_{sin}	353	70	AP_2	231	15	L_{sin}	72	4	L_1
0	82	S_2	124	90	C_{sin}	150	76	AP_2	228	27	L_{sin}	261	21	L_1
153	74	S_2	136	87	C_{sin}	357	68	AP_2	228	22	L_{sin}	267	24	L_1
152	67	S_2	305	78	C_{sin}	12	53	AP_2	230	21	L_{sin}	243	8	L_1
355	80	S_2	317	75	C_{sin}	282	50	AP_2	222	22	L_{sin}	224	14	L_1
331	86	S_2	149	84	C_{sin}	273	46	AP_2	236	12	L_{sin}	59	8	L_1
340	80	S_2	150	84	C_{sin}	213	60	AP_2	233	37	L_{sin}	38	24	L_1
350	80	S_2	145	80	C_{sin}	208	56	AP_2	234	37	L_{sin}	232	1	L_1
159	90	S_2	144	78	C_{sin}	337	28	AP_2	244	12	L_{sin}	248	5	L_1
148	89	S_2	130	61	C_{sin}	23	46	AP_2	243	17	L_{sin}	270	14	L_1

Domain A			Domain A			Domain C			Domain A			Domain A		
335	81	S_2	94	64	C_{sin}	2	85	AP_2	240	18	L_{sin}	218	38	L_1
343	74	S_2	114	72	C_{sin}	346	77	AP_2	232	8	L_{sin}	160	67	L_1
336	89	S_2	117	70	C_{sin}	111	33	AP_2	232	8	L_{sin}	220	49	L_1
339	78	S_2	129	68	C_{sin}	233	56	AP_2	233	9	L_{sin}	215	13	L_1
152	84	S_2	108	54	C_{sin}	223	78	AP_2	230	10	L_{sin}	219	21	L_1
173	78	S_2	115	64	C_{sin}	194	71	AP_2	235	14	L_{sin}	233	20	L_1
142	83	S_2	136	82	C_{sin}	298	84	AP_2	226	12	L_{sin}	234	12	L_1
314	85	S_2	130	75	C_{sin}	139	78	AP_2	251	7	L_{sin}	250	38	L_1
330	69	S_2	140	80	C_{sin}	299	75	AP_2	260	24	L_{sin}	256	12	L_1
341	37	S_2	148	90	C_{sin}	129	65	AP_2	77	14	L_{sin}	76	11	L_1
331	67	S_2	135	79	C_{sin}	117	75	AP_2	42	1	L_{sin}	250	9	L_1
339	62	S_2	133	75	C_{sin}	104	72	AP_2	42	15	L_{sin}	222	3	L_1
341	54	S_2	325	89	C_{sin}	171	42	AP_2	229	29	L_{sin}	266	7	L_1
298	65	S_2	330	87	C_{sin}	343	51	AP_2	222	24	L_{sin}	260	6	L_1
346	62	S_2	150	89	C_{sin}	338	49	AP_2	239	16	L_{sin}	248	18	L_1
323	74	S_2	338	64	C_{sin}	32	55	AP_2	217	26	L_{sin}	226	4	L_1
320	77	S_2	277	90	C_{sin}	45	61	AP_2	203	7	L_{sin}	269	14	L_1
312	81	S_2	122	82	C_{sin}	279	10	AP_2	262	28	L_{sin}	248	17	L_1
323	85	S_2	292	83	C_{sin}	279	32	AP_2	244	24	L_{sin}	329	22	L_1
319	70	S_2	282	72	C_{sin}	338	28	AP_2	262	21	L_{sin}	240	22	L_1
324	73	S_2	276	67	C_{sin}	332	32	AP_2	42	37	L_{sin}	330	24	L_1
321	60	S_2	275	70	C_{sin}	340	22	AP_2	249	12	L_{sin}	264	10	L_1
323	78	S_2	130	72	C_{sin}	326	40	AP_2	253	5	L_{sin}	261	3	L_1
169	72	S_2	135	70	C_{sin}	131	78	AP_2	256	11	L_{sin}	82	2	L_1
141	90	S_2	132	85	C_{sin}	111	75	AP_2	58	2	L_{sin}	81	24	L_1
149	84	S_2	297	83	C_{sin}	133	74	AP_2	79	19	L_{sin}	96	28	L_1
141	89	S_2	299	80	C_{sin}	116	67	AP_2	82	22	L_{sin}	85	32	L_1
313	74	S_2	304	82	C_{sin}	101	90	AP_2	261	15	L_{sin}	76	36	L_1
327	63	S_2	113	80	C_{sin}	310	90	AP_2	256	17	L_{sin}	43	20	L_1
332	63	S_2	133	71	C_{sin}	319	90	AP_2	66	6	L_{sin}	44	17	L_1
325	68	S_2	306	74	C_{sin}	151	68	AP_2	230	25	L_{sin}	64	7	L_1
319	65	S_2	104	87	C_{sin}	150	76	AP_2	49	5	L_{sin}	58	4	L_1
306	61	S_2	289	74	C_{sin}	326	46	AP_2	48	14	L_{sin}	252	24	L_1
267	74	S_2	296	84	C_{sin}	349	39	AP_2	245	10	L_{sin}	248	22	L_1
295	65	S_2	297	68	C_{sin}	175	45	AP_2	69	32	L_{sin}	252	12	L_1
302	67	S_2	319	85	C_{sin}	181	61	AP_2	86	30	L_{sin}	275	22	L_1
294	66	S_2	139	82	C_{sin}	175	59	AP_2	83	31	L_{sin}	275	26	L_1
305	53	S_2	305	72	C_{sin}	202	84	AP_2	254	24	L_{sin}	264	17	L_1
314	73	S_2	127	81	C_{sin}	340	82	AP_2	46	38	L_{sin}	256	4	L_1
288	50	S_2	294	89	C_{sin}	359	70	AP_2	29	58	L_{sin}	260	3	L_1
310	62	S_2	241	71	C_{sin}	5	87	AP_2	247	37	L_{sin}	259	8	L_1
137	62	S_2	106	69	C_{sin}	5	72	AP_2	242	37	L_{sin}	256	12	L_1
143	63	S_2	150	83	C_{sin}	348	69	AP_2	93	29	L_{sin}	240	45	L_1
137	54	S_2	144	90	C_{sin}	200	32	AP_2	234	12	L_{sin}	238	32	L_1
141	55	S_2	118	72	C_{sin}	220	32	AP_2	26	44	L_{sin}	222	52	L_1

Domain A			Domain A			Domain C			Domain A			Domain A		
143	50	S_2	135	83	C_{sin}	210	88	AP_2	37	36	L_{sin}	242	40	L_1
149	74	S_2	136	82	C_{sin}	197	5	AP_2	41	35	L_{sin}	228	38	L_1
141	68	S_2	314	88	C_{sin}	11	64	AP_2	40	25	L_{sin}	241	20	L_1
121	90	S_2	143	78	C_{sin}	13	66	AP_2	33	37	L_{sin}	239	21	L_1
149	61	S_2	143	89	C_{sin}	24	48	AP_2	71	34	L_{sin}	240	28	L_1
138	70	S_2	308	84	C_{sin}	21	65	AP_2	72	56	L_{sin}	107	11	L_1
155	67	S_2	137	82	C_{sin}	29	86	AP_2	75	14	L_{sin}	267	13	L_1
151	75	S_2	78	37	AP_1	323	87	AP_2	77	31	L_{sin}	267	7	L_1
142	75	S_2	359	64	AP_1	340	84	AP_2	264	13	L_{sin}	100	29	L_1
145	80	S_2	22	70	AP_1	304	40	AP_2	277	3	L_{sin}	105	8	L_1
142	80	S_2	131	36	AP_1	77	75	AP_3	287	33	L_{sin}	0	76	L_1
150	54	S_2	45	26	AP_1	88	81	AP_3				72	7	L_1
129	53	S_2	104	42	AP_1	86	77	AP_3				232	18	L_1
81	50	S_2	155	43	AP_1	90	90	AP_3				4	90	L_1
337	75	S_2	146	34	AP_1	80	79	AP_3				209	40	L_1
347	88	S_2	73	56	AP_1	95	78	AP_3				257	10	L_1
342	82	S_2	83	29	AP_1	251	49	L_1				255	24	L_2
353	86	S_2	10	54	AP_1	263	48	L_1				252	16	L_2
341	88	S_2	353	61	AP_1	290	41	L_1				254	12	L_2
347	87	S_2	277	32	AP_1	345	17	L_1				259	6	L_2
321	84	S_2	198	58	AP_1	341	39	L_1				214	15	L_2
172	90	S_2	177	44	AP_1	8	47	L_1				239	12	L_2
333	75	S_2	173	82	AP_1	357	43	L_1				265	3	L_2
3	82	S_2	166	72	AP_1	320	58	L_1				260	7	L_2
336	84	S_2	351	56	AP_1	232	24	L_1				255	13	L_2
357	80	S_2	328	24	AP_1	42	1	L_1				260	6	L_2
339	84	S_2	327	28	AP_1	25	17	L_1				262	3	L_2
171	84	S_2	298	24	AP_1	29	32	L_1				80	18	L_2
171	87	S_2	166	15	AP_1	36	27	L_1				254	4	L_2
167	86	S_2	12	33	AP_1	10	16	L_1				265	1	L_2
354	86	S_2	321	45	AP_1	240	6	L_1				260	26	L_2
170	86	S_2	335	45	AP_1	56	20	L_1				254	23	L_2
155	81	S_2	146	9	AP_1	58	13	L_1				276	24	L_2
161	75	S_2	173	33	AP_1	63	2	L_1				251	14	L_2
162	75	S_2	165	43	AP_1	62	13	L_1				251	16	L_2
150	73	S_2	188	38	AP_1	112	40	L_1				64	6	L_2
151	73	S_2	169	28	AP_1	109	14	L_1				264	21	L_2
159	76	S_2	153	60	AP_1	108	24	L_1				241	13	L_2
163	82	S_2	168	64	AP_1	268	35	L_1				256	5	L_2
149	74	S_2	170	37	AP_1	279	24	L_1				258	1	L_2
152	72	S_2	22	71	AP_1	289	28	L_1				262	17	L_2
165	84	S_2	133	18	AP_1	195	36	L_1				102	6	L_2
162	83	S_2	338	72	AP_2	196	31	L_1				258	23	L_2
171	79	S_2	332	74	AP_2	3	9	L_1				240	16	L_2
163	81	S_2	344	80	AP_2	18	25	L_1				258	19	L_2

Supporting Table 1: raw data of structural measurements

Domain A			Domain A			Domain C			Domain A		
158	81	S_2	335	89	AP_2	355	9	L_1	256	17	L_2
176	85	S_2	346	83	AP_2	248	22	L_2	260	7	L_2
168	83	S_2	169	89	AP_2	248	10	L_2	251	8	L_2
180	81	S_2	11	69	AP_2	243	37	L_2	60	11	L_2
178	79	S_2	11	60	AP_2	252	32	L_2	276	6	L_2
191	75	S_2	153	80	AP_2	251	5	L_2	269	3	L_2
310	75	S_2	160	82	AP_2	245	21	L_2	231	17	L_2
320	81	S_2	331	70	AP_2	250	22	L_2	254	29	L_2
320	76	S_2	338	65	AP_2	244	25	L_2	252	14	L_2
176	67	S_2	344	80	AP_2	255	23	L_2	262	10	L_2
170	87	S_2	335	79	AP_2	231	23	L_2	240	6	L_2
168	86	S_2	6	77	AP_2	241	24	L_2	261	5	L_2
156	90	S_2	354	83	AP_2	299	72	L_2	252	4	L_2
152	83	S_2	160	88	AP_2	292	72	L_2	75	2	L_2
152	87	S_2	342	65	AP_2	240	25	L_2	253	24	L_2
156	81	S_2	157	68	AP_2	244	22	L_2	258	24	L_2
158	82	S_2	165	72	AP_2	238	45	L_2	81	24	L_2
144	87	S_2	345	84	AP_2	260	64	L_2	249	9	L_2
152	71	S_2	340	75	AP_2	266	58	L_2	238	16	L_2
159	74	S_2	325	86	AP_2	260	61	L_2	258	13	L_2
149	72	S_2	339	77	AP_2	266	56	L_2	250	8	L_2
336	84	S_2	332	71	AP_2	304	60	L_2	264	22	L_2
335	88	S_2	190	71	AP_2	300	64	L_2	264	16	L_2
169	83	S_2	335	90	AP_2	306	64	L_2	253	11	L_2
159	83	S_2	156	75	AP_2	262	50	L_2	75	1	L_2
149	88	S_2	164	78	AP_2	262	24	L_2	79	14	L_2
346	85	S_2	337	81	AP_2	250	28	L_2	64	12	L_2
328	85	S_2	187	50	AP_2	253	29	L_2	272	55	L_2
156	81	S_2	167	82	AP_2	262	26	L_2	252	25	L_2
148	85	S_2	339	80	AP_2	249	25	L_2	253	30	L_2
340	75	S_2	131	88	AP_2	257	31	L_2	260	41	L_2
340	78	S_2	135	80	AP_2	232	36	L_2	266	43	L_2
326	84	S_2	159	81	AP_2	274	17	L_2	226	35	L_2
315	80	S_2	342	62	AP_2	262	3	L_2	244	20	L_2
351	72	S_2	4	62	AP_2	250	7	L_2	253	16	L_2
343	84	S_2	176	74	AP_2	34	39	L_2	228	22	L_2
146	84	S_2	5	81	AP_2	13	45	L_2	253	28	L_2
150	87	S_2	342	73	AP_2	31	46	L_2	51	9	L_2
323	85	S_2	344	43	AP_2	46	44	L_2	256	9	L_2
168	76	S_2	341	41	AP_2	37	49	L_2	251	6	L_2
158	80	S_2	170	53	AP_2	247	3	L_2	245	5	L_2
163	77	S_2	145	82	AP_2	253	16	L_2	246	2	L_2
170	80	S_2	298	78	AP_2	263	9	L_2	242	0	L_2
152	78	S_2	147	48	AP_2	292	18	L_2	247	4	L_2
148	75	S_2	163	71	AP_2	288	9	L_2	249	19	L_2

Domain A			Domain A			Domain C		
152	75	S_2	155	80	AP_2	289	11	L_2
140	90	S_2	329	77	AP_2	249	19	L_{dex}
148	90	S_2	333	63	AP_2	266	0	L_{dex}
146	90	S_2	317	80	AP_2	313	7	L_{nor}
314	49	S_2	135	75	AP_2	315	12	L_{nor}
328	47	S_2	136	84	AP_2	314	8	L_{nor}
330	46	S_2	327	73	AP_2	316	20	L_{nor}
340	84	S_2	156	87	AP_2	310	16	L_{nor}
161	90	S_2	159	90	AP_2	240	30	L_{sin}
337	65	S_2	332	84	AP_2	246	26	L_{sin}
344	73	S_2	332	54	AP_2	306	45	L_{sin}
129	76	S_2	349	56	AP_2	292	44	L_{sin}
145	78	S_2	13	46	AP_2	310	48	L_{sin}
177	81	S_2	140	75	AP_2	283	46	L_{sin}
151	71	S_2	144	66	AP_2	225	26	L_{sin}
160	69	S_2	356	51	AP_2	287	39	L_{sin}
163	80	S_2	343	63	AP_2	285	52	L_{sin}
152	75	S_2	343	53	AP_2	305	52	L_{sin}
165	84	S_2	352	35	AP_2	271	65	L_{sin}
163	81	S_2	348	55	AP_2	269	39	L_{sin}
153	77	S_2	358	62	AP_2	259	27	L_{sin}
160	86	S_2	342	54	AP_2	266	3	FA_1
157	85	S_2	348	52	AP_2	275	19	FA_1
150	75	S_2	346	59	AP_2	343	10	FA_1
348	74	S_2	19	76	AP_2	33	16	FA_1
343	67	S_2	10	76	AP_2	37	11	FA_1
346	69	S_2	10	80	AP_2	130	12	FA_1
339	79	S_2	9	89	AP_2	108	22	FA_1
343	76	S_2	11	90	AP_2	107	26	FA_1
341	80	S_2	181	81	AP_2	195	23	FA_1
350	75	S_2	181	82	AP_2	68	24	FA_1
356	77	S_2	163	81	AP_2	125	54	FA_1
354	75	S_2	178	74	AP_2	175	7	FA_1
348	90	S_2	348	89	AP_2	293	8	FA_1
353	90	S_2	348	90	AP_2	250	10	FA_1
349	87	S_2	26	25	AP_2	274	15	FA_1
349	85	S_2	80	38	AP_2	91	4	FA_1
344	87	S_2	46	39	AP_2	158	15	FA_1
352	84	S_2	12	86	AP_2	254	6	FA_1
343	85	S_2	6	82	AP_2	203	4	FA_1
342	72	S_2	1	67	AP_2	285	22	FA_1
350	74	S_2	357	73	AP_2	96	15	FA_1
174	83	S_2	336	65	AP_2	267	20	FA_1
308	78	S_2	349	86	AP_2	265	12	FA_1
348	86	S_2	349	62	AP_2	261	24	FA_1

Domain A		
255	20	L_2
248	6	L_2
254	14	L_2
260	18	L_2
252	14	L_2
246	8	L_2
243	7	L_2
242	11	L_2
233	37	L_2
258	4	L_2
261	11	L_2
90	29	L_2
92	22	L_2
279	2	L_2
87	11	L_2
266	4	L_2
175	2	L_2
85	3	L_2
94	0	L_2
269	4	L_2
275	6	L_2
270	4	L_2
266	5	L_2
268	4	L_2
265	4	L_2
88	28	L_2
90	44	L_2
91	32	L_2
91	25	L_2
83	22	L_2
94	34	L_2
100	27	L_2
92	21	L_2
67	27	L_2
278	6	L_2
62	12	L_2
69	12	L_2
75	20	L_2
64	2	L_2
45	7	L_2
61	17	L_2
74	5	L_2
62	28	L_2
234	3	L_2
93	28	L_2

Supporting Table 1: raw data of structural measurements

Domain A		
324	59	S_2
330	72	S_2
334	65	S_2
345	64	S_2
351	60	S_2
306	87	S_2
127	67	S_2
332	70	S_2
339	76	S_2
322	83	S_2
323	90	S_2
320	90	S_2
153	84	S_2
151	78	S_2
328	72	S_2
324	78	S_2
328	75	S_2
311	81	S_2
127	53	S_2
129	62	S_2
147	75	S_2
144	82	S_2
155	61	S_2
153	61	S_2
316	87	S_2
134	85	S_2
316	87	S_2
134	85	S_2
126	69	S_2
127	69	S_2
133	80	S_2
135	62	S_2
132	58	S_2
149	77	S_2
150	80	S_2
324	75	S_2
332	75	S_2
314	79	S_2
313	84	S_2
154	88	S_2
335	67	S_2
338	75	S_2
329	69	S_2
176	67	S_2
321	87	S_2

Domain A		
159	82	AP_2
163	78	AP_2
342	84	AP_2
154	76	AP_2
340	88	AP_2
328	67	AP_2
344	84	AP_2
186	84	AP_2
182	78	AP_2
149	80	AP_2
167	82	AP_2
348	86	AP_2
346	80	AP_2
354	79	AP_2
8	81	AP_2
13	86	AP_2
13	85	AP_2
9	66	AP_2
344	72	AP_2
181	86	AP_2
352	86	AP_2
355	83	AP_2
1	85	AP_2
5	88	AP_2
173	88	AP_2
180	90	AP_2
2	87	AP_2
134	73	AP_2
356	87	AP_2
176	85	AP_2
174	81	AP_2
168	81	AP_2
176	84	AP_2
6	83	AP_2
355	86	AP_2
170	84	AP_2
176	86	AP_2
359	70	AP_2
4	76	AP_2
313	13	AP_2

Domain C		
258	13	FA_1
9	65	FA_2
30	60	FA_2
225	26	FA_2
214	23	FA_2
226	41	FA_2
205	13	FA_2
51	4	FA_2
264	13	FA_2
76	2	FA_2
77	7	FA_2
29	0	FA_2
34	14	FA_2
40	23	FA_2
26	18	FA_2
26	10	FA_2
28	32	FA_2
13	33	FA_2
357	12	FA_2
2	13	FA_2
189	13	FA_2
190	20	FA_2
13	17	FA_2
12	14	FA_2
237	4	FA_2
258	40	FA_2
80	15	FA_2
227	16	FA_2
238	20	FA_2
190	20	FA_2
194	15	FA_2
164	8	FA_2
164	8	FA_2
56	8	FA_2
242	29	FA_2
241	40	FA_2
241	30	FA_2
243	13	FA_2
72	29	FA_2
318	40	FA_2
243	13	FA_2
333	36	FA_2
230	9	FA_2
243	9	FA_2
230	60	FA_2

Domain A		
76	35	L_2
70	26	L_2
90	25	L_2
262	28	L_2
258	25	L_2
232	12	L_2
49	11	L_2
226	24	L_2
235	10	L_2
251	30	L_2
176	68	L_2
244	16	L_2
242	37	L_2
236	30	L_2
237	48	L_2
241	30	L_2
252	14	L_2
254	12	L_2
254	14	L_2
261	20	L_2
242	12	L_2
242	4	L_2
274	2	L_2
94	14	L_2
58	53	L_2
250	7	L_2
252	13	L_2
242	8	L_2
254	9	L_2
254	0	L_2
250	0	L_2
245	1	L_2
76	15	L_2
82	18	L_2
280	6	L_2
78	39	L_2
51	41	L_2
98	26	L_2
91	27	L_2
88	25	L_2
83	23	L_2
272	2	L_2
83	34	L_2
87	30	L_2
96	26	L_2

Domain A		
329	85	S_2
300	57	S_2
328	77	S_2
328	85	S_2
322	86	S_2
316	84	S_2
318	68	S_2
324	73	S_2
325	85	S_2
328	89	S_2
152	87	S_2
306	81	S_2
323	81	S_2
166	78	S_2
171	75	S_2
346	80	S_2
176	77	S_2
160	73	S_2
149	88	S_2
148	87	S_2
164	86	S_2
191	78	S_2
170	79	S_2
178	76	S_2
182	74	S_2
185	72	S_2
180	76	S_2
191	72	S_2
177	87	S_2
346	86	S_2
340	86	S_2
318	70	S_2
308	67	S_2
292	65	S_2
292	64	S_2
279	65	S_2
317	74	S_2
348	84	S_2
311	63	S_2
319	58	S_2
333	75	S_2
330	68	S_2
164	90	S_2
338	77	S_2
138	62	S_2

Domain C		
240	45	FA_2
225	18	FA_2
240	14	FA_2
293	42	FA_2
339	28	FA_2
351	20	FA_2
329	5	FA_2
346	21	FA_2
77	34	FA_2
269	68	FA_2
267	60	FA_2
295	14	FA_2
101	8	FA_2
290	53	FA_2
101	43	FA_2
238	30	FA_2
47	17	FA_2
194	8	FA_2
194	59	FA_2
197	27	FA_2
237	21	FA_2
122	18	FA_2
124	23	FA_2
19	12	FA_2
13	26	FA_2
20	4	FA_2
19	28	FA_2
8	31	FA_2
47	14	FA_2
59	18	FA_2
35	25	FA_2
57	4	FA_2
126	2	FA_2
248	7	FA_2
11	24	FA_2
90	71	FA_3
129	74	FA_3
87	70	FA_3
86	85	FA_3
120	75	FA_3
93	78	FA_3

Domain A		
98	27	L_2
92	35	L_2
69	87	L_2
94	25	L_2
90	34	L_2
94	24	L_2
96	9	L_2
101	14	L_2
92	30	L_2
87	14	L_2
119	34	L_2
81	24	L_2
87	7	L_2
94	35	L_2
92	17	L_2
92	35	L_2
95	17	L_2
94	41	L_2
91	17	L_2
92	26	L_2
96	3	L_2
112	29	L_2
86	16	L_2
86	26	L_2
88	12	L_2
87	12	L_2
250	21	L_2
251	21	L_2
240	40	L_2
234	35	L_2
237	41	L_2
243	38	L_2
41	18	L_2
40	11	L_2
235	28	L_2
234	35	L_2
45	8	L_2
90	47	L_2
84	55	L_2
82	40	L_2
251	16	L_2
88	65	L_2
67	31	L_2
68	29	L_2
267	5	L_2

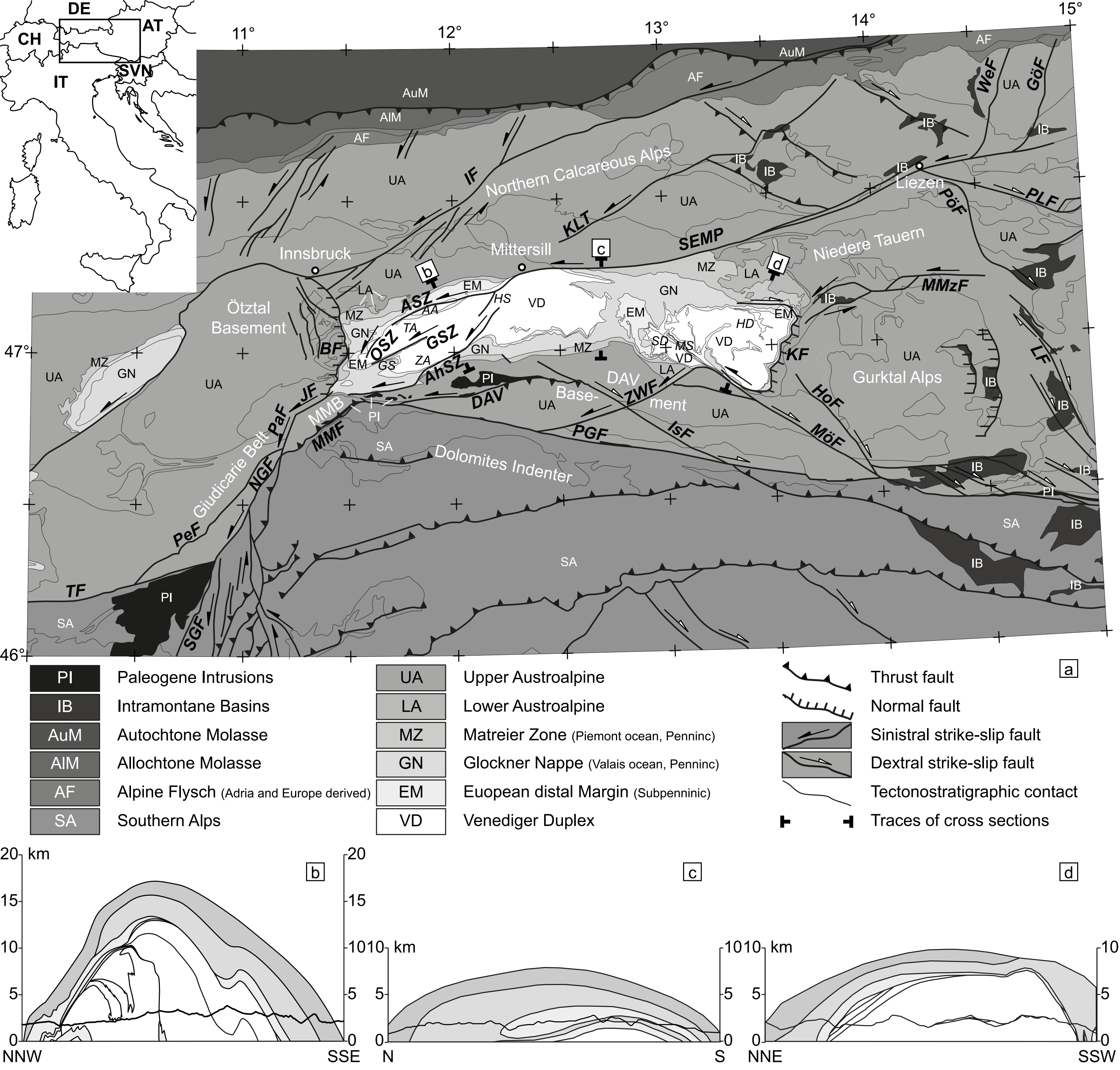

AhSZ: Ahrntal Shear Zone, ASZ: Ahorn Shear Zone, BF: Brenner Fault, DAV: Defereggen-Antholz-Vals Fault, GöF:Görtschitztal Fault, GSZ: Greiner Shear Zone, HoF:Hochstuhl Fault, IF: Inntal Fault, IS: Iseltal Fault, JF: Jaufen Fault, KLT: Königssee-Lammertal-Traunsee Fault, KF: Katschberg Fault, LF: Lavanttal Fault, MMB: Meran-Mauls Basement, MMF: Meran-Mauls Fault, MMZF: Mur-Mürz Fault; MöF: Mölltal Fault, NGF: Northern Giudicarie Fault, OSZ: Olperer Shear Zone, PaF: Passeier Fault, PeF: Pejo Fault, PLF: Palten-Liesing-Fault, PöF: Pöls Fault, PGF: Pustertal-Gailtal Fault, SEMP: Salzach-Ennstal-Mariazell-Puchberg Fault, SGF: Southern Giudicarie Fault, TF: Tonale Fault, WeF: Wyer Fault, ZWF: Zwischenberge-Wöllentratten Fault, AA: Ahorn Antiform, GS: Greiner Synform, HD: Hochalm Dome, HS: Habach Synform, MS: Mallnitz Synform, SD: Sonnblick Dome, TA: Tuxer Antiform, ZA: Zillertaler Antiform

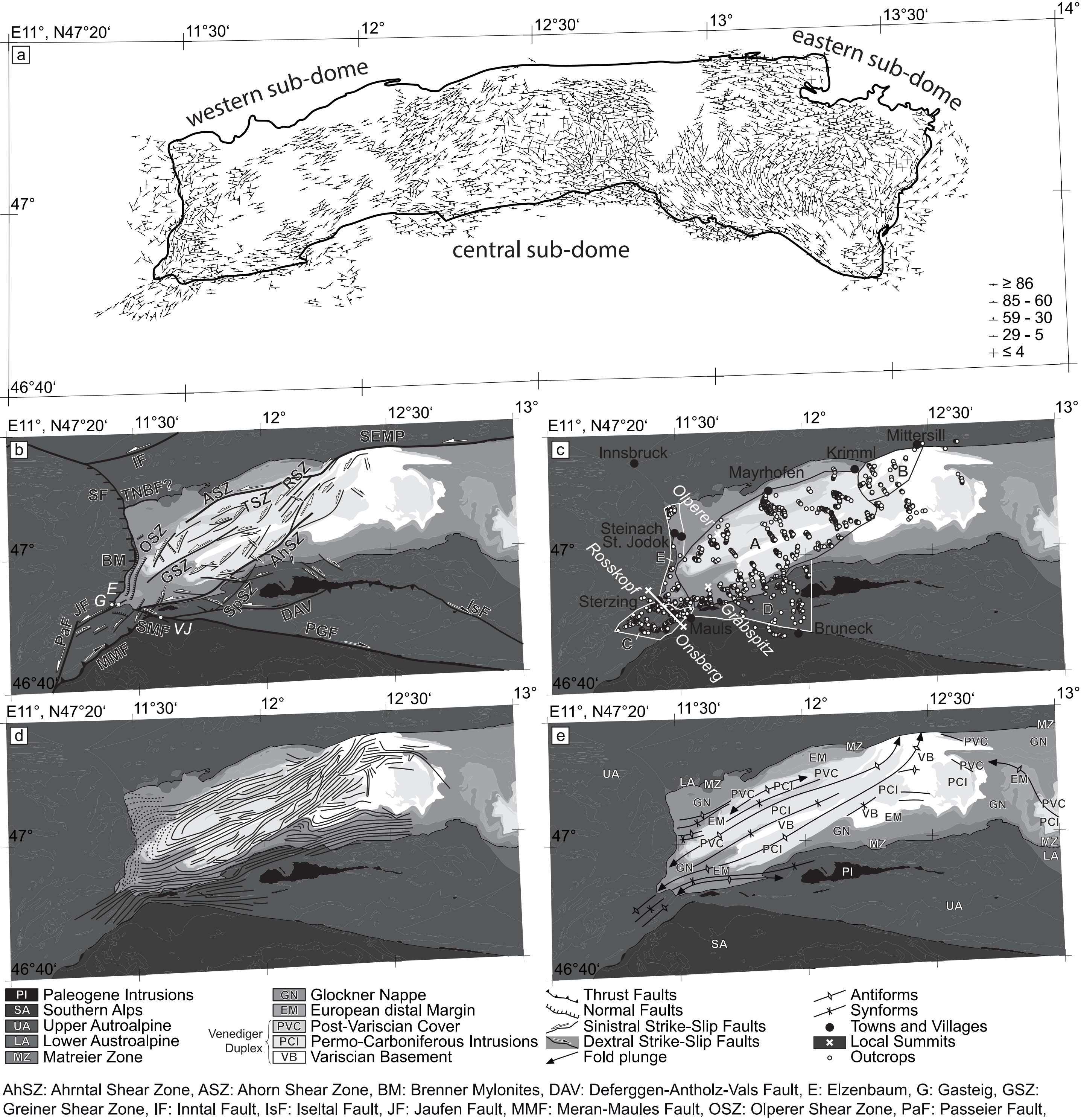

AhSZ: Ahrntal Shear Zone, ASZ: Ahorn Shear Zone, BM: Brenner Mylonites, DAV: Deferggen-Antholz-Vals Fault, E: Elzenbaum, G: Gasteig, GSZ: Greiner Shear Zone, IF: Inntal Fault, IsF: Iseltal Fault, JF: Jaufen Fault, MMF: Meran-Maules Fault, OSZ: Olperer Shear Zone, PaF: Passeier Fault, PGF: Pustertal Fault, RSZ: Rinderkar Shear Zone, SEMP: Salzach-Ennstal-Puchberg-Mariazell Fault, SF: Silltal Fault, SMF: Sprechenstein-Mauls Fault, SpSZ: Speikboden Shear Zone, TNBF: Tauern Northern Boundary Fault, TSZ: Tuxer shear zones, VJ: Valler Jöchl

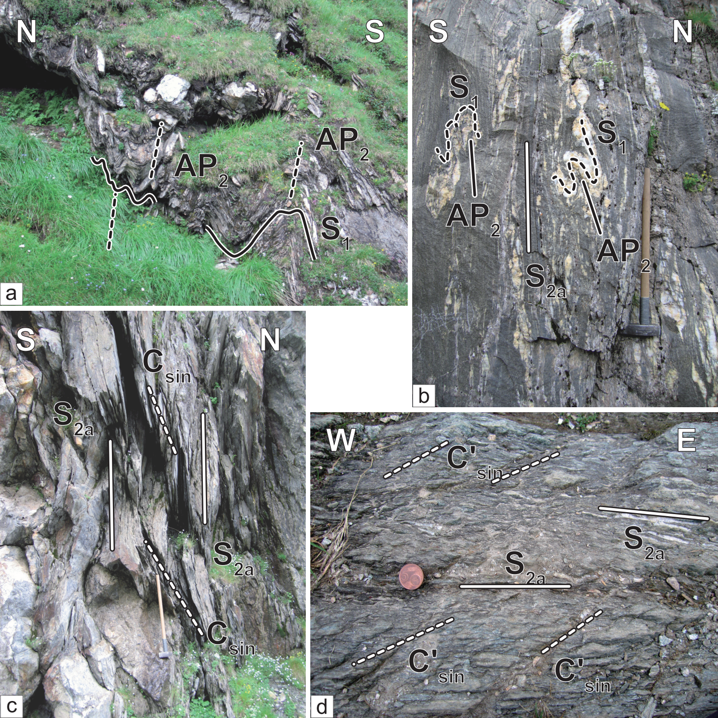

N
S
AP2
AP2
S1
a
S
N
S1
S1
AP2
AP2
S2a
b
S
N
Csin
S2a
S2a
Csin
c
W
E
C'sin
S2a
S2a
C'sin
C'sin
d

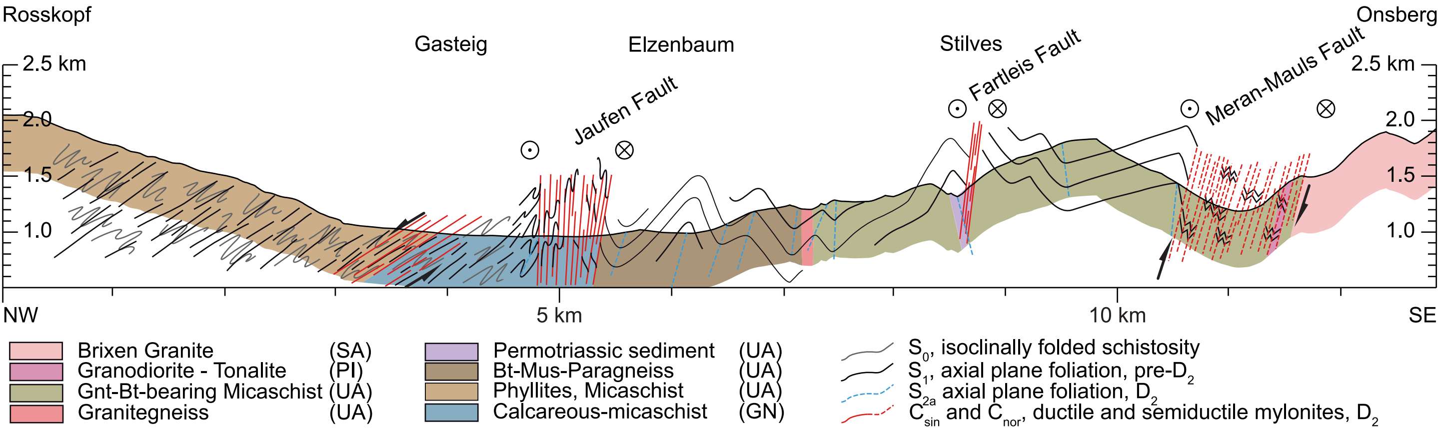

Rosskopf
Onsberg
Gasteig
Elzenbaum
Stilves
Jaufen Fault
Fartleis Fault
Meran-Mauls Fault
2.5 km
2.0
1.5
1.0
NW
5 km
10 km
SE
Brixen Granite (SA)
Granodiorite - Tonalite (PI)
Gnt-Bt-bearing Micaschist (UA)
Granitegneiss (UA)
Permotriassic sediment (UA)
Bt-Mus-Paragneiss (UA)
Phyllites, Micaschist (UA)
Calcareous-micaschist (GN)
S0, isoclinally folded schistosity
S1, axial plane foliation, pre-D2
S2a axial plane foliation, D2
Csin and Cnor, ductile and semiductile mylonites, D2

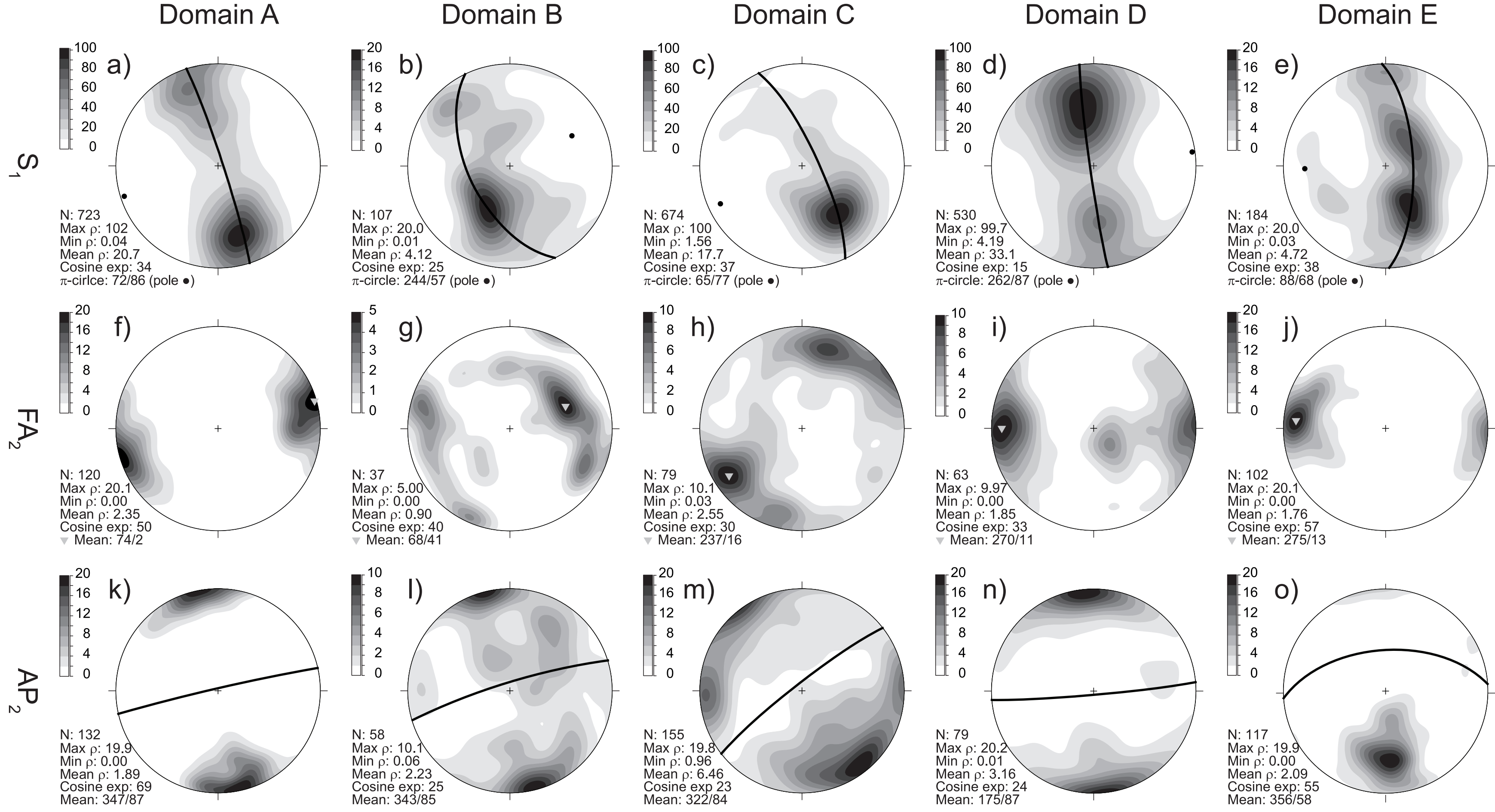

Domain A
Domain B
Domain C
Domain D
Domain E
S1
FA2
AP2
a)
N: 723
Max ρ: 102
Min ρ: 0.04
Mean ρ: 20.7
Cosine exp: 34
π-cirlce: 72/86 (pole ●)
b)
N: 107
Max ρ: 20.0
Min ρ: 0.01
Mean ρ: 4.12
Cosine exp: 25
π-circle: 244/57 (pole ●)
c)
N: 674
Max ρ: 100
Min ρ: 1.56
Mean ρ: 17.7
Cosine exp: 37
π-circle: 65/77 (pole ●)
d)
N: 530
Max ρ: 99.7
Min ρ: 4.19
Mean ρ: 33.1
Cosine exp: 15
π-circle: 262/87 (pole ●)
e)
N: 184
Max ρ: 20.0
Min ρ: 0.03
Mean ρ: 4.72
Cosine exp: 38
π-circle: 88/68 (pole ●)
f)
N: 120
Max ρ: 20.1
Min ρ: 0.00
Mean ρ: 2.35
Cosine exp: 50
▼ Mean: 74/2
g)
N: 37
Max ρ: 5.00
Min ρ: 0.00
Mean ρ: 0.90
Cosine exp: 40
▼ Mean: 68/41
h)
N: 79
Max ρ: 10.1
Min ρ: 0.03
Mean ρ: 2.55
Cosine exp: 30
▼ Mean: 237/16
i)
N: 63
Max ρ: 9.97
Min ρ: 0.00
Mean ρ: 1.85
Cosine exp: 33
▼ Mean: 270/11
j)
N: 102
Max ρ: 20.1
Min ρ: 0.00
Mean ρ: 1.76
Cosine exp: 57
▼ Mean: 275/13
k)
N: 132
Max ρ: 19.9
Min ρ: 0.00
Mean ρ: 1.89
Cosine exp: 69
Mean: 347/87
l)
N: 58
Max ρ: 10.1
Min ρ: 0.06
Mean ρ: 2.23
Cosine exp: 25
Mean: 343/85
m)
N: 155
Max ρ: 19.8
Min ρ: 0.96
Mean ρ: 6.46
Cosine exp 23
Mean: 322/84
n)
N: 79
Max ρ: 20.2
Min ρ: 0.01
Mean ρ: 3.16
Cosine exp: 24
Mean: 175/87
o)
N: 117
Max ρ: 19.9
Min ρ: 0.00
Mean ρ: 2.09
Cosine exp: 55
Mean: 356/58

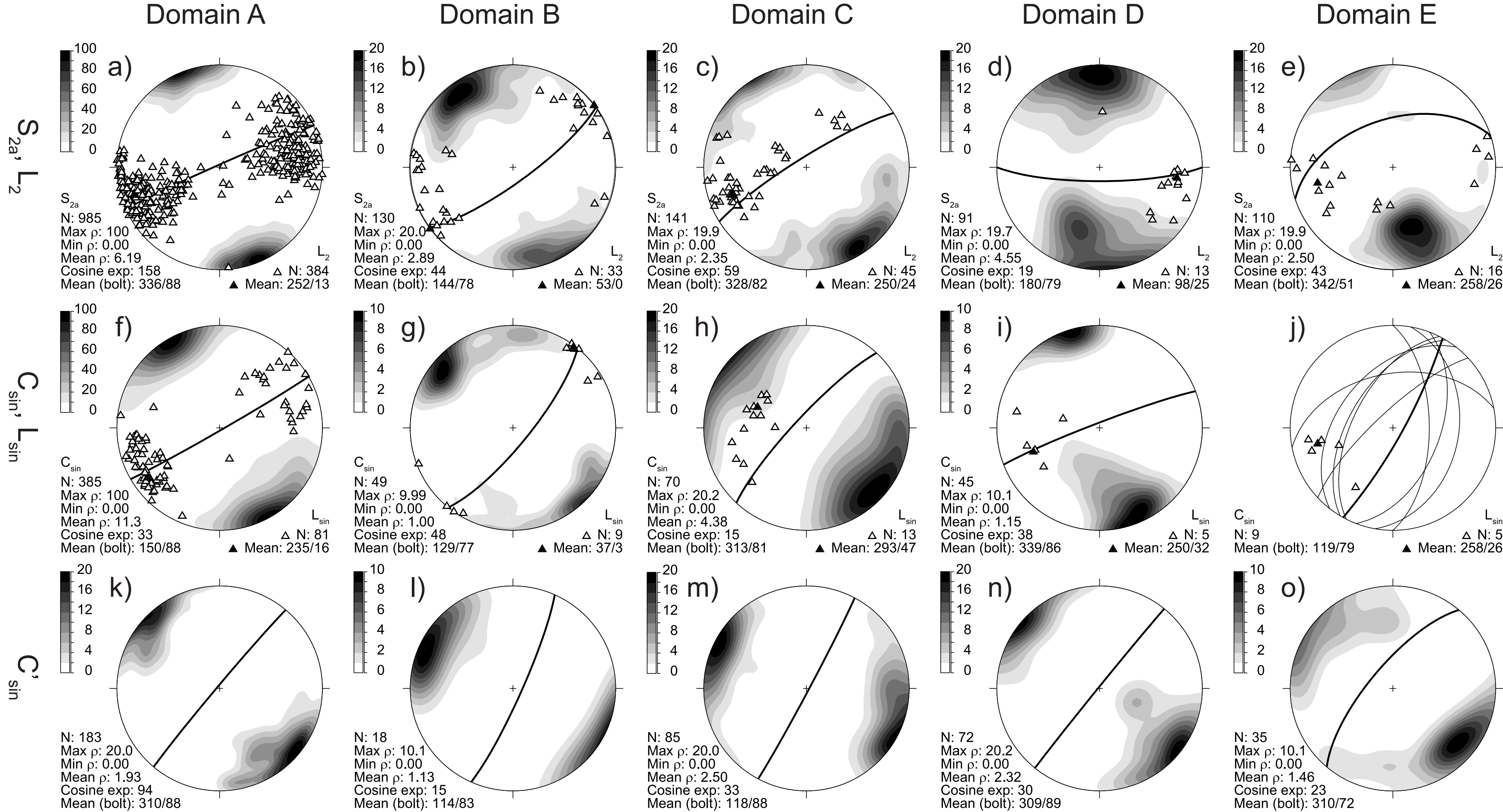

Domain A
Domain B
Domain C
Domain D
Domain E
S2a, L2
Csin, Lsin
C'sin
a)
S2a
N: 985
Max ρ: 100
Min ρ: 0.00
Mean ρ: 6.19
Cosine exp: 158
Mean (bolt): 336/88
L2
N: 384
Mean: 252/13
b)
S2a
N: 130
Max ρ: 20.0
Min ρ: 0.00
Mean ρ: 2.89
Cosine exp: 44
Mean (bolt): 144/78
L2
N: 33
Mean: 53/0
c)
S2a
N: 141
Max ρ: 19.9
Min ρ: 0.00
Mean ρ: 2.35
Cosine exp: 59
Mean (bolt): 328/82
L2
N: 45
Mean: 250/24
d)
S2a
N: 91
Max ρ: 19.7
Min ρ: 0.00
Mean ρ: 4.55
Cosine exp: 19
Mean (bolt): 180/79
L2
N: 13
Mean: 98/25
e)
S2a
N: 110
Max ρ: 19.9
Min ρ: 0.00
Mean ρ: 2.50
Cosine exp: 43
Mean (bolt): 342/51
L2
N: 16
Mean: 258/26
f)
Csin
N: 385
Max ρ: 100
Min ρ: 0.00
Mean ρ: 11.3
Cosine exp: 33
Mean (bolt): 150/88
Lsin
N: 81
Mean: 235/16
g)
Csin
N: 49
Max ρ: 9.99
Min ρ: 0.00
Mean ρ: 1.00
Cosine exp: 48
Mean (bolt): 129/77
Lsin
N: 9
Mean: 37/3
h)
Csin
N: 70
Max ρ: 20.2
Min ρ: 0.00
Mean ρ: 4.38
Cosine exp: 15
Mean (bolt): 313/81
Lsin
N: 13
Mean: 293/47
i)
Csin
N: 45
Max ρ: 10.1
Min ρ: 0.00
Mean ρ: 1.15
Cosine exp: 38
Mean (bolt): 339/86
Lsin
N: 5
Mean: 250/32
j)
Csin
N: 9
Mean (bolt): 119/79
Lsin
N: 5
Mean: 258/26
k)
N: 183
Max ρ: 20.0
Min ρ: 0.00
Mean ρ: 1.93
Cosine exp: 94
Mean (bolt): 310/88
l)
N: 18
Max ρ: 10.1
Min ρ: 0.00
Mean ρ: 1.13
Cosine exp: 15
Mean (bolt): 114/83
m)
N: 85
Max ρ: 20.0
Min ρ: 0.00
Mean ρ: 2.50
Cosine exp: 33
Mean (bolt): 118/88
n)
N: 72
Max ρ: 20.2
Min ρ: 0.00
Mean ρ: 2.32
Cosine exp: 30
Mean (bolt): 309/89
o)
N: 35
Max ρ: 10.1
Min ρ: 0.00
Mean ρ: 1.46
Cosine exp: 23
Mean (bolt): 310/72

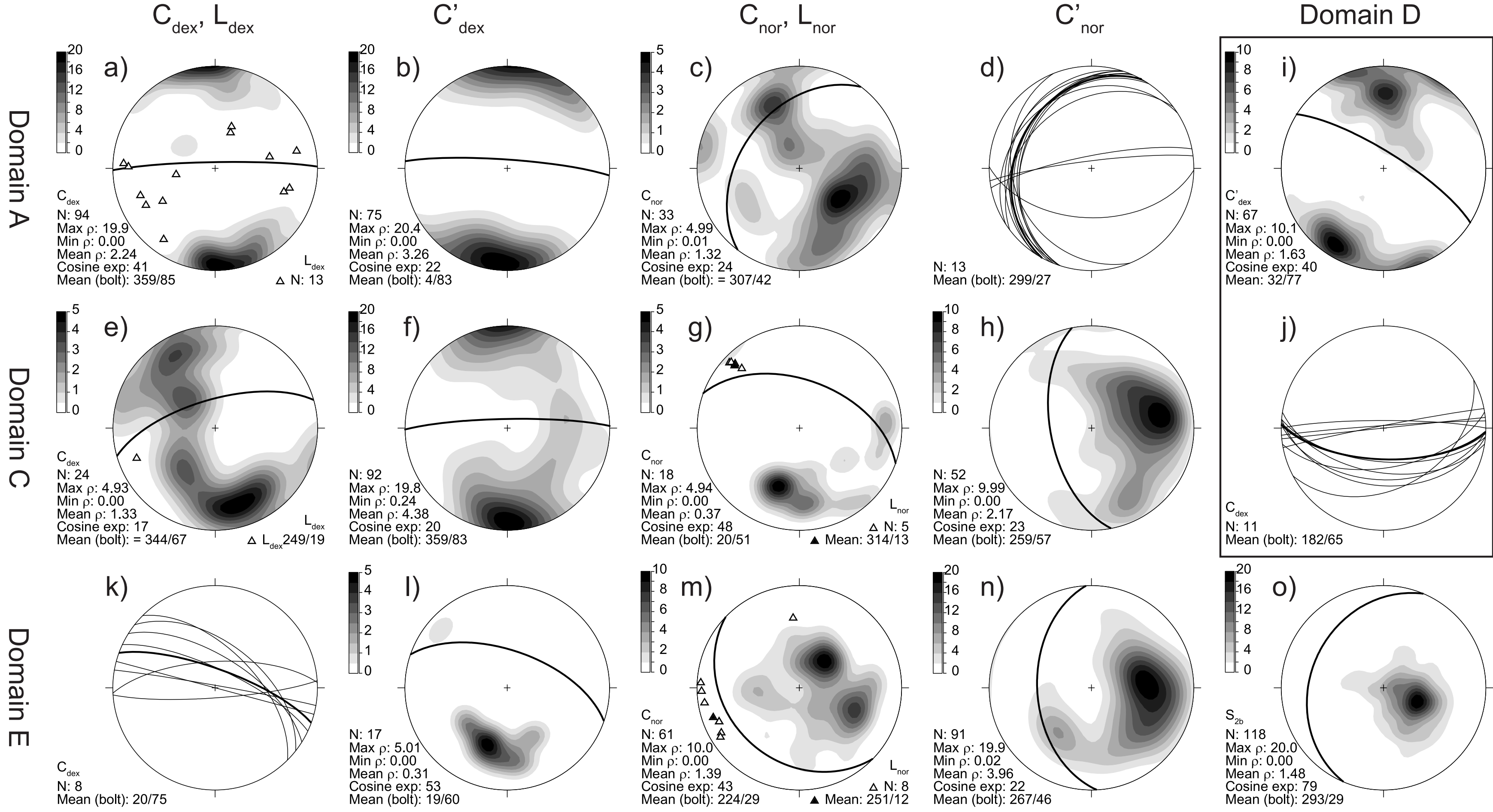

C_{dex}, L_{dex}
C'_{dex}
C_{nor}, L_{nor}
C'_{nor}
Domain D
Domain A
Domain C
Domain E
a)
C_{dex}
N: 94
Max ρ: 19.9
Min ρ: 0.00
Mean ρ: 2.24
Cosine exp: 41
Mean (bolt): 359/85
L_{dex}
△ N: 13
b)
N: 75
Max ρ: 20.4
Min ρ: 0.00
Mean ρ: 3.26
Cosine exp: 22
Mean (bolt): 4/83
c)
C_{nor}
N: 33
Max ρ: 4.99
Min ρ: 0.01
Mean ρ: 1.32
Cosine exp: 24
Mean (bolt): = 307/42
d)
N: 13
Mean (bolt): 299/27
i)
C'_{dex}
N: 67
Max ρ: 10.1
Min ρ: 0.00
Mean ρ: 1.63
Cosine exp: 40
Mean: 32/77
e)
C_{dex}
N: 24
Max ρ: 4.93
Min ρ: 0.00
Mean ρ: 1.33
Cosine exp: 17
Mean (bolt): = 344/67
L_{dex}
△ L_{dex}249/19
f)
N: 92
Max ρ: 19.8
Min ρ: 0.24
Mean ρ: 4.38
Cosine exp: 20
Mean (bolt): 359/83
g)
C_{nor}
N: 18
Max ρ: 4.94
Min ρ: 0.00
Mean ρ: 0.37
Cosine exp: 48
Mean (bolt): 20/51
L_{nor}
△ N: 5
▲ Mean: 314/13
h)
N: 52
Max ρ: 9.99
Min ρ: 0.00
Mean ρ: 2.17
Cosine exp: 23
Mean (bolt): 259/57
j)
C_{dex}
N: 11
Mean (bolt): 182/65
k)
C_{dex}
N: 8
Mean (bolt): 20/75
l)
N: 17
Max ρ: 5.01
Min ρ: 0.00
Mean ρ: 0.31
Cosine exp: 53
Mean (bolt): 19/60
m)
C_{nor}
N: 61
Max ρ: 10.0
Min ρ: 0.00
Mean ρ: 1.39
Cosine exp: 43
Mean (bolt): 224/29
L_{nor}
△ N: 8
▲ Mean: 251/12
n)
N: 91
Max ρ: 19.9
Min ρ: 0.02
Mean ρ: 3.96
Cosine exp: 22
Mean (bolt): 267/46
o)
S_{2b}
N: 118
Max ρ: 20.0
Min ρ: 0.00
Mean ρ: 1.48
Cosine exp: 79
Mean (bolt): 293/29

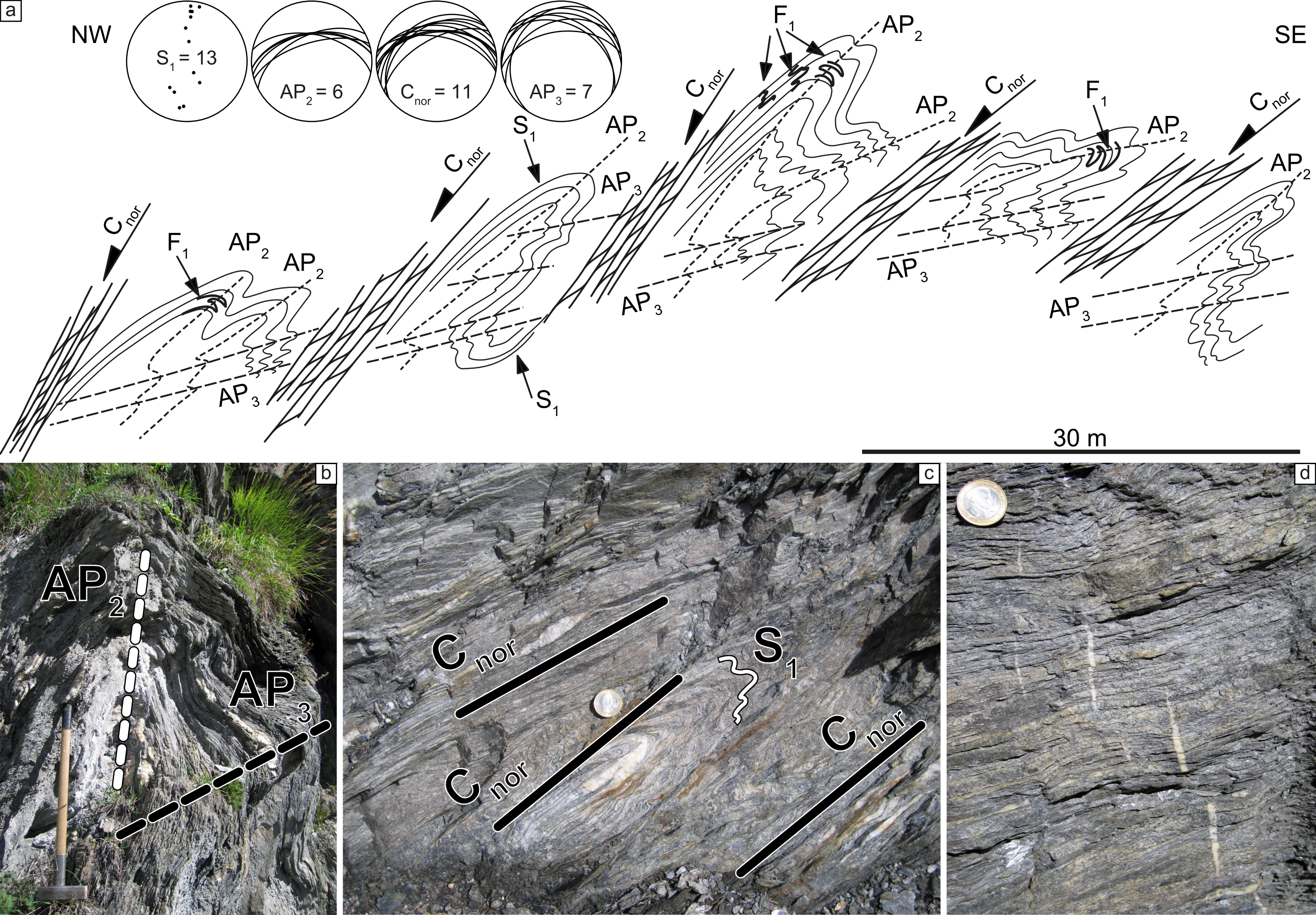
a
NW
SE
S1 = 13
AP2 = 6
Cnor = 11
AP3 = 7
F1
AP2
AP3
Cnor
S1
30 m
b
AP2
AP3
c
Cnor
S1
d

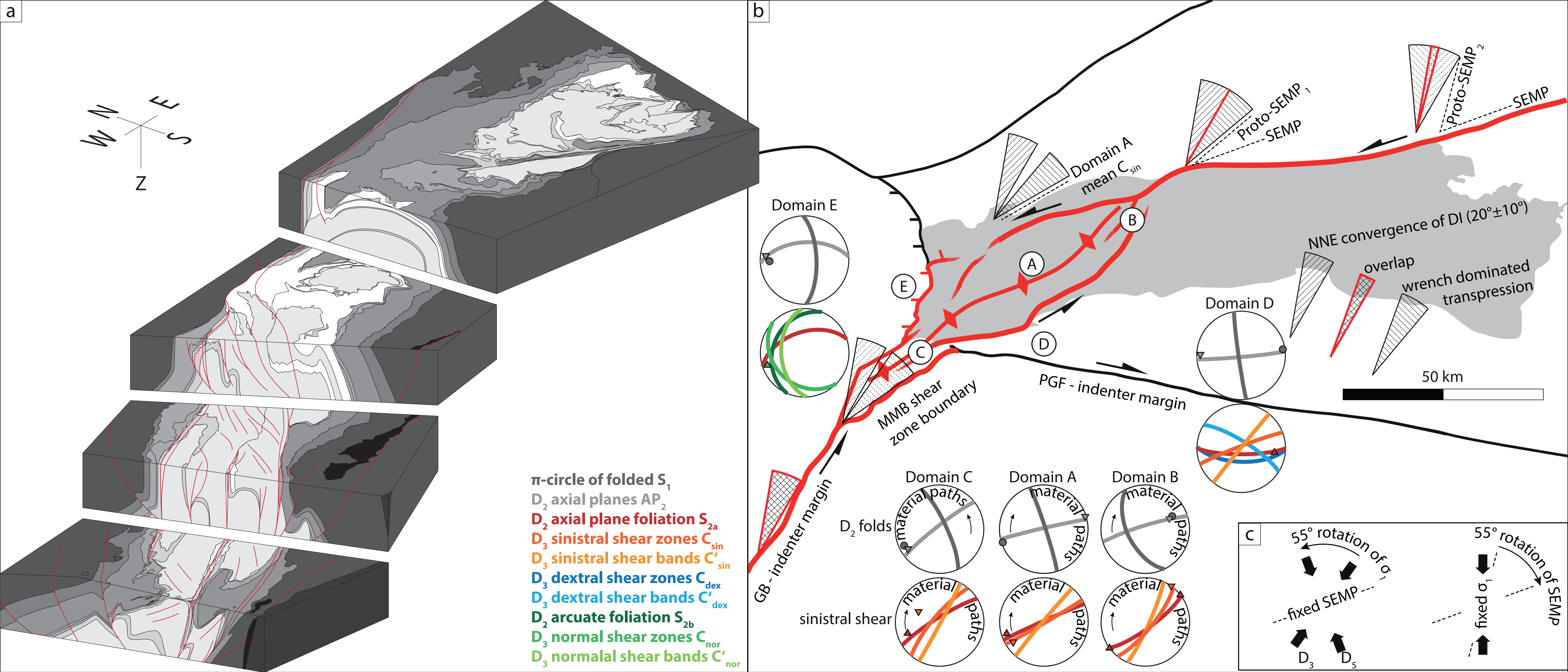
a
W N E S
Z
π-circle of folded S_1
D_2 axial planes AP_2
D_2 axial plane foliation S_{2a}
D_3 sinistral shear zones C_{sin}
D_3 sinistral shear bands C'_{sin}
D_3 dextral shear zones C_{dex}
D_3 dextral shear bands C'_{dex}
D_2 arcuate foliation S_{2b}
D_3 normal shear zones C_{nor}
D_3 normalal shear bands C'_{nor}
b
Domain E
E
Domain A mean C_{sin}
A
B
C
D
Proto-SEMP $_1$
SEMP
Proto-SEMP $_2$
SEMP
NNE convergence of DI (20°±10°)
overlap
wrench dominated transpression
Domain D
50 km
MMB shear zone boundary
PGF - indenter margin
GB - indenter margin
Domain C
Domain A
Domain B
D_2 folds
sinistral shear
material paths
material paths
material paths
material paths
material paths
material paths
c
55° rotation of σ_1
fixed SEMP
D_3
D_5
55° rotation of SEMP
fixed σ_1

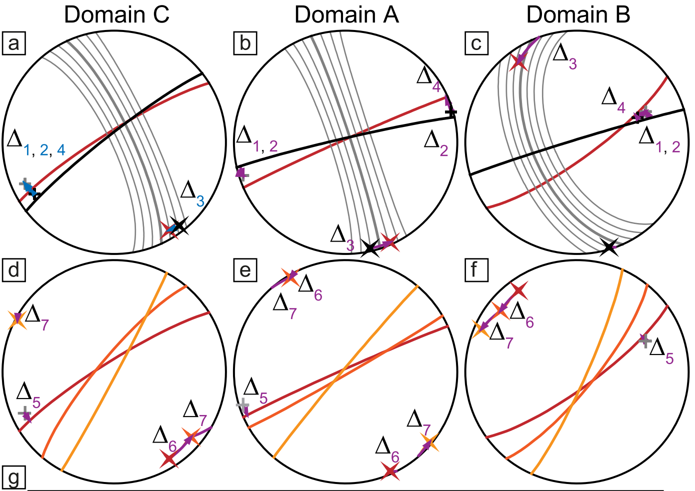

g

Dihedral angles (in degree °)		Domain C	Domain A	Domain B
Δ_1 = (AP_2 – π-axis)	(,)	11	-5	-5
Δ_2 = (FA_2 – π-axis)	(,)	8	-6	-8
Δ_3 = (AP_2 – S_{2a})	(,)	6	-11	-25
Δ_4 = (FA_2 – S_{2a})	(,)	3	-9	-3
Δ_5 = (π-axis – S_{2a})	(,)	-5	-6	-4
Δ_6 = (S_{2a} – C_{sin})	(,)	-18	-7	-15
Δ_7 = (C_{sin} – C'_{sin})	(,)	-18	-20	-16

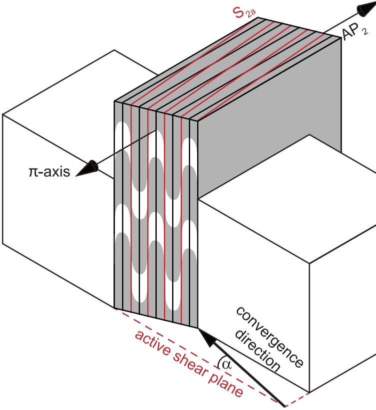

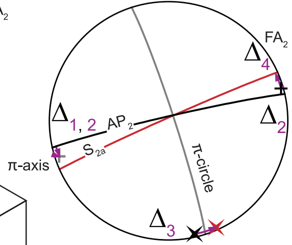

Dihedral angles (D_2 folding)	
Δ_1 = (AP_2 – π-axis)	(/, +)
Δ_2 = (FA_2 – π-axis)	(+, +)
Δ_3 = (AP_2 – S_{2a})	(×, ×)
Δ_4 = (FA_2 – S_{2a})	(+, /)

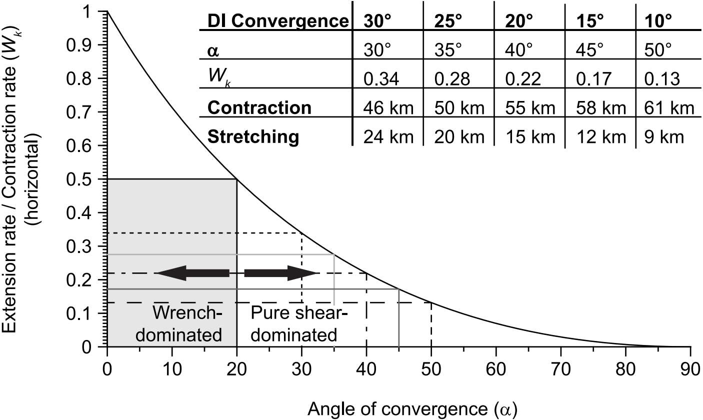

DI Convergence	30°	25°	20°	15°	10°
α	30°	35°	40°	45°	50°
W_k	0.34	0.28	0.22	0.17	0.13
Contraction	46 km	50 km	55 km	58 km	61 km
Stretching	24 km	20 km	15 km	12 km	9 km

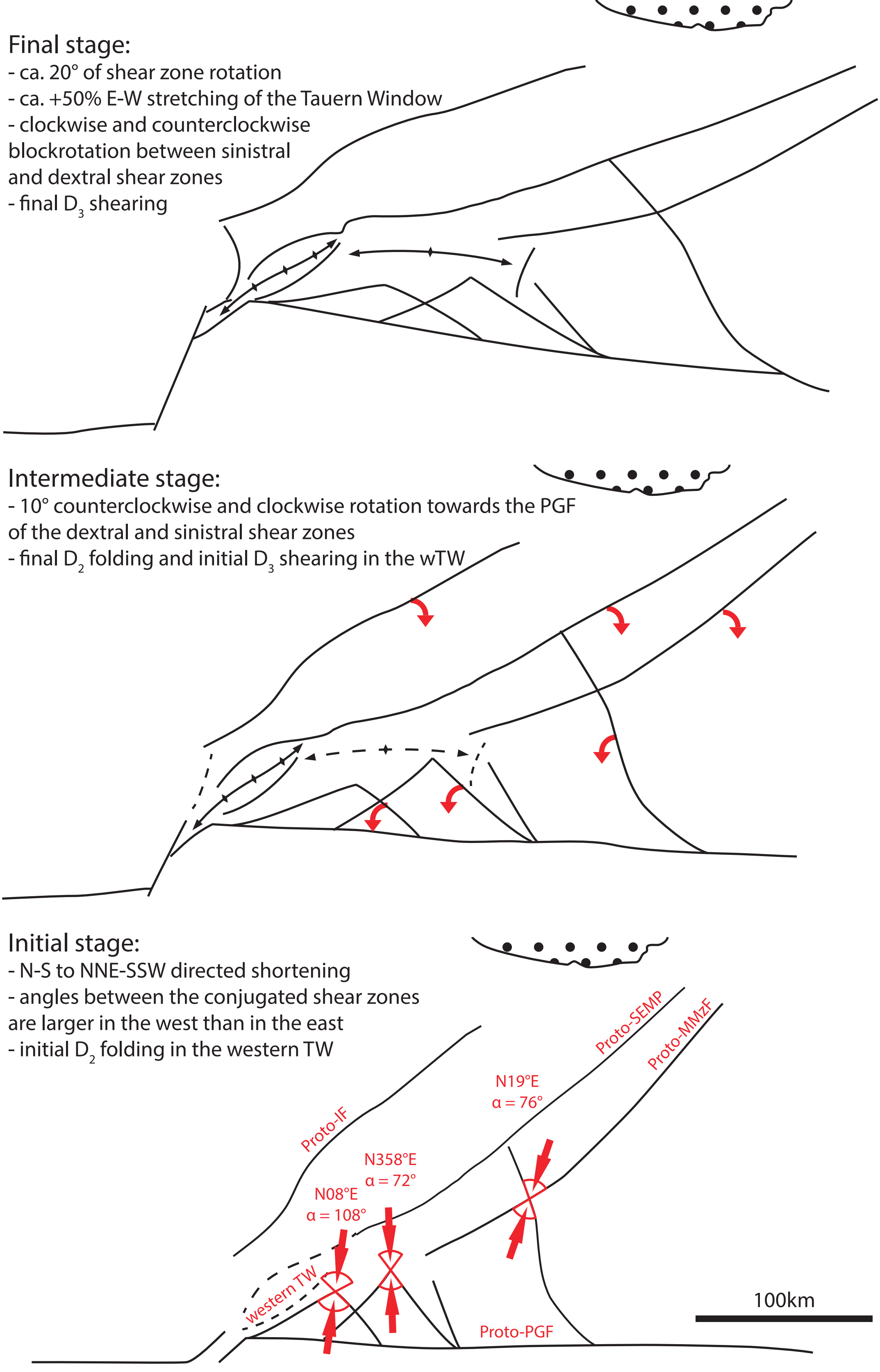

Final stage:
- ca. 20° of shear zone rotation
- ca. +50% E-W stretching of the Tauern Window
- clockwise and counterclockwise blockrotation between sinistral and dextral shear zones
- final D3 shearing
Intermediate stage:
- 10° counterclockwise and clockwise rotation towards the PGF of the dextral and sinistral shear zones
- final D2 folding and initial D3 shearing in the wTW
Initial stage:
- N-S to NNE-SSW directed shortening
- angles between the conjugated shear zones are larger in the west than in the east
- initial D2 folding in the western TW
Proto-SEMP
Proto-MMzF
Proto-IF
N19°E
α = 76°
N358°E
α = 72°
N08°E
α = 108°
western TW
Proto-PGF
100km